### POLITECNICO DI TORINO

MASTER's Degree in Civil Engineering



### MASTER's Degree Thesis

# Numerical model of constructed wetland in Lesbos, Greece

Supervisors

Candidate

Prof. FULVIO BOANO

VERONICA YEPES CARDONA

PHD. ANACLETO RIZZO

OCTOBER 2025

In the midst of hardship, when nothing makes sense, dare to set sail and head for deeper waters

#### Abstract

Constructed wetlands (CWs) represent a natural solution for sustainable wastewater treatment, combining hydraulic processes with biochemical pathways for the removal of organic matter and nutrients. Despite their widespread application, vertical flow CWs under unsaturated conditions remain underexplored, especially with regard to oxygen dynamics and substrate degradation. This thesis develops and applies a one-dimensional numerical model of an unsaturated vertical CW, designed with reference to the HYDROUSA project facility in Lesbos, Greece, to simulate water flow and pollutant removal processes under realistic operating conditions. The model combines the Richards equation for variably saturated flow with the Dilute Species Transport module of COMSOL Multiphysics, allowing for the simultaneous description of water movement and solute transport. To capture the biochemical transformations of organic matter, nitrogen species, and oxygen, the BIO PORE conceptual framework was implemented and adapted to unsaturated vertical conditions. Particular attention was paid to oxygen exchange between pore water and the atmosphere, reformulating it to reflect its dependence on water content and saturation, thus expanding the model's applicability beyond traditional saturated systems. Calibration and validation were performed using field data of inlet and outlet chemical oxygen demand (COD), measured weekly at the Lesvos pilot plant. COD was separated into soluble and particulate fractions, which were dynamically simulated through hydrolysis reactions, substrate degradation, and microbial growth. The oxygen balance was analyzed using an additional sourcesink formulation that considers diffusion and replenishment from the atmosphere. Sensitivity analyses were performed to assess the role of hydraulic parameters (Van Genuchten-Mualem functions), biodegradation constants, and oxygen mass transfer coefficients in treatment efficiency. The results demonstrate that the adapted Bio-Pore scheme can successfully reproduce the temporal dynamics of COD removal in an unsaturated vertical wetland. The integration of an oxygen exchange mechanism significantly improved the accuracy of dissolved oxygen predictions, crucial for maintaining aerobic degradation. The model also provided insight into the interaction between flow variability, substrate removal pathways, and longterm treatment performance. This thesis helps bridge the gap between empirical observations and process-based modeling of unsaturated constructed wetlands. By integrating advanced hydraulic formulations with a network of biogeochemical reactions, it offers a flexible framework for simulating pollutant removal and optimizing wetland design. This approach supports the development of more resilient and efficient constructed wetlands, highlighting their potential to provide

decentralized was tewater treatment while protecting environmental quality and promoting circular water use.

## Acknowledgements

With this thesis, my academic journey at Politecnico di Torino comes to an end. I would like to begin by expressing my deepest gratitude to my family, who supported me in the decision to move abroad and who have always been by my side, even from afar. To my mom and dad, who are not only my greatest supporters but also my biggest inspiration in pursuing a life in civil engineering: thank you for raising me with a thirst for knowledge and for giving me the wings to fly.

I am also grateful to my lifelong friends, who have always cheered for me and stood behind every decision I have made, and to the friends I found in Torino, who became my family away from home. Without their love and encouragement, this experience would not have been the same. A very special thanks goes to Dani, who has been by my side every step of the way, helping me through the hardest times and sharing with me one of the most meaningful experiences of my life.

I would also like to sincerely thank Professor Fulvio Boano and Doctor Anacleto Rizzo for believing in me and for their guidance and support throughout the thesis work. Finally, I am thankful to all my classmates, who made this journey not only a period of learning, but an unforgettable experience filled with friendship and growth.

## Table of Contents

Li	st of	Table	S	VI
Li	st of	Figur	es	VIII
A	crony	m ms		XII
1	Intr	oduct	ion	1
2	Stat	te of t	he Art	3
	2.1	Proble	em Statement	3
	2.2	Theor	etical Framework: Constructed Wetlands	4
		2.2.1	Basic concepts	4
		2.2.2	Key treatment mechanisms	4
		2.2.3	Types of constructed wetland	5
		2.2.4	Applications	9
		2.2.5	Contaminant Removal Processes	10
	2.3	Nume	rical Framework	13
		2.3.1	Numerical Framework for Flow in Porous Media	13

		2.3.2	Numerical Framework of the BIO_PORE Model	19
3	Met	hodolo	$_{ m pgy}$	35
	3.1	Site De	escription	35
		3.1.1	Location: Island of Lesvos, Greece	35
		3.1.2	Case Study: HYDROUSA Constructed Wetland in Lesvos $$ .	36
	3.2	Model		45
		3.2.1	Software: COMSOL Multiphysics	45
		3.2.2	System to be Modeled: VFInsat	47
		3.2.3	Input flowrate characteristics	49
		3.2.4	Simulation's parameters	50
4	Res	ults		75
	4.1	Hydraı	ulic verification	75
	4.2	Couple	ed hydraulic-biochemical results	80
		4.2.1	Corrected simulation	83
5	Con	clusior	ns	91
A	Inpu	ıt data	for the model	94
Bi	bliog	raphy		100

## List of Tables

2.1	Components adapted from the transport model of reactors described in [19]	24
2.2	Process rates of particulate components in the liquid phase $X_{S,m}$ and $X_{I,m}$ , and in the solid phase $X_{S,f}$ and $X_{I,f}$ (kg/m <sup>3</sup> ·s), adapted from [19]	25
2.3	Bacterial groups considered in CMW1 (adapted from Samsó [19]).	25
2.4	Stoichiometric matrix (adapted from [20, 19])	26
2.5	Reaction rates from CMW1 in $\rm kgm^{-3}s^{-1}$ (adapted from [20, 19])	27
2.6	Stoichiometric parameters related to organic matter and bacterial groups [20]	29
2.7	Composition parameters [20]	29
2.8	Stoichiometric factors $v_{5,i}$ related to ammoniacal nitrogen $S_{NH}$ and factor $v_{9,\text{lisi}}$ related to the production of $X_{S,f}$ [20]	30
2.9	Kinetic parameters at 20°C [20, 19]	30
3.1	Molar masses used for unit conversion in the biochemical model	69
3.2	COD fractionation adopted in the biochemical model	69
3.3	Initial concentrations of microbial groups	71

A.1	VF CW monitoring data: flow, saturation depth and effluent con-	
	centrations (sat/unsat) for COD, $NO_3$ -N and $NH_4$ -N 94	

## List of Figures

2.1	Representation of a Free Water Surface system [5]	5
2.2	Representation of a Horizontal Sub Surface Flow [5]	7
2.3	Representation of a Vertical Sub Surface Flow [5]	8
2.4	Porous media element crossed by a flow of speed V in the three directions	14
2.5	graphical representation of Darcy's experiment	15
2.6	Full filtration network diaphragm	16
2.7	Van Genuchten equations	18
2.8	Bacterial distribution representation [16]	22
2.9	Principal interactions between bacterial groups and substrate $[16]$ .	24
3.1	Blueprint of the site of the Constructed Wetland in Lesvos	37
3.2	Phragmites Australis	37
3.3	Transversal section of the VFSat	38
3.4	Blueprint of the VFSat	38
3.5	Typha latifolia	39
3.6	Iris pseudacorus	39

3.7	Carex spp	40
3.8	Scirpus lacustris	40
3.9	Transversal section of the VFInsat	41
3.10	Pumping section of the VFInsat	41
3.11	Blueprint of the VFInsat	42
3.12	Model geometry	51
3.13	Model geometry for the second hydraulic version	51
3.14	Material properties	52
3.15	Daily flowrate function	66
3.16	Q inlet for 6 days zoom	67
3.17	Total daily number of pulses	67
3.18	$f_oxy$	70
3.19	Solver configuration	72
3.20	Time stepping configuration	73
4.1	Series of inlet pulses for 30 days	76
4.2	Series of inlet pulses for 1 days	77
4.3	Flushes inflow verification	77
4.4	Effective saturation over one day	78
4.5	Liquid volume fraction over one flush for the first hydraulic simulation	79
4.6	Simulated oxygen concentrations in time for the first hydraulic simulation	81
4.7	Simulated NH4 concentrations in time for the first hydraulic simulation	81
4.8	Simulated NO3 concentrations in time for the first hydraulic simulation	82

4.9	Simulated COD concentrations in time for the first hydraulic simulation	82
4.10	Simulated COD concentrations in time for the second hydraulic simulation	83
4.11	Simulated NH4 concentrations in time for the second hydraulic simulation	84
4.12	Simulated NO3 concentrations in time for the second hydraulic simulation	84
4.13	Simulated O2 concentrations in time for the second hydraulic simulation	85
4.14	Simulated Xa concentrations in time for the second hydraulic simulation	85
4.15	Simulated Xh concentrations in time for the second hydraulic simulation	86
4.16	Simulated COD concentrations in profile for the second hydraulic simulation during the last flush	87
4.17	Simulated SNH concentrations in profile for the second hydraulic simulation during the first flush	87
4.18	Simulated SNO concentrations in profile for the second hydraulic simulation during the first flush	88
4.19	Simulated SO concentrations in profile for the second hydraulic simulation during the first flush	88
4.20	Daily mean OCR comparison between real and model data	89

## Acronyms

 $\mathbf{C}\mathbf{W}$ 

Constructed Wetland

VFCW

Vertical Flow Constructed wetland

**HFCW** 

Horizontal flow constructed wetland

COD

Chamical oxygen demand

### Chapter 1

### Introduction

Constructed Wetlands (CWs) consist of engineered ecosystems that aim to treat wastewater by replicating the natural process of wetland environments, in a sustainable way against traditional treatment systems as this alternative is: eco-friendly, low-energy and cost effective [1, 2]. This system is particularly utilized in rural or decentralized areas, where they are presented as a more feasible option, and commonly used in a vertical subsurface flow constructed wetland (VFCWs) configuration, as they are able to considerably remove organic matter and nutrients by maintaining at the same time a lower footprint [3]. These types of systems purify wastewater before it is returned to the environment based on a combination of physical filtration, microbial degradation and plant uptake.

Recent concern arises in the optimization of CWs, to ensure not only environmental compliance with regulations, but also to improve its long-term sustainability and efficiency. It has been identified that its performance is strongly influenced by interacting factors such as the hydraulic flow regime, the characteristics of the substrate, seasonal variations, and loading strategy. Particularly, a potential method to remove contaminants such as nitrogen and organic matter would be the recirculation of treated effluent back to the inlet. Nevertheless, this method lacks a complete understanding of how recirculation influences the system's behavior in the real world in full-scale systems.

This challenge is addressed by this thesis, assessing the knowledge gap with the development of a numerical model of a VFCWs that treats blackwater in the island of Lesvos, Greece. The model, was developed using COMSOL Multiphysics ®, incorporating Richards' equation for the simulation of unsaturated flow and biopore-based reaction scheme for the biochemical processes. Using real data,

hydraulic conductivity and the removal efficiency of key pollutants, the goal is to assess the impact of strategies of recirculation on the performance of the treatment and to establish a basis for optimization of the operations.

### Chapter 2

### State of the Art

#### 2.1 Problem Statement

CWs have gained popularity in recent times to be used as sustainable solutions for decentralized water treatment, particularly in rural areas or small communities in which the use of conventional systems is ineffective or infeasible. These systems are a nature-based approach to purify water by combining physical, chemical and biological processes happening in both saturated and unsaturated zones. For this solution, it is fundamental to comprehend the behavior of pollutants such as carbon and nitrogen compounds during treatment cycles, in order to guarantee that effluent water quality follows environmental discharge regulations and standards, specifically when being discharged into more sensitive ecosystems such as rivers.

This study focuses on the evaluation of both the hydraulic and biochemical performance of a real-life vertical flow-built wetland in charge of blackwater treatment in Lesvos, Greece. The main goal was to quantify how efficiently the system is able to remove chemical oxygen demand (COD), ammonium and nitrates through a single treatment cycle. Additionally, it was possible to quantify how recirculation strategies would be able to enhance the removal of these pollutants.

Due to the continuous monitoring of the existing system during the past three years, there is enough data for the calibration and validation of a model. Nevertheless, its complexity is given by the absence of defined relationships between the quantity of recirculation events and the consequent effluent quality, leading to difficulties in getting proper prediction of the behavior of the system without using extensive manual testing or simulation. Therefore, to approach this challenge, a numerical

model was developed with the use of the software COMSOL Multiphysics ®, applying Richard's equation for the simulation of unsaturated flow, along with a biopore-based approach for the representation of biochemical reactions. Real operation data will therefore be used for the calibration of the model in order to assess the effects of varying recirculation strategies on contaminant removal and hydraulic connectivity. In such way, this work contributes to an optimized operation of CWs through a model-based decision support, guaranteeing both environmental compliance and an efficient system.

## 2.2 Theoretical Framework: Constructed Wetlands

#### 2.2.1 Basic concepts

As previously introduced, CWs are an engineering system that stimulate and the natural water cleansing process in a controlled way. This is a nature-based approach as it occurs naturally in humid and swampy environments, therefore its usually referred to as "artificial wetland".

Among the advantages that this water cleansing method offers is resource efficiency, as it operates under low-energy demand, requires low human intervention for its maintenance, and relatively low cost of construction in comparison to traditional treatment plants.

In such way, artificial wetlands are specially well suited for more remote locations where space is limited and financial resources are scarce as is the case of smaller communities in mountains, islands, or regions with limited economic resources being low-cost and low-impact, and allowing for wastewater to be reused for irrigation or sanitation purposes.

#### 2.2.2 Key treatment mechanisms

CWs are typically built as an underground, impermeable basin filled in with porous mineral layers of different grain sizes. Then, wastewater is introduced through a feeding system, while drainage network at the bottom collects and discharges the treated effluent. On the bed's surface, usually at ground level, aquatic macrophytes al planted, which are wetland plants that are naturally adapted to marshy ecosystems, and have a fundamental participation in nutrient

cycling, and especially contribute to nitrogen transformation within the system.

#### 2.2.3 Types of constructed wetland

Several Types of constructed wetland may be designed, including free water surface, subsurface flow, horizontal subsurface flow, and vertical subsurface flow.

1. Free water surface (FWS) Wetland- This type of wetland is designed to imitate natural marshals. They are built in sealed basins with shallow water, at a shallow depth of 0.3 to 0.6m, that stays in direct contact with the atmosphere [1]. The movement of water is slowed down and guided through an inlet zone and moves across the wetland surface, to finally exit through one or more outlet areas. This process of slow flow velocities happens thanks to a network of micro-channels, created by a combination of shallow regions and dense vegetation. It is fundamental for a design that keeps wastewater in contact with biologically active surfaces to have adequate hydraulic retention times and lower risk of hydraulic short-circuiting, [3].

The plants used in FWS wetlands are usually native marsh species, where an emergent species dominates, or there's a combination with submerged plants. By having an adequate planting strategy, it's possible for portions of the water surface to stay exposed to the atmosphere, which allows for oxygen transfer and a process known as nitrification, needed for nitrogen removal. Common species include rushes, water lilies and duckweed [4]:

- Emergent macrophytes such as rushes (*Juncus* spp.) and reed canary grass (*Glyceria maxima*);
- Submerged species like water milfoil (Myriophyllum spicatum);
- Floating plants such as white-water lily (Nymphaea alba);
- Pleustophyte such as duckweed (*Lemna* spp.) is also frequently used. Even if it covers the water surface, it has a high nutrient uptake capacity, and a significant contribution to water purification.



Figure 2.1: Representation of a Free Water Surface system [5]

FWS wetlands are known for their capacity to remove a wide range of pollutants. For instance, this type of wetlands uses oxygen-rich (aerobic) processes near the surface, and instead, for deeper areas, use low-oxygen (anoxic) processes to break down organic matter and nitrogen, helping in this way the reduction of biochemical oxygen demand (BOD). They may also remove suspended solids through the slow water flow and dense plants that cause particles to settle and then be filtered. Plants themselves may also absorb and store both nutrients and heavy metals, meaning they are removed from the water. Finally, micropollutants and pathogens or disease-causing organisms may be potentially removed based on specific environmental conditions. [1].

2. Subsurface Flow (SSF) Wetlands- This type of treatment system is composed of impermeabilized basins where wastewater flows through a porous substrate or fill material with a high hydraulic conductivity so that water properly moves such as gravel, sand or other natural soil. This material not only guarantees water movement but is also the physical medium that anchors the root systems of emergent macrophytes, and a vast surface area for microbial biofilm growth. Many of the purification processes actually happen thanks to these microorganisms, for instance degradation of organic matter and transformation of nutrients.[1].

One of the major benefits of SSF wetlands is that they have larger contact area provided to microbial communities in comparison FWS. Given this, bacteria have a greater surface area to colonize on the fill material and therefore become more effective at removing pollutants since biofilm activity is more intense. This allows for SSF wetlands to be built on a smaller footprint or a more compact form, saving space in comparison to FWS systems for the same level of treatment [4]. Additionally, since the wastewater flows beneath the surface, this kind of system reduces issues like odor generation, mosquitoes, or direct human exposure, increasing in this way a better option for populated areas in peri-urban or rural communities.

There's two possible configurations of SSF wetlands according to the movement of water. Usually, the two designs are combined in a hybrid system for a more optimal treatment performance. The configurations are:[3].

- Horizontal subsurface flow (HSSF): in this case wastewater flows sideways through the substrate from the inlet to the outlet. This system is particularly useful for removing organic matter and suspended soil.
- Vertical subsurface flow (VSSF): in this system water is added intermittently from the top and filters down vertically through unsaturated and saturated zones before being collected in the bottom. This process has an

additional benefit as it helps with oxygen transfer, making it better at removing nitrogen through nitrification processes.

Horizontal Subsurface Flow(HSSF) As previously introduced, HSSF wetlands are made of sealed impermeabilized basins, usually lined with plastic geomembranes, and filled with porous material of suitable grain size [1]. Wastewater moves laterally through the saturated bed, generally following a plug-flow regime. To facilitate movement from the inlet to the outlet, a slight slope of 1% is usually present at the bottom of the bed, often achieved by placing a sand layer below the liner. Vegetation commonly used includes emergent rooted macrophytes such as common reed (Phragmites australis), cattail (Typha minima), and rushes (Juncus spp.), which not only provide hydraulic regulation but also come with several ecological benefits [6].

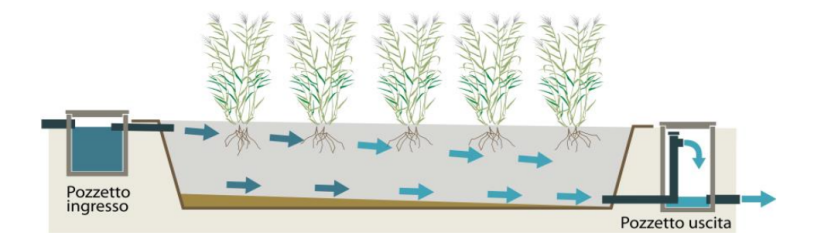


Figure 2.2: Representation of a Horizontal Sub Surface Flow [5]

As in HHSF wetlands the water level stays below the surface of the substrate, the treatment environment is predominantly without oxygen but still has numerous aerobic micro zones around plant root systems, since the macrophytes exchange oxygen from the atmosphere into the rhizosphere. This transfer leads to an enhanced oxidative capacity of the filler material improving the process of degradation of pollutants.

Microbial communities colonizing the substrate are key for this treatment process as follows: [3].

- Aerobic bacteria that are around support the oxidation and nitrification of organic matter.
- Anaerobic and anoxic bacteria contribute to denitrification and efficient transformation of organic matter and nitrogenous compounds.

Additionally, the treatment performance is further enhanced by the porous medium which contributes by itself to remove pollutants and absorb phosphorus and heavy metals.

These systems present multiple advantages. Thanks to the coexistence of various redox conditions within a single system along with plant-microbe interactions, HSSF wetlands effectively treat a wide range of types of wastewaters and of pollutant loads. This makes this type of system very robust, making them suitable for various climatic conditions due to the fact that the thermal mass of the substrate protects against seasonal temperature variations. This leads to HSSF being very versatile and reliable and capable of providing stable performance in any environment.

Vertical Subsurface Flow (VSSF) They consist of impermeabilized basins filled with porous material of appropriate grain size, in this case, usually coarse sand. Vegetation, like in the case of HSSF, also usually includes emergent rooted macrophytes, such as Phragmites australis and Juncus spp. In this system, wastewater is introduced intermittently at the surface, and it percolates vertically through the filler material under alternative saturated and unsaturated conditions, which is a similar behavior to a type of batch reactor.[1, 3].

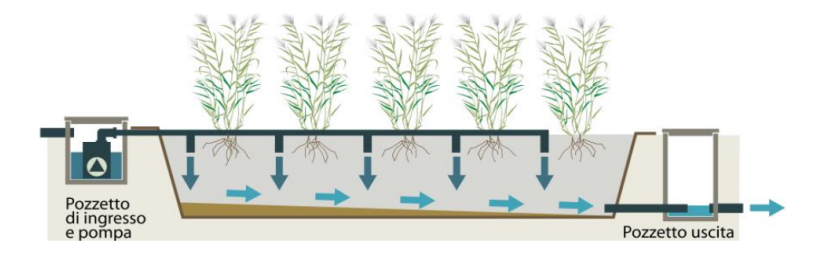


Figure 2.3: Representation of a Vertical Sub Surface Flow [5]

The filler medium in VSSF requires a finer material than HSSF, in order to ensure a slower vertical filtration and a more uniform distribution of influent within the substrate, this is why coarse sand is commonly used, as its properties allow for both suitable hydraulics conductivity and effective pollutant filtration. [7].

A key aspect of VSSF systems is its feeding strategy, as wastewater is supplied intermittently, meaning it is alternating between filling and draining phases in function of either a time distribution device or self-priming siphons. In practice, two parallel beds often operate alternately for enough re-aeration between cycles. This type of method, in which loading is not continuous, allows for an enhancement of the oxygen transfer within the substrate and stimulates the development of aerobic microbial populations, and therefore improve the removal of both organic matter and nitrogen [1]. Nevertheless, for long-term operations is fundamental to

have carful monitoring of the clogging processes within the filter material, as an excessive deposition at the bed surface may create stagnant layers, which limit the diffusion of oxygen from the atmosphere, inhibiting the nitrification and other aerobic processes. In order to prevent this, the design and operation of VSSF wetlands has to consider hydraulic loading rates and the frequency of dosing to maintain a sustainable treatment performance over time. [7].

#### 2.2.4 Applications

Constructed wetlands are designed to improve wastewater quality through the removal a a wide range of pollutants, among the list, there are suspended soils, organic matter, nutrients, and fecal bacteria. They can also help in the removal or less predominant but still environmentally important contaminants like heavy metals, pharmaceuticals, surfactants and other cleaning and personal care products that are present in waste water [1, 3]. Even though they have many advantages, they still carry many challenges, one of the most important ones is that in the long term operation of the Subsurface flow constructed wetlands (SSCW) there tends to be clogging in the porous medium. This process reduces the infiltration capacity of the substrate, and therefore limits the percolation of water, compromising the performance and results of the treatment [8].

Clogging can happen due to multiple causes, one of them might be the accumulation of suspended soils that are contained in the influent, the creation of biofilm due to bacterial and fungal growth, the formation of chemical precipitates, or the expansion of plant roots within the substrate. When talking about this causes, suspended soils tend to be identified as the most critical factor, this happens because they can block pore spaces and granular interstices, progressively reducing the hydraulic conductivity [9, 3].

To mitigate this problem, one of the recommendations is to pretreat wastewater before entering the wetland. Pretreatment processes have the goal of reducing the load of suspended soils and organic matter, therefore minimizing the risk of clogging and ensuring long-term sustainability and system efficiently. Pretreatment combined with an appropriate design, operational strategy and good management can amplify the lifespan of the subsurface flow wetland while maintaining the removal efficiency [10].

#### 2.2.5 Contaminant Removal Processes

In wastewater treatment systems, generally purification occurs through two fundamental mechanics, the first one is the physical separation of solids from the liquid phase, and the second one is the degradation or transformations of chemical compounds present in the effluent. Constructed wetlands work as a fixed-bed bioreactors in which wastewater goes through the porous medium that is colonized by plants and microorganisms. Within this environment, pollutants and organic matter are removed by the combination of biological, chemical and physical processes. While the physical and chemical mechanisms play the biggest role in the contaminant removal, biological transformations still play a decisive role in determining the long-term efficiency of this type of system [1, 3].

#### Particulate Organic Matter (POM)

The presences of POM in the inflow can compromise the performance of CWs. As wastewater percolates though the porous substrate, particles are kept by the physical and chemical interactions with the granular medium, leading to gradual accumulation. This happens because of the mechanisms, like particle impaction on grain surfaces, low percolation velocities, changes in the trajectory within pore species, and surface interaction forces. Resulting in a tendency for POM to concentrate near the inlet zone of the wetland, while progressing removal happening along the length of the bed [11]. In the long-term, excessive accumulation may contribute to clogging of the porous medium and reduce hydraulic conductivity.

#### Hydrolysis

The following process occurs once POM is trapped, it undergoes hydrolysis, during this process, complex particulate material is broken down into dissolved organic compounds (DOM). This process is driven by enzymatic and microbial activity, that can happen under aerobic, anoxic and anaerobic conditions [11]. Therefore, hydrolysis represents a crucial step in the transformation of particulate matter into soluble substrate that can be further metabolized in following biochemical steps.

#### Aerobic Respiration

Dissolved organic matter, both the one already present in the wastewater or the one produced through the hydrolysis, is primarily degraded by this process, it is mediated by heterotrophic bacteria that utilize oxygen as the terminal electron acceptor. Oxygen availability within the wetland substrate is therefore a determining factor for treatment quality [12, 13]. Besides respiration, there are other aerobic biochemical reactions that can contribute to the reduction of organic matter, helping to further stabilize the waste water before discharge.

#### Denitrification

Denitrification is the microbial reduction of oxidized nitrogen species ( $NO_3^-$ ,  $NO_2^-$ ) into  $N_2$ . This process joins the carbon and nitrogen cycles, this happens because denitrifying bacteria requires both an organic carbon source and electron acceptors provided by nitrogen oxides. Denitrification happens mainly under anoxic conditions, that is when oxygen is low and the bacteria switch from oxygen to nitrate or nitrate for respiration. Facultative heterotrophs do this process, always preferring oxygen when available but carrying on with nitrogen when the environment oxygen availability is scarce or null.

#### Nitrification

Is an aerobic process performed by autotrophic bacteria. During this process, ammonium  $(NH_4^+)$  and ammonia  $(NH_3)$  are oxidised to nitrite and later to nitrate. It usually occurs in two steps: the first one is called *Nitrosomonas* spp, which oxidizes ammonium into nitrite, the second one is called *Nitrobacter* spp. and converts nitrite into nitrate. The nitrate produced in the reaction will later serve for denitrification of the substrate [1].

#### **Fermentation**

In conditions in which there is an oxygen limitation, soluble organic compounds are generated that were generated by hydrolysis can undergo fermentation. Anaerobic heterotrophic bacteria converts these substrates into short-chain fatty acids, that go together with the release of carbon dioxide. Fermentation is a very important process in strictly anaerobic parts of the CW, because it provides intermediate

products such as acetate and lactate that feed into other anaerobic processes, including both methanogenesis and sulfate reduction.

#### Phosphorus Removal

Phosphorus is present in wastewater in both organic and inorganic form, its removal can happen through adsorption and precipitation, and also by biological uptake. Phosphorus-accumulating organisms (PAOs), like Acinetobacter spp., store the phosphorus as an intercellular polyphosphate. When it is exposed to the alternation between aerobic and anaerobic conditions, these bacteria accumulates phosphorus beyond their metabolic requirements, leading to the reduction of the overall phosphorus concentration in the outflow.

#### **Sulfate Reduction**

Sulfate  $(SO_4^{2-})$  can fill the propuse of electron acceptor for sulfate reducing bacteria, that is in charge of the metabolization fermentation products, like acetate, lactate or butyrate. These microorganisms produce hydrogen sulfide  $(H_2S)$  as a by-product, which may inhibit plant growth while it contributes to organic matter degradation [14].

#### Methanogenesis

Is a process carried out strictly only by anaerobic arches that convert hydrogen, carbon dioxide and simple organic into methane. This process prevents the accumulation of fermentation intermediates in anaerobic zones. The process sometimes also coexists with sulphate reduction, but how it balances depends on the COD to sulfate ratio, creating two scenarios, when it is low, sulfate reducers dominate, on the contrary, when it is high, mathanogens dominate [14].

#### 2.3 Numerical Framework

#### 2.3.1 Numerical Framework for Flow in Porous Media

In variably saturated porous media, like the soils that are used for constructed wetlands, water movements happens in laminar flow conditions given that there are very slow velocities that get imposed by the pore structure. This flow can happen both under saturated or unsaturated conditions depending on the position of the water table. The functions that govern the water particle motion are among others: gravity, viscous resistance, adhesion, cohesion, and in the case of unsaturated media, capillarity. When the last one rises, it produces a fringe above the water table where pore water pressures are negative, leading to partially saturated conditions [15]

#### **Continuity Equation**

The continuity principle establishes that the difference between inflow and outflow water that go through an element of volume soil, equals the variation of water that is stored in the volume over time.

$$Q_e - Q_u = \frac{\partial P_w}{\partial t},\tag{2.1}$$

where  $Q_e$  and  $Q_u$  are inflow and outflow water weights and Pw is the water weight in the soil element. When velocity gets induced and there is a simplification, the differential form of the equation is:

$$-\gamma_w \left( \frac{\partial V_x}{\partial x} + \frac{\partial V_y}{\partial y} + \frac{\partial V_z}{\partial z} \right) dx \, dy \, dz = \frac{\partial P_w}{\partial t}, \tag{2.2}$$

with  $\gamma_w$  the specific weight of water and  $V_i$  the filtration velocities. In steady conditions,  $\partial P_w/\partial t = 0$ , recovering the mass conservation principle.

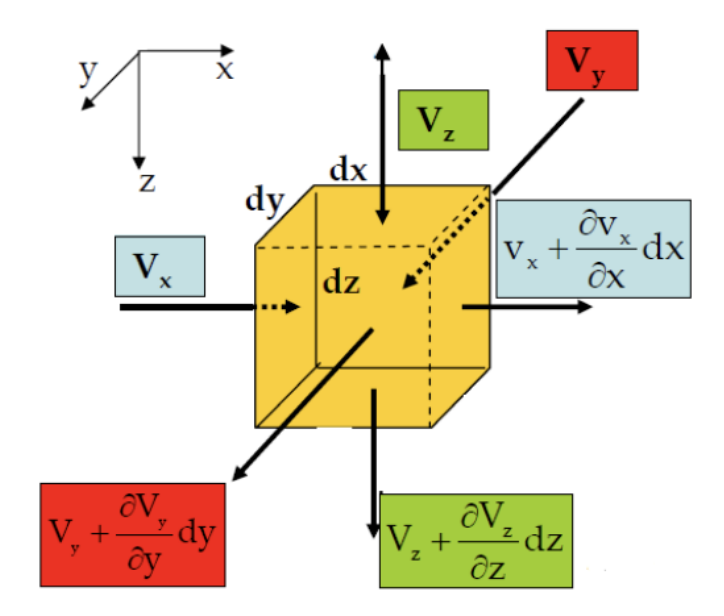


**Figure 2.4:** Porous media element crossed by a flow of speed V in the three directions

#### Darcy's Law

The experiments Darcy performed in 1856 established the empirical law:

$$Q = VA = KA \frac{\Delta h}{L},\tag{2.3}$$

where Q is discharge, K hydraulic conductivity,  $\Delta h$  hydraulic head drop, L sample length, and A cross-sectional area. In differential form:

$$q = -K\frac{dH}{dl},\tag{2.4}$$

with q specific discharge and H hydraulic head. Conductivity depends both on fluid and porous medium properties, and can be written as:

$$K = \frac{k\gamma}{\mu},\tag{2.5}$$

where k is intrinsic permeability,  $\gamma = \rho g$  the specific weight of the fluid, and  $\mu$  its viscosity.

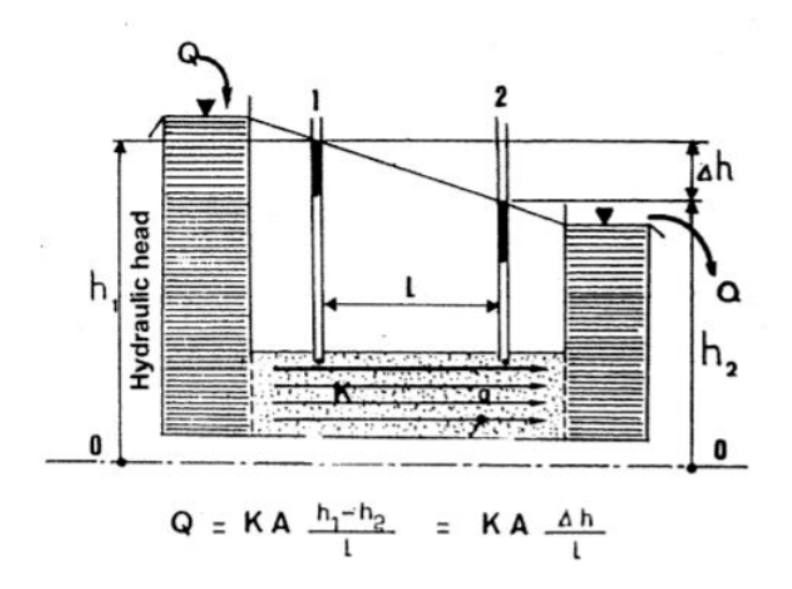


Figure 2.5: graphical representation of Darcy's experiment

#### General Flow Equation

When combining the continuity equation with Darcy's law in the case for homogeneous isotropic medium leads to:

$$K_x \frac{\partial^2 h}{\partial x^2} + K_y \frac{\partial^2 h}{\partial y^2} + K_z \frac{\partial^2 h}{\partial z^2} = \frac{1}{1+e} \left( e \frac{\partial S_r}{\partial t} + S_r \frac{\partial e}{\partial t} \right), \tag{2.6}$$

where h is piezometric head,  $S_r$  the degree of saturation and e the void ratio.

The general flow equation through porous medium is represented by the previous expression and in it special cases can be simplified:

- Permanent flow: e and  $S_r$  constant
- Consolidation: e variable and  $S_r$  constant
- Drainage / inhibition:  $S_r$  variable and e constant
- Combinations of them

#### Laplace Equation

Assuming steady flow, isotropy and constant porosity / saturation, the flow equation can get reduced to the Laplace form:

$$\frac{\partial^2 h}{\partial x^2} + \frac{\partial^2 h}{\partial y^2} + \frac{\partial^2 h}{\partial z^2} = 0. {(2.7)}$$

Which in two dimensions can be written as:

$$\frac{\partial^2 h}{\partial x^2} + \frac{\partial^2 h}{\partial z^2} = 0. {(2.8)}$$

The mathematical basis for flow nets is based on this equation, and it provides the numerical solution for them.

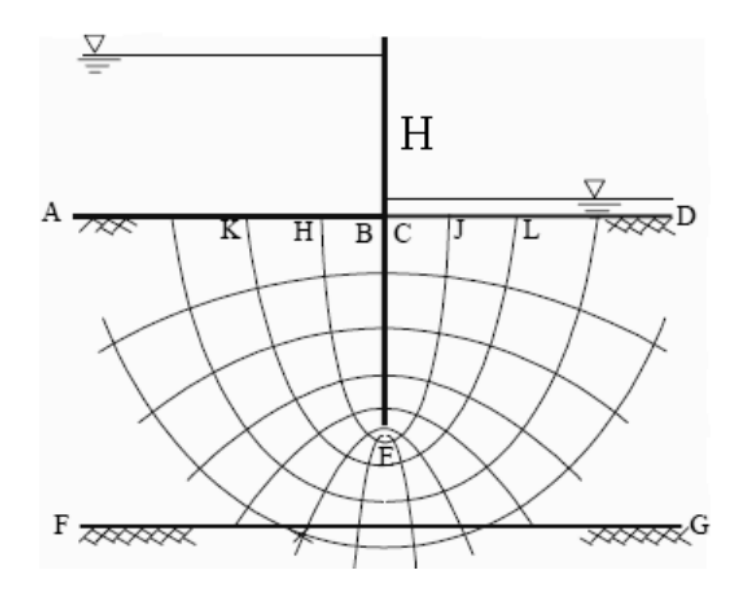


Figure 2.6: Full filtration network diaphragm

#### **Richards Equation**

With the purpose of understanding soils, and extending into Darcy's law, the evaluation of hydraulic conductivity becomes very important. Hydraulic conductivity depends on water content  $\vartheta$ :  $K = K(\vartheta)$ . Therefore, in terms of water content a

general continuity equation can be built, leading to Richard's equation.

$$\frac{\partial \vartheta}{\partial t} = \frac{\partial}{\partial z} \left( D \frac{\partial \vartheta}{\partial z} - K \right), \tag{2.9}$$

where  $D = K \partial \psi / \partial \vartheta$  is the hydraulic diffusivity and  $\psi$  the suction head.

Therefore, in terms of water content a general continuity equation can be built, leading to Richard's equation.

#### **COMSOL** Formulation

During the development of this work, the Richard's equation was used inside of the software COMSOL Multiphysics, which implements a pressure-based mixed formulations:

$$Q_m = \rho \left( \frac{C_m}{\rho g} + S_e S \right) \frac{\partial p}{\partial t} + \nabla \cdot \rho \left( -\frac{K_s}{\mu} K_r \left( \nabla p + \rho g \nabla D \right) \right), \qquad (2.10)$$

where:

- p is pore pressure
- $\rho$  fluid density
- q gravity
- $C_m$  specific moisture capacity
- $S_e$  effective saturation
- S storage coefficient
- $K_s$  saturated permeability
- $K_r$  relative permeability
- $K_r$  relative permeability
- $\mu$  dynamic viscosity
- D elevation
- $Q_m$  volumetric source/sink

The hydraulic part of the model formulated for this work has the same numerical framework that was explained.

#### Van Genuchten Relations

Whenever there are unsaturated conditions, the water content parameter chages the hydraulic properties at that point in time, the ones that change are  $\vartheta$ ,  $S_e$ ,  $C_m$ , and  $K_r$ .

In the Van Genuchten equations, the terrain situation is defined when the pressure in the fluid is the atmospheric pressure,

$$Hp = \frac{p}{pg} \tag{2.11}$$

The equations mentioned are as the following one:

$$\begin{split} \theta &= \begin{cases} \theta_{\mathrm{r}} + \mathrm{Se}(\theta_{\mathrm{s}} - \theta_{\mathrm{r}}) & H_{p} < 0 \\ \theta_{\mathrm{s}} & H_{p} \geq 0 \end{cases} \\ \mathrm{Se} &= \begin{cases} \frac{1}{\left[1 + \left|\alpha H_{p}\right|^{n}\right]^{m}} & H_{p} < 0 \\ H_{p} \geq 0 \end{cases} \\ C_{\mathrm{m}} &= \begin{cases} \frac{\alpha m}{1 - m} (\theta_{\mathrm{s}} - \theta_{\mathrm{r}}) \mathrm{Se}^{\frac{1}{m}} \left(1 - \mathrm{Se}^{\frac{1}{m}}\right)^{m} & H_{p} < 0 \\ H_{p} \geq 0 \end{cases} \\ k_{\mathrm{r}} &= \begin{cases} \mathrm{Se}^{l} \left[1 - \left(1 - \mathrm{Se}^{\frac{1}{m}}\right)^{m}\right]^{2} & H_{p} < 0 \\ H_{p} \geq 0 \end{cases} \end{split}$$

Figure 2.7: Van Genuchten equations

In order to use these equations some parameters are necessary, those parameters can be obtained from experimental work. The mentioned parameters are a, n, l

and

$$m = 1 - \frac{1}{n}.$$

And hydraulic pressure is

$$H_p = \frac{\sqrt[n]{\left(\sqrt[n]{\frac{1}{S_e}} - 1\right)}}{\sqrt[n]{\alpha}} \tag{2.12}$$

# 2.3.2 Numerical Framework of the BIO PORE Model

The model implemented for the biochemical part of the present work is called BIO\_PORE, The model was originally formulated by Samsó and García [16, 17], and it is process based model that was originally conceived to describe biochemical interactions inside horizontal subsurface flow constructed wetland (HSSF-CWs). Even though the framework of this model was a horizontal flow model, the present work has beed adapted and implemented for a vertical flow constructed wetland (VF-CW) that is operating under variably unsaturated conditions. In order to do so, it was very important to reinterpret the boundary conditions and the hydraulic formulation without changing the biokinetic structure.

#### **Definitions**

The components that were used in the model can be divided into mainly two categories, soluble which are denotated as Ss, and particulate that are denotated as  $X_x$ . Usually, microorganisms belong to the solid part and are reperesnted by the bacterial groups. In the following section there are the definitions of each of the eight soluble, ten particulate and seventeen processes that govern the phenomena inside the CW and at the end there are the summary tables with all the formulas and parameters implemented in the original Samsó and Gracía [16] and where explained in the work of Santelia [18].

#### Dissolved Components $S_s$

1.  $SO \rightarrow$  dissolved oxygen  $O_2$  [M( $O_2$ )/L<sup>3</sup>] Represents the dissolved oxygen inside the CW that is subject to the gas exchange that happens with the atmosphere. This quantity can be directly measured.

- 2. **SF**  $\rightarrow$  soluble, fermentable COD fraction, readily biodegradable [M(COD)/L<sup>3</sup>]. This fraction of COD is immediately available for biodegradation, as is the case for the growth of heterotrophic bacteria  $(X_H)$  and fermenting bacteria  $(X_{FB})$ . This fraction is mainly produced by hydrolysis and to a lower scale to bacterial lysis.
- 3. **SA**  $\rightarrow$  soluble acetate COD fraction [M(COD)/L<sup>3</sup>] In this fraction all fermentation products are considered completely acetate. SA is consumed during anoxic and aerobic growth of heterotrophs  $(X_H)$  and also during anaerobic growth of acetotrophic methanogens  $(X_{AMB})$ .
- 4.  $SI \rightarrow$  inert soluble COD fraction [M(COD)/L<sup>3</sup>] This soluble component cannot be further degraded during treatment. The particle is created by hydrolysis and is treated as part of the incoming organic matter.
- 5.  $\mathbf{SNH} \to \text{ammoniacal nitrogen (NH}_4^+ \text{ and NH}_3\text{-N) [M(N)/L}^3]$  This soluble component represents all ammoniacal species in the CW (NH}\_4^+\text{-N and NH}\_3\text{-N)}. It is produced by biomass reduction and hydrolysis, and at the same time, it is consumed by nitrification and microbial assimilation during growth.
- 6. **SNO**  $\rightarrow$  nitrites and nitrates (NO<sub>2</sub><sup>-</sup> and NO<sub>3</sub><sup>-</sup>-N) [M(N)/L<sup>3</sup>] Both oxygen containing compounds are included even though only nitrates are considered in stoichiometric calculations. This compounds are produced by nitrification and consumed by anoxic growth of heterotropghs ( $X_H$ ) and sulfide-oxidizing bacteria ( $X_{SOB}$ ) produce sulfate.
- 7.  $SSO_4 \rightarrow sulfate [M(S)/L^3]$  This compound represents sulfur in oxidized form. In order to oxide acetate, the acetotrophic sulfate-reducing bacteria  $(X_{ASRB})$  uses sulfate as electro acceptor, while aerobic and anoxic growth of sulfide-oxidizing bacteria  $(X_{SOB})$  produce sulfate.
- 8.  $\mathbf{SH}_2\mathbf{S} \to \text{hydrogen sulfide } [\mathrm{M}(\mathrm{S})/\mathrm{L}^3]$  This compound is considered as a sulfur species and is subjected to gas exchange. It has two process, it gets consumed by sulfide oxidizing bacteria  $(X_{SOB})$  to regenerate sulfate and at the same time it is produced by sulfate reduction. In the case of high concentrations,  $\mathrm{SH}_2\mathrm{S}$  can be toxic for the bacterial populations in the wetland.

### Particulate Components $X_x$ [18]

9. **XS**  $\rightarrow$  slowly biodegradable COD particles [M(COD)/L<sup>3</sup>] In the BIO\_PORE model there is a distinction between (XS, f) in aqueous phase and solid phase. (XS, m) represents the part of COD that requires hydrolysis before degradation.

It is mainly generated by bacterial death, when the biodegradable parts of the cells are released. In any case, the fraction is consumed by heterotrophs  $(X_H)$  through hydrolysis.

- 10.  $XI \rightarrow$  inert COD particles [M(COD)/L<sup>3</sup>] In the same way as XS, BIO\_PORE also breaks into aqueous and solid. The solid part cannot be degraded by the system and it can be assumed to remain in the pores until removed by higher flows. This solid part is produced by bacterial death but in a much smaller proportion in comparison to the solid fraction of XS.
- 11.  $\mathbf{XH} \to \text{heterotrophic bacteria } [M(COD)/L^3]$  These types of bacteria are in charge of hydrolysis, aerobic mineralization of organic matter, and anoxic denitrification.
- 12.  $\mathbf{XA} \to \text{autotrophic nitrifying bacteria } [M(COD)/L^3]$  These types of microorganisms are in charge of nitrification, a process in which SNH is assumed to be directly converted into SNO, meanwhile, nitrites are not really considered intermediate products.
- 13. **XFB**  $\rightarrow$  fermenting bacteria [M(COD)/L<sup>3</sup>] Anaerobic microorganisms that consume SF to produce acetate SA.
- 14. **XAMB**  $\rightarrow$  acetotrophic methanogenic bacteria [M(COD)/L<sup>3</sup>] They are anaerobic microorganisms that consume acetate SA to produce methane CH<sub>4</sub>, and this in not exactly considered in the model.
- 15. **XASRB**  $\rightarrow$  acetotrophic sulfate-reducing bacteria [M(COD)/L<sup>3</sup>] Using sulfate SSO<sub>4</sub> as an electro acceptor during the oxidation of acetate SA, anaerobic organisms produce SH<sub>2</sub>S.
- 16. **XSOB**  $\rightarrow$  sulfide-oxidizing bacteria [M(COD)/L<sup>3</sup>] Chemolithautotrophs that use either dissolved oxygen SO or nitrate/nitrite SNO to oxidize SH<sub>2</sub>S into sulfate SSO<sub>4</sub>.

In figure 2.8, it is possible to see a schematic representation of the distribution of bacterial groups in the longitudinal direction of the CW.

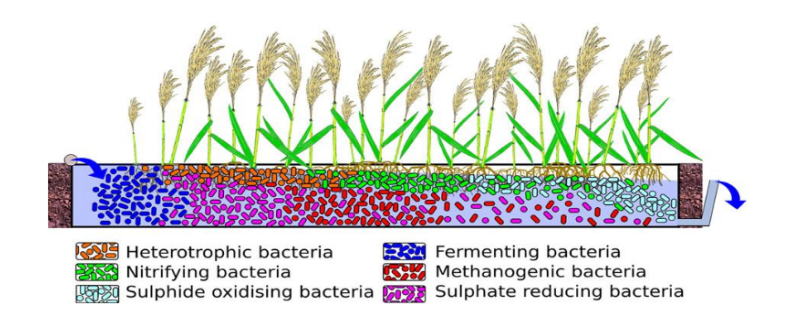


Figure 2.8: Bacterial distribution representation [16]

#### **Processes**

According to Santelia [18], the main biochemical processes that were included in the BIO\_PORE model are summarized into:

- 1. **Hydrolysis** This process changes the slowly biodegradable particulate matter XS and makes it readily fermentable soluble COD (SF), and to a smaller portion, into inert soluble COD SI. Particularly, in this model, the production of SI through hydrolysis is neglected. Nevertheless, the reaction takes place even without the presence of oxygen SO, and releases ammoniacal nitrogen SNH as well. This process is mainly driven by heterotrophic bacteria  $X_H$  and in a smaller proportion, fermenting bacteria  $X_{FB}$ , this last one acts more slowly and that factor is taken into account by the  $\eta_H$  factor.
- 2. Aerobic growth of  $X_H$  on SF In this process, heterotrophic bacteria mineralizes organic matter by consuming the fraction of COD ready to be degrated SF. At the same time, oxygen SO serves as electron acceptor and SNH is assimilated into biomass.
- 3. Anoxic growth of  $X_H$  on SF In this process, under anoxic conditions, XH consumes the faction of COD ready to be degraded SF while expending nitrites and nitrates SNO as electron acceptors. This process represents the denitrification because SNH is once more assimilated into biomass.
- 4. **Aerobic growth of**  $X_H$  **on** SA This process is quite similar to process 2 but instead of SF, SA gets degraded with oxygen as the terminal electron acceptor.
- 5. Anoxic growth of  $X_H$  on SA This process is quite similar to process 3 but instead of SF, SA replaces SF as carbon source.

- 6. Aerobic growth of XA on SNH This is the main nitrification step, in it, ammoniacal nitrogen SNH is oxidized in the presence of oxygen SO to produce nitrites and nitrates SNO. In this process, a small part of SNH is assimilated into biomass at the same time.
- 7. Growth of  $X_{FB}$  In this process the fermenting bacteria  $X_{FB}$  gorws anaerobically by consuming SF, and at the same time it produces acetate SA and incorporates SNH into their biomass.
- 8. Growth of  $X_{AMB}$  In this process, acetotrophic methanogens  $X_{AMB}$  grow under anaerobic conditions, while consuming acetate SA and assimilating ammoniacal nitrogen SNH. On the other hand, methane  $CH_4$  is also generated through this process, but this part is not explicitly considered in this model.
- 9. **Growth of**  $X_{ASRB}$  In this process, acetotrophic sulfate-reducing bacteria  $X_{ASRB}$  operates under anaerobic conditions, in it, they use sulfate SSO<sub>4</sub> as electron acceptor while oxidizing acetate SA, which results in the creation of hydrogen sulfide SH<sub>2</sub>S and at the same time assimilating SNH into biomass.
- 10. Aerobic growth of  $X_{SOB}$  on  $SH_2S$  this process is the reverse process of 9, in this case sulfide oxidizing bacteria  $X_{SOB}$  consumes both oxygen SO and hydrogen sulfide  $SH_2S$ , which ends up in the production of sulfate  $SSO_4$  and the assimilation of SNH.
- 11. Anoxic growth of  $X_{SOB}$  on  $SH_2S$  This process assimilates to process 10, but differing to that one, it occurs under anoxic conditions, so in this case SNO replaces oxygen as the electron acceptor in the oxidation of  $SH_2S$ .
- 12. Bacterial lysis (processes 6, 8, 10, 12, 14, 17) The processes of lysis represent the decay of microbial populations across all bacterial groups. These processes generate important amounts of slowly biodegradable COD XS, smaller quantities of inert particles XI, and traces of readily biodegradable COD SF. At the same time ammoniacal nitrogen SNH also gets released.

In order to illustrate the interactions between the substances in the wetland, Figure 2.9 explains schematically the cycle of carbon, nitrogen and sulfur. In this diagram, the incoming compounds enter from the top, while oxygen SO enters the system through passive diffusion from the atmosphere and through the root release from microphytes. Both inert fractions XI soluble and particulate, and SI are not degraded or transformed and therefore do not appear in the schematic. The components that have an asterisk besides them are not included or taken into account in the model.

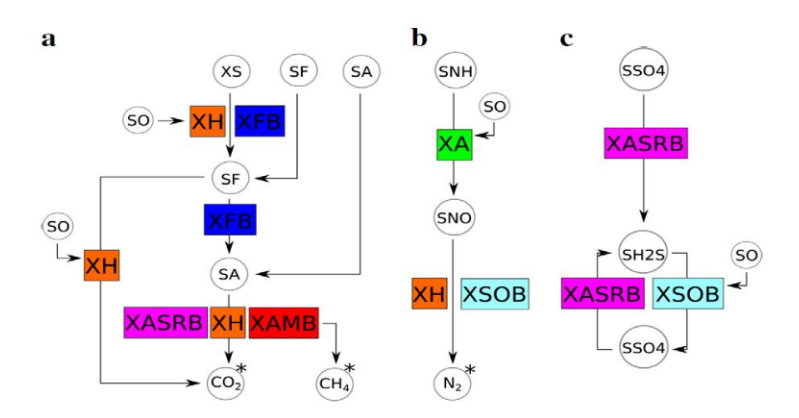


Figure 2.9: Principal interactions between bacterial groups and substrate [16]

# Model equations

The following equations were used from the model implemented by Santelia [18]:

**Table 2.1:** Components adapted from the transport model of reactors described in [19].

Component	Unit	Phase	Description
$S_O$	$mg O_2/l$	Aqueous	Dissolved oxygen
$S_F$	mg COD/l	Aqueous	Fermentable soluble COD fraction
$S_A$	mg COD/l	Aqueous	Soluble acetate COD fraction
$S_I$	mg COD/l	Aqueous	Inert soluble COD fraction
$X_{S,m}$	mg COD/l	Aqueous	Slowly biodegradable soluble COD par-
			ticles
$X_{S,f}$	mg COD/l	Solid	Slowly biodegradable solid COD parti-
			cles
$X_{I,m}$	mg COD/l	Aqueous	Inert soluble COD particles
$X_{I,f}$	mg COD/l	Solid	Inert solid COD particles
$S_{NH}$	mg N/l	Aqueous	Ammoniacal nitrogen
$S_{NO}$	mg N/l	Aqueous	Nitrites – nitrates
$S_{H_2S}$	mg S/l	Aqueous	Hydrogen sulfide
$S_{SO_4}$	mg S/l	Aqueous	Sulfate

**Table 2.2:** Process rates of particulate components in the liquid phase  $X_{S,m}$  and  $X_{I,m}$ , and in the solid phase  $X_{S,f}$  and  $X_{I,f}$  (kg/m<sup>3</sup>·s), adapted from [19].

**Table 2.3:** Bacterial groups considered in CMW1 (adapted from Samsó [19]).

Component	Unit	Phase	Description			
$X_H$	$mg O_2/l$	Solid	Heterotrophic bacteria			
$X_A$	$mg O_2/l$	Solid Autotrophic nitrifying bacteria				
$X_{FB}$	$mg O_2/l$	Solid	Fermenting bacteria			
$X_{AMB}$	$mg O_2/l$	Solid	Acetotrophic methanogenic bacteria			
$X_{ASRB}$	$mg O_2/l$	Solid	Acetotrophic sulfate-reducing bacteria			
$X_{SOB}$	$mg O_2/l$	Solid	Sulfide-oxidizing bacteria			

State of the Art

Table 2.4: Stoichiometric matrix (adapted from [20, 19]).

Process $j$	$S_O$	$S_F$	$S_A$	$S_I$	$S_{NH}$	$S_{NO}$	$S_{SO4}$	$S_{H_2S}$	$X_{S,f}$	$X_{S,m}$	$X_{I,f}$	$X_{I,m}$	$X_H$	$X_A$	$X_{FB}$	$X_{AMB}$	$X_{ASRB}$	$X_{SOB}$
1 Hydrolysis $X_{S,f}$				$f_{\text{hyd},SI}$					-1									
1 Hydrolysis $X_{S,m}$										-1								
2 Aerobic growth $X_H$ on $S_F$	1	$-1/Y_H$																
3 Anoxic growth $X_H$ on $S_F$		$-1/Y_H$																
4 Aerobic growth $X_H$ on $S_A$	1		$-1/Y_H$															
5 Anoxic growth $X_H$ on $S_A$			$-1/Y_H$															
6 Lysis of $X_H$		$f_{BM,SF}$									$f_{BM,XI}$		-1					
7 Aerobic growth $X_A$ on $S_{NH}$	-4.57				$-1/Y_A$									1				
8 Lysis of $X_A$		$f_{BM,SF}$									$f_{BM,XI}$			-1				
9 Growth of $X_{FB}$		$-1/Y_{FB}$	$-1/Y_{FB}$												1			
10 Lysis of $X_{FB}$		$f_{BM,SF}$									$f_{BM,XI}$				-1			
11 Growth of $X_{AMB}$			$-1/Y_{AMB}$													1		
12 Lysis of $X_{AMB}$		$f_{BM,SF}$									$f_{BM,XI}$					-1		
13 Growth of $X_{ASRB}$			$-1/Y_{ASRB}$														1	
14 Lysis of $X_{ASRB}$		$f_{BM,SF}$									$f_{BM,XI}$						-1	
15 Aerobic growth $X_{SOB}$ on $S_{H_2S}$								$-Y_{SOB}$										1
16 Anoxic growth $X_{SOB}$ on $S_{H_2S}$								$-Y_{SOB}$										1
17 Lysis of $X_{SOB}$		$f_{BM,SF}$									$f_{BM,XI}$							-1

**Table 2.5:** Reaction rates from CMW1 in  $kg m^{-3} s^{-1}$  (adapted from [20, 19]).

Process	Rate expression
Hydrolysis of $X_{S,m}$	$k_h \left[ \frac{X_{S,m}}{K_X \left( \frac{X_{S,m}}{X_H + X_{FB}} \right)} \right] (X_H + \eta_h X_{FB})$
Hydrolysis of $X_{S,f}$	$k_{L}\left(\frac{X_{S,m}}{X_{H}+X_{FB}}\right)^{\left(HH+\eta_{h}X_{FB}\right)}$ $k_{h}\left[\frac{X_{S,f}}{K_{X}\left(\frac{X_{S,f}}{X_{H}+X_{FB}}\right)}\right]\left(X_{H}+\eta_{h}X_{FB}\right)$ $\mu_{K,f}\left(\frac{S_{F}}{X_{FB}}\right)\left(\frac{S_{O}}{X_{FB}}\right)$
Aerobic growth of $X_H$ on $S_F$	$ ^{\mu H, l \ JGL} \setminus K_{GE, H} + S_E \rangle \setminus K_{GO, H} + S_O \rangle$
	$\left(\frac{S_{NH}}{K_{SNH,H} + S_{NH}}\right) \left(\frac{K_{SH2S,H}}{K_{SH2S,H} + S_{H_2S}}\right) X_{H}$ $\eta_g \mu_{H,l}  f_{GL} \left(\frac{S_F}{K_{SF,H} + S_F}\right) \left(\frac{K_{SO,H}}{K_{SO,H} + S_O}\right)$
Anoxic growth of $X_H$ on $S_F$	$\eta_g  \mu_{H,l}  f_{GL} \left( \frac{S_F}{K_{SF,H} + S_F} \right) \left( \frac{K_{SO,H}}{K_{SO,H} + S_O} \right)$
~ r	$ \left( \frac{S_{NH}}{K_{SNH,H} + S_{NH}} \right) \left( \frac{S_{NO}}{K_{SNO,H} + S_{NO}} \right) \left( \frac{K_{SH2S,H}}{K_{SH2S,H} + S_{H_2S}} \right) X_{H} $ $ \mu_{H,l} f_{GL} \left( \frac{S_{A}}{K_{SA,H} + S_{A}} \right) \left( \frac{S_{O}}{K_{SO,H} + S_{O}} \right) $
Aerobic growth of $X_H$ on $S_A$	$\mu_{H,l} f_{GL} \left( \frac{S_A}{K_{SA,H} + S_A} \right) \left( \frac{S_O}{K_{SO,H} + S_O} \right)$
	$\left(\frac{S_{NH}}{K_{SNH,H} + S_{NH}}\right) \left(\frac{K_{SH2S,H}}{K_{SH2S,H} + S_{H_2S}}\right) X_{H}$ $\eta_g  \mu_{H,l}  f_{GL} \left(\frac{S_A}{K_{SA,H} + S_A}\right) \left(\frac{K_{SO,H}}{K_{SO,H} + S_O}\right)$
Anoxic growth of $X_H$ on $S_A$	
$S_A$	$\left(\frac{S_{NH}}{K_{SNH,H} + S_{NH}}\right) \left(\frac{S_{NO}}{K_{SNO,H} + S_{NO}}\right) \left(\frac{K_{SH2S,H}}{K_{SH2S,H} + S_{H_2S}}\right) X_{H}$
Lysis of $X_H$	$b_H X_H$
Aerobic growth of $X_A$ on $S_{NH}$	$\mu_{A,i} f_{GL} \left( \frac{S_O}{K_{SO,A} + S_O} \right) \left( \frac{S_{NH}}{K_{SNH,A} + S_{NH}} \right)$
NH	$\left(\frac{K_{SH2S,A}}{K_{SH2S,A} + S_{H_2S}}\right) X_A$
Lysis of $X_A$	$b_A X_A$
	Continued on next page

27

Continued on next page

Table 2.5 — continued from previous page

	Table 2.5 — continued from previous page
Process	Rate expression
Growth of $X_{FB}$	$\mu_{FB,l} f_{GL} \left( \frac{S_F}{K_{SF,FB} + S_F} \right) \left( \frac{K_{SO,FB}}{K_{SO,FB} + S_O} \right)$
	$\left(\frac{S_{NH}}{K_{SNH,FB} + S_{NH}}\right) \left(\frac{K_{SNO,FB}}{K_{SNO,FB} + S_{NO}}\right) \left(\frac{K_{SH2S,FB}}{K_{SH2S,FB} + S_{H_2S}}\right) X_{FB}$
Lysis of $X_{FB}$	$ b_{FB} X_{FB} $
Growth of $X_{AMB}$	$\mu_{AMB,l} f_{GL} \left( \frac{S_A}{K_{SA,AMB} + S_A} \right) \left( \frac{K_{SO,AMB}}{K_{SO,AMB} + S_O} \right)$
	$\left(\frac{S_{NH}}{K_{SNH,AMB} + S_{NH}}\right) \left(\frac{K_{SNO,AMB}}{K_{SNO,AMB} + S_{NO}}\right) \left(\frac{K_{SH2S,AMB}}{K_{SH2S,AMB} + S_{H_2S}}\right) X_{AMB}$
Lysis of $X_{AMB}$	$b_{AMB} X_{AMB}$
Growth of $X_{ASRB}$	$\frac{\mu_{ASRB,l} f_{GL} \left(\frac{S_A}{K_{SA,ASRB} + S_A}\right) \left(\frac{K_{SO,ASRB}}{K_{SO,ASRB} + S_O}\right)}{\left(\frac{S_{NH}}{K_{SNH,ASRB} + S_{NH}}\right) \left(\frac{K_{SNO,ASRB}}{K_{SNO,ASRB} + S_{NO}}\right) \left(\frac{S_{SO4}}{K_{SSO4,ASRB} + S_{SO4}}\right) X_{ASRB}}$
	$\left(\frac{S_{NH}}{K_{SNH,ASRB} + S_{NH}}\right) \left(\frac{K_{SNO,ASRB}}{K_{SNO,ASRB} + S_{NO}}\right) \left(\frac{S_{SO4}}{K_{SSO4,ASRB} + S_{SO4}}\right) X_{ASRB}$
Lysis of $X_{ASRB}$	$b_{ASRB}  X_{ASRB}$
Aerobic growth of $X_{SOB}$	$\mu_{SOB,i} f_{GL} \left( \frac{S_O}{K_{SO,SOB} + S_O} \right) \left( \frac{S_{NH}}{K_{SNH,SOB} + S_{NH}} \right)$
on $S_{H_2S}$	$b_{ASRB} X_{ASRB}$ $\mu_{SOB,i} f_{GL} \left( \frac{S_O}{K_{SO,SOB} + S_O} \right) \left( \frac{S_{NH}}{K_{SNH,SOB} + S_{NH}} \right)$ $\left( \frac{S_{H_2S}}{K_{SH2S,SOB} + S_{H_2S}} \right) X_{SOB}$ $\eta_{SOB} \mu_{SOB,i} f_{GL} \left( \frac{K_{SO,SOB}}{K_{SO,SOB} + S_O} \right) \left( \frac{S_{NH}}{K_{SNH,SOB} + S_{NH}} \right)$ $\left( S_{NO} \right) \left( S_{H_2S} \right) V$
Anoxic growth of $X_{SOB}$ on	$ \eta_{SOB}  \mu_{SOB,i}  f_{GL} \left( \frac{K_{SO,SOB}}{K_{SO,SOB} + S_O} \right) \left( \frac{S_{NH}}{K_{SNH,SOB} + S_{NH}} \right) $
$SH_2S$	$\left(\frac{S_{NO}}{K_{SNO,SOB} + S_{NO}}\right) \left(\frac{S_{H_2S}}{K_{SH2S,SOB} + S_{H_2S}}\right) X_{SOB}$
Lysis of $X_{SOB}$	$b_{SOB} X_{SOB}$

**Table 2.6:** Stoichiometric parameters related to organic matter and bacterial groups [20].

Parameter	Value	Unit	Description
$f_{{ m Hyd},SI}$	0	$g_{COD,SI}/g_{COD,XS}$	Production of $S_I$ during the hydrolysis process
$f_{BM,SF}$	0.05	$g_{COD,SF}/g_{COD,BM}$	Fraction of $S_F$ produced from total biomass lysis
$f_{BM,XI}$	0.1	$g_{COD,XI}/g_{COD,BM}$	Fraction of $X_I$ produced from total biomass lysis
$Y_H$	0.63	$g_{COD,BM}/g_{COD,SF}$	Yield coefficient for heterotrophic bacteria $X_H$
$Y_A$	0.24	$g_{COD,BM}/g_N$	Yield coefficient for autotrophic nitrifying bacteria $X_A$
$Y_{FB}$	0.053	$g_{COD,BM}/g_{COD,SF}$	Yield coefficient for fermenting bacteria $X_{FB}$
$Y_{AMB}$	0.032	$g_{COD,BM}/g_{COD,SA}$	Yield coefficient for acetotrophic methanogenic bacte-
			ria $X_{AMB}$
$Y_{ASRB}$	0.05	$g_{COD,BM}/g_{COD,SA}$	Yield coefficient for acetotrophic sulfate-reducing bac-
			teria $X_{ASRB}$
$Y_{SOB}$	0.12	$g_{COD,BM}/g_S$	Yield coefficient for sulfide-oxidizing bacteria $X_{SOB}$

Table 2.7: Composition parameters [20].

Parameter	Value	${f Unit}$	Description
$i_{N,SF}$	0.03	$g_N/g_{COD,SF}$	Nitrogen fraction contained in $S_F$
$i_{N,SI}$	0.01	$g_N/g_{COD,SI}$	Nitrogen fraction contained in $S_I$
$i_{N,XS}$	0.04	$g_N/g_{COD,XS}$	Nitrogen fraction contained in $X_S$
$i_{N,XI}$	0.03	$g_N/g_{COD,XI}$	Nitrogen fraction contained in $X_I$
$i_{N,BM}$	0.07	$g_N/g_{COD,BM}$	Nitrogen fraction contained in the total biomass

**Table 2.8:** Stoichiometric factors  $v_{5,i}$  related to ammoniacal nitrogen  $S_{NH}$  and factor  $v_{9,lisi}$  related to the production of  $X_{S,f}$  [20].

Expression	Value
$v_{5,1} = i_{N,XS} - (1 - f_{\text{Hyd},SI}) \cdot i_{N,SF} - f_{\text{Hyd},SI} \cdot i_{N,SI}$	0.01
$v_{5,2} = v_{5,3} = rac{i_{N,SF}}{Y_H} - i_{N,BM}$	-0.0224
$v_{5,4} = v_{5,5} = v_{5,9} = v_{5,11} = v_{5,13} = v_{5,15} = v_{5,16} = -i_{N,BM}$	-0.07
	0.0315
$v_{5,7} = -i_{N,BN} - \frac{1}{Y_A}$	-4.2367
$v_{9,\text{lisi}} = 1 - f_{BM,SF} - f_{BM,XI}$	0.85

Table 2.9: Kinetic parameters at  $20^{\circ}$ C [20, 19].

Parameter	Value	Unit	Description
$k_h$	3	1/d	Hydrolysis rate constant
$K_X$	0.1	$g_{COD,SF}/g_{COD,BM}$	Saturation/inhibition coefficient for hydroly-
			sis
$\eta_H$	0.1	-	Correction factor for hydrolysis by $X_{FB}$
$\mu_{H,l}$	6	1/d	Maximum growth rate of $X_H$ on $S_F$ and $S_A$
$\eta_g$	0.8	-	Correction factor for denitrification by $X_H$
$b_H$	0.4	1/d	Lysis rate constant of $X_H$
$K_{SO,H}$	0.2	$mg O_2/l$	Saturation/inhibition coefficient for $S_O$
$K_{SF,H}$	2	$mg_{COD,SF}/l$	Saturation/inhibition coefficient for $S_F$
$K_{SA,H}$	4	${ m mg}_{COD,SA}/{ m l}$	Saturation/inhibition coefficient for $S_A$
$K_{SNH,H}$	0.05	mgN/l	Saturation/inhibition coefficient for $S_{NH}$
$K_{SNO,H}$	0.5	m mgN/l	Saturation/inhibition coefficient for $S_{NO}$
$K_{SH2S,H}$	140	mgS/l	Saturation/inhibition coefficient for $S_{H_2S}$
$\mu_{A,i}$	1	1/d	Maximum growth rate of $X_A$ on $S_{NH}$
$b_A$	0.15	1/d	Lysis rate constant of $X_A$
$K_{SO,A}$	0.4	$mg O_2/l$	Saturation/inhibition coefficient for $S_O$
$K_{SNH,A}$	1	m mgN/l	Saturation/inhibition coefficient for $S_{NH}$
$K_{SH2S,A}$	140	mgS/l	Saturation/inhibition coefficient for $S_{H_2S}$
$\mu_{FB,i}$	3	1/d	Maximum growth rate of $X_{FB}$
$b_{FB}$	0.02	1/d	Lysis rate constant of $X_{FB}$
$K_{SO,FB}$	0.002	$mg O_2/l$	Saturation/inhibition coefficient for $S_O$
$K_{SF,FB}$	28	${\rm mg}_{COD,SF}/{\rm l}$	Saturation/inhibition coefficient for $S_F$

Parameter	Value	$\mathbf{Unit}$	Description
$K_{SNH,FB}$	0.01	m mgN/l	Saturation/inhibition coefficient for $S_{NH}$
$K_{SNO,FB}$	0.005	m mgN/l	Saturation/inhibition coefficient for $S_{NO}$
$K_{SH2S,FB}$	140	mgS/l	Saturation/inhibition coefficient for $S_{H_2S}$
$\mu_{AMB,i}$	0.085	1/d	Maximum growth rate of $X_{AMB}$
$b_{AMB}$	0.008	1/d	Lysis rate constant of $X_{AMB}$
$K_{SO,AMB}$	0.002	$mg O_2/l$	Saturation/inhibition coefficient for $S_O$
$K_{SA,AMB}$	56	$\mathrm{mg}_{COD,SA}/\mathrm{l}$	Saturation/inhibition coefficient for $S_A$
$K_{SNH,AMB}$	0.01	m mgN/l	Saturation/inhibition coefficient for $S_{NH}$
$K_{SNO,AMB}$	0.005	m mgN/l	Saturation/inhibition coefficient for $S_{NO}$
$K_{SH2S,AMB}$	140	mgS/l	Saturation/inhibition coefficient for $S_{H_2S}$
$\mu_{ASRB,i}$	0.18	1/d	Maximum growth rate of $X_{ASRB}$
$b_{ASRB}$	0.012	1/d	Lysis rate constant of $X_{ASRB}$
$K_{SO,ASRB}$	0.002	${ m mg~O_2/l}$	Saturation/inhibition coefficient for $S_O$
$K_{SA,ASRB}$	24	$\mathrm{mg}_{COD,SA}/\mathrm{l}$	Saturation/inhibition coefficient for $S_A$
$K_{SNH,ASRB}$	0.01	m mgN/l	Saturation/inhibition coefficient for $S_{NH}$
$K_{SNO,ASRB}$	0.0005	m mgN/l	Saturation/inhibition coefficient for $S_{NO}$
$K_{SH2S,ASRB}$	140	mgS/l	Saturation/inhibition coefficient for $S_{H_2S}$
$K_{SSO4,ASRB}$	19	mgS/l	Saturation/inhibition coefficient for $S_{SO4}$
$\mu_{SOB,i}$	5.28	1/d	Maximum growth rate of $X_{SOB}$
$b_{SOB}$	0.15	1/d	Lysis rate constant of $X_{SOB}$
$K_{SO,SOB}$	0.2	$mg O_2/l$ Saturation/inhibition coefficient for $S_C$	
$K_{SNH,SOB}$	0.05	mgN/l	Saturation/inhibition coefficient for $S_{NH}$
$K_{SNO,SOB}$	0.5	mgN/l	Saturation/inhibition coefficient for $S_{NO}$
$K_{SH2S,SOB}$	0.24	mgS/l	Saturation/inhibition coefficient for $S_{H_2S}$

Taking into account that the BIO\_PORE model is an innovation of the CWM1 model, it is important to highlight that one of the most important innovations is the treatment of particulate components of COD. More specifically, particulate organic matter is divided into particulate and soluble phases for  $XS_{part}$  and  $XI_{part}$  for the first and  $XS_{infl}$  and  $XI_{infl}$  for the second, therefore, allowing the simulation of attachment and detachment processes occurring at particle scale. Moreover, this model takes into account 18 substances divided between 8 dissolved species in aqueous phase, 4 organic particulate species (that are both aqueous and solid) and finally 6 functional bacterial groups.

The principal features of the BIO PORE model are:

• Explicit representation of attachment and detachment processes for particulate COD, simulating accumulation within the granular medium.

- A hydraulic sub-model that calculates the exact water level at each instant, crucial in a vertical-flow wetland to distinguish between saturated and unsaturated zones.
- A biofilm sub-model that avoids unrealistic unlimited biomass growth and incorporates the effects of solid deposition on bacterial proliferation.

#### Hydraulic Sub-Model

The hydraulic sub-model describes the variating saturated flow within the porous bed. This flow is governed by the Richards equation [21]

$$\frac{\partial h}{\partial t} = \nabla \cdot (K(h) \nabla h) + s_s, \qquad (2.13)$$

where h [L] is the hydraulic head, t [T] time,  $\sigma(h)$  [L<sup>-1</sup>] storage coefficient, K(h) [L T<sup>-1</sup>] hydraulic conductivity, and  $s_s$  [L T<sup>-1</sup>] source/sink term.

In this work, the Richards equation is applied in a vertical unsaturated flow constructed wetland, that is differentiated from the original horizontal flow model, that is dominated by gravity percolation and the pulses in the hydraulic loading.

The soil water retention curve is described using the Van Genuchten 1980 equation:

$$\theta(h) = \theta_r + (\theta_s - \theta_r) S_e(h), \tag{2.14}$$

with  $S_e(h)$  the effective saturation:

$$S_e(h) = [1 + (\alpha |h|)^n]^{-m}, \qquad m = 1 - \frac{1}{n}.$$
 (2.15)

#### Transport of Dissolved and Particulate Species

The transport sub-model works with both soluble species (COD fractions, nitrogen and sulfur) and particulate components (XS and XI). The general equation for transport of soluble species  $C_k$  is:

$$\frac{\partial(\theta C_k)}{\partial t} = \nabla \cdot (\theta D \nabla C_k - q C_k) + r_{C_k} + r_{att} - r_{det} + s_{C_k}. \tag{2.16}$$

This equation is still valid for the vertical constructed wetland, in this case the adjective-dispersive transport interacts with saturated flow conditions.

Attachment and detachment are described as first-order processes:

$$r_{att} = \lambda_{att} C_m \left( 1 - \frac{M_T}{M_{cap}} \right), \tag{2.17}$$

$$r_{det} = \lambda_{det} C_f, \tag{2.18}$$

with  $\lambda_{att}, \lambda_{det}$  [T<sup>-1</sup>] the attachment/detachment coefficients.

#### Biofilm Sub-Model

Thanks to the biofilm sub-model, a logistic growth limiter is introduced

$$f_{bio} = \left(1 - \frac{M_{bio}}{M_{bio,max}}\right) \left(1 - \frac{M_{XI,f}}{M_{cap}}\right),\tag{2.19}$$

This interaction is particularly particularly important for vertical systems, due to the clogging phenomena that occurs in the infiltration surface and has an extraordinarily strong impact in the infiltration dynamics.

#### Plant Sub-Model

In this sub-model, an additional source term represents the root oxygen release and nutrient uptake. In the case of a vertical wetland, these contributions are concentrated near the surface layers, which interacts with the inflow that occurs in pulses loading both saturated and unsaturated conditions and contaminants load.

#### Reaction Rates and Stoichiometry

Substrate transformation is expressed as:

$$r_i = \sum_{j=1}^{R} v_{i,j} \, \rho_j. \tag{2.20}$$

In this model seventeen process are included, among them there is hydrolysis, nitrification, fermentation, aerobic heterotrophic growth, methanogenesis, sulfate reduction, anoxic heterotrophic growth, sulfide oxidation and lysis. Those seventeen processes interact with eighteen components, in this work, the stoichimetric framework that includes the mentioned interactions is preserved, but applied under a vertical flow regime. The tables on [19, 20] define the stoichiometric and kinetic tables of parametrization.

#### Clogging Sub-Model

The clogging is a factor that the bio-bore model takes into account, it is defined as a porosity reduction that happens due to solid accumulation and dead biomass. According to [22], clogging is modeled through a reduction in effective hydraulic conductivity:

$$K_b(h) = K(h) k_b(h).$$
 (2.21)

In the case of vertical systems, this mechanism is extremely important in the infiltrations surface, because this is the locations where particulate matter accumulates and progressively reduces the permeability.

After reviewing all the literature mentioned in this chapter, it is possible to conclude that even though the bio-pore model was originally designed for the horizontal sub-surface flow constructed wetland, it is still a modular process-based structure, this allows the model be adapted for different configurations and systems. The following work done in this thesis is to implement the bio-pore for a vertical flow constructed wetland with unsaturated conditions.

# Chapter 3

# Methodology

# 3.1 Site Description

# 3.1.1 Location: Island of Lesvos, Greece

Lesvos (or Lesbos) is a Greek island, the third biggest one in the country, it covers 1630 km2 and it is located in the North-Eastern Aegean Sea [23], very close to the coast of Turkey. In the coastline of the island that is 320 km long, there are two important gulfs, Kalloni and Gera, both covered in hilly and mountainous terrains, among them Mount Lepetymnos (968 m) and Olympus (967 m).

The geology of the island is of volcanic type, especially in the west side which can be seen in the many hot springs and petrified forests fossilized from the Miocene era present in the zone.

The climate in the island is classic Mediterranean with mild wet winters and hoy dry summers, the average temperature throughout the year is close to 18 degrees Celsius and there is a mean accumulated annual rainfall of 750 mm. It is also known to be one of the sunniest islands in the region.

The flora of the island is mainly dominated by olive trees, there are over eleven million of them, which covers around 40% of the islands terrain, 20% of the remaining land is covered in pine and chestnut and then the remaining is divided into a few other species like scrub and grassland.

The residents in the island are a population of about 85 to 90 thousand, the capital

is a city called Mytiline and it is the main quantity of people concentration, their main economic activies are agriculture of products like olive oil, ouzo, cheese, figs and almonds, there is also fishing and tourism.

Historically, Lesvos has been inhabited since prehistoric times, artefacts dating back millennia from the Neolithic and Mycenaean eras have been found in the island. Recent history tells that the aeolian Greeks settle there around the 11<sup>th</sup> century BC, some important historical cities were located there, like Mytilene, Methymna and Eresos, where the poet Sappho and the philosopher Theophratus.

Lesvos has been an important place in history and due to its location, which has made it part of many civilizations and cultures settlements, Persian and Athenian rule, later Byzantine, Genoese and Ottoman control, all of those before joining modern Greece in 1912. On the following years to this, the Asia-Menor population exchange gave new shape to the cultural context of the island and that change is still seen in the island today. [24, 25]

# 3.1.2 Case Study: HYDROUSA Constructed Wetland in Lesvos

The HYDROUSA project was authorized through H2020, Grant Agreement Number 776643, and the project was to implement an innovative constructed wetland (CW) system in Antissa, Lesvos (Greece), the purpose of the project was to treat wastewater produced by a high fluctuation seasonal turistic site. The system projected is one of the first large-scale hybrid constructed wetlands in the Mediterranean, and its main objective is to comply with the very strict Greek standards for wastewater reuse in irrigatio9n and fertigation. [26, 27]

#### System Layout

The treatment follows a line pathway sequence: Upflow Anaerobic Sludge Blanket (UASB) reactor that works as pre-treatment followed by a hybrid subsurface flow contructed wetland made of two stages, then a membrane ultrafiltration (UF) and finally ultraviolet (UV) disinfection. The CW in this case represents the secondary and tertiary treatments, meanwhile, the ultrafiltration and ultraviolet act as quaternary treatment polishing the results to ensure safe reuse.



Figure 3.1: Blueprint of the site of the Constructed Wetland in Lesvos

The CW consists of two vertical flow units:

• VF1 SAT (saturated downflow unit): Consists of a bed with measurements of 17.5 x 14 m creating a total surface of 245 m<sup>2</sup>, it is filled with gravel layers with gravel sizes that go form 30-50 mm, 10-20 mm and 5-10 mm, up to reaching 1 meter depth, all planted with Phragmites australis.



Figure 3.2: Phragmites Australis

The system is operated under saturation conditions, which is a very helpful part for the removal of BOD and TSS (Total suspended soils), and plays an important role in denitrification when performed with recirculation.

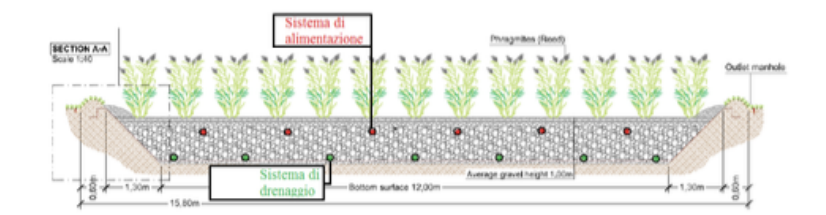


Figure 3.3: Transversal section of the VFSat

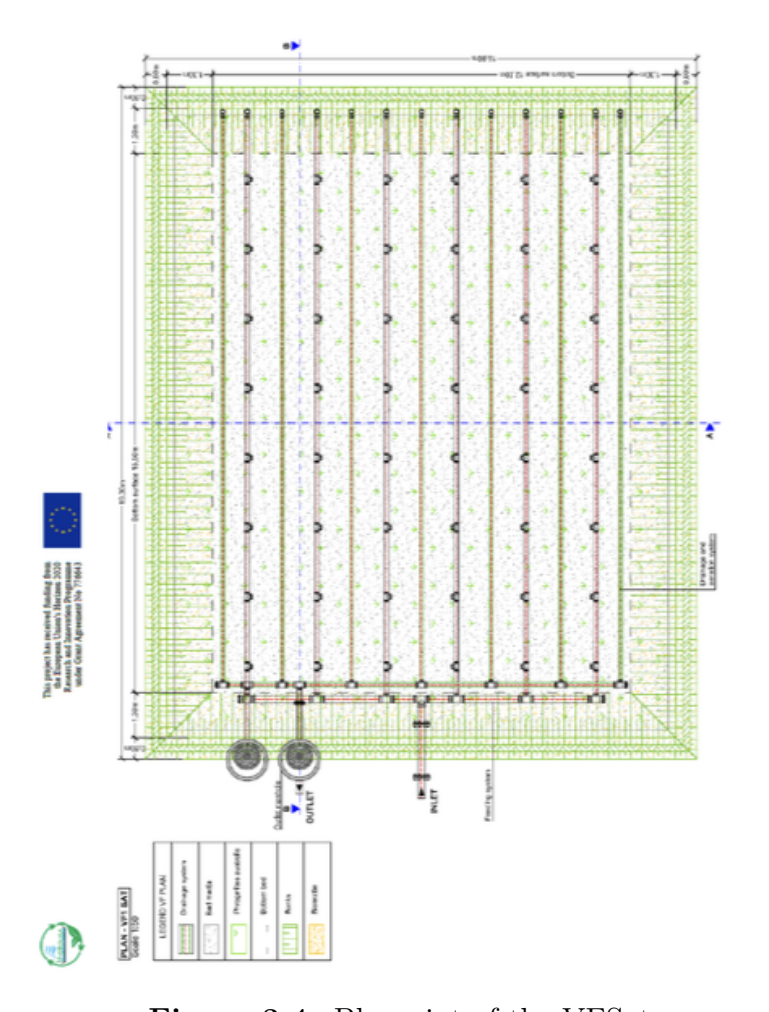


Figure 3.4: Blueprint of the VFSat

• VF2 UNSAT (unsaturated intermittently-loaded unit): It is constituted by three beds that contain four parallel lines from A to D, each of  $18 \times 8.5$  m creating each a surface of about 150 m2 and therefore a total area of about

600 m2. The beds are layered with gravel composed of grain sizes that vary in layers from 20-40 mm and 5-10 mm, and sand layer of 0.2-5 mm and finally some upper gravel creating a total depth of 1 m. The vegetation includes *Typha latifolia*, *Iris pseudacorus*, *Carex spp.*, and *Scirpus lacustris*.



Figure 3.5: Typha latifolia



Figure 3.6: Iris pseudacorus



Figure 3.7: Carex spp.



Figure 3.8: Scirpus lacustris

This part of the treatment operates wit intermitting feeding, created by pulses of water flow, which ensures oxygenation and enhances nitrification.

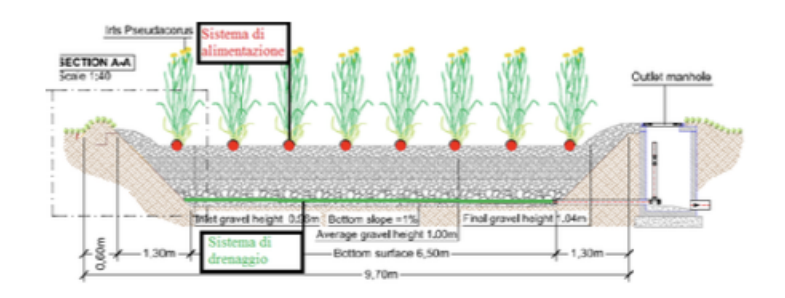


Figure 3.9: Transversal section of the VFInsat

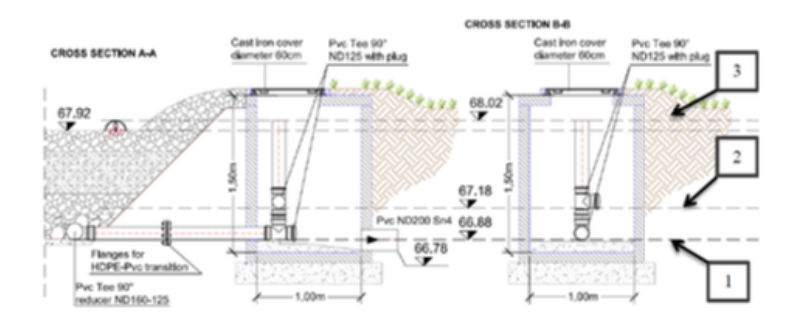


Figure 3.10: Pumping section of the VFInsat

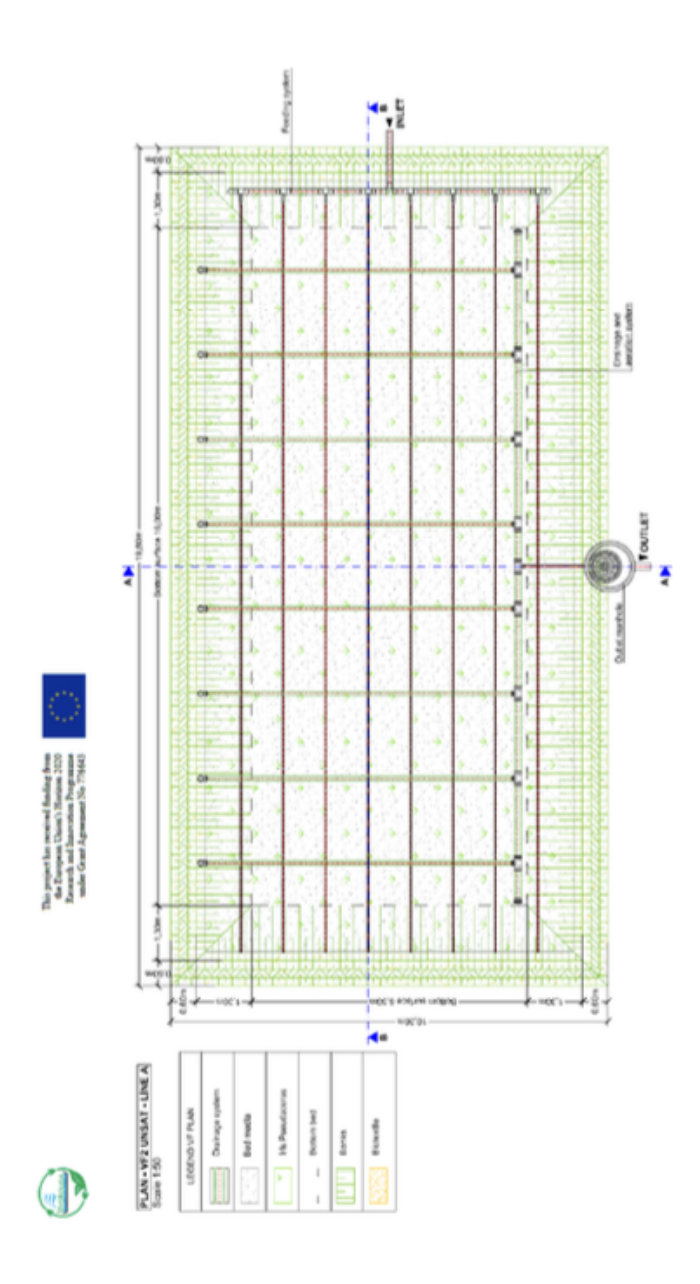


Figure 3.11: Blueprint of the VFInsat

#### **Operational Modes**

The system was designed with some flexibility, all with the purpose of it being able to operate under different configurations, which allows to test for different removal efficiencies for Mediterranean conditions. After testing, four main operation modes where stablished:

- 1. Mode 1: UASB  $\rightarrow$  VF2 UNSAT  $\rightarrow$  UV (nitrification only).
- 2. Mode 2: UASB  $\rightarrow$  VF1 SAT  $\rightarrow$  VF2 UNSAT  $\rightarrow$  UV (enhanced COD, BOD<sub>5</sub>, and TSS removal).
- 3. **Mode 3:** UASB  $\rightarrow$  VF1 SAT  $\rightarrow$  VF2 UNSAT  $\rightarrow$  UV with recirculation to VF1 SAT (combined nitrification and partial denitrification).
- 4. **Mode 4:** UASB  $\rightarrow$  UF  $\rightarrow$  UV (bypassing CWs; no nitrogen removal).

The approach created by the modules implementation allows the system to adapt to different water quality inflows and different water quality outflows, for example, nitrogen or the reuse standards fro irrigation systems.

#### Pilot Systems

As an aggregate to the full scale CW, there are also four pilot-scale units from  $0.5-1~\rm m^3/d$  each, that were implemented to test intensified and innovative CW configurations:

- The first one is an aerated constructed wetland (AEW) that uses Forced Bed Aeration  $^{\rm TM}$ ,
- The other three are bio-electrified constructed wetlands (MFC units), that are constructed wetlands filled with electroconductive material and an inoculated Geobacter spp., that is designed to couple wastewater with bioelectricity generation.

The purpose of these pilots is to investigate both integration of energy recovery and footprint reduction in the CW technology development.

#### Post-Treatment Units

The water inflow of both the full-scale and pilot constructed wetland systems undergoes an improvement through compact post treatment modules:

- Full scale: membrane ultrafiltration (pore size 0.02 µm, dizzer® XL modules) followed by UV disinfection (Viqua F4+ lamps).
- **Pilot scale:** sand filtration (downflow configuration) followed by UV disinfection (Viqua E4+).

These units were implemented to guarantee the compliance with Greek regulation and standards for water reuse for irrigation in the case of variations in the influent water quality.

#### Construction and Start-up

The construction process included activities such as excavation of basins, installation of HDPE liners, drainages and distribution systems, gravel and sand filling, and planting the selected macrophytes. The initial stage of construction was done on phases:

- 1. Initial planting under fresh water
- 2. Temporary flooding to promote establishment and weed control
- 3. Gradual transition to design loading conditions
- 4. Hydraulic testing for water tightness and proper pump automation

#### Relevance to the Thesis

This HYDROUSA CW in Lesvos, in particular the unsaturated unit, is the case study for the present work. The hybrid VF configuration, constituted by a saturated and unsaturated stage, can be implemented together with flexible operation and advanced post treatment, and this can provide a perfect experimental environment to evaluate hydraulics, water quality processes and applicability of processed-based models under Mediterranean weather conditions and high seasonal variability.

# 3.2 Model

# 3.2.1 Software: COMSOL Multiphysics

In this thesis, the software chosen to hold the main simulation and develop the proposed model is COMSOL Multiphysics. This software is a powerful and versatile platform, which is broadly used by engineers and scientists to simulate various types of designs, devices and processes across different fields such as engineering, manufacturing and scientific research. It allows for both single physics and coupled Multiphysics modeling, while allowing a comprehensive representation of real-world phenomena without removing the complexity of the situations represented.

The software guides its users through its model builder, which takes them step by step along the workflow, which goes from geometrical and materials selection and properties definition of the problem, until the setup of the physical properties; which allows to perform simulations and analyze the obtained results.

Additionally, this software on its platform allows the integration of add-on modules which can be adjusted to specific requirements, without changing or damaging the consistent user interface.

All of the above mentioned functions and their flexibility while being implemented make COMSOL Multiphysics a good fit for the development of advanced models in research applications, like the one done and presented on this work.

COMSOL Multiphysics is a numerical simulation software based on the Finite Element Method (FEM), it works as a Multiphysics platform in which it is possible to simulate and model phenomena that occur at the same time and in a coupled way, like fluid flow, heat transfer, structural mechanics, electromagnetics and chemical reactions, all on the same single environment.

Thanks to its modular structure, it can address problems in different areas:

- electrical (AC/DC, plasma, RF, MEMS)
- mechanical (heat mechanics, geomechanics, fatigue)
- fluids (CFD, microfluidics, subsurface flow)
- chemical processes (batteries, fuel cells, corrosion)

Furthermore, the interface of the software can interact with external softwares such

as Matlab, all allowing easier integration with data and work that help improve the engineering workflows.

The software follows a structured work flow divided into seven steps:

- 1. **Problem Definition and Geometry:** The first step is to clearly define the problem and construct the geometry of the system, either in 2D or 3D.
- 2. Material Assignment and Physics: Materials are assigned to the geometry, and the governing physics (such as fluid dynamics, heat transfer, or structural mechanics) are defined.
- 3. **Boundary Conditions:** Physical constraints such as inlet velocity, wall conditions (e.g., no-slip), or fixed supports are specified.
- 4. **Meshing:** The geometry is discretized into small finite elements to approximate the solution of the governing differential equations.
- 5. **Study Definition:** The user selects the type of analysis to be performed, which can be *stationary*, *time-dependent*, or in the *frequency domain*.
- 6. **Solver Configuration:** COMSOL provides powerful solvers that can be configured as *segregated* or *fully coupled*, depending on the complexity of the multiphysics interactions.
- 7. **Post-processing:** Once the solution is obtained, the results are analyzed through 3D plots, 2D surfaces, graphs, and streamlines, which provide physical insight into the problem.

Through the implementation of this workflow it is possible for engineers and researchers to systematically go from the first moments of conceptualization of the problem until reaching the numerical solution and both numerical and graphical interpretation of the results. This is possible due to the flexibility in the physics definition and the advancement and robustness of the solver and the good visualization tools. All of the mentioned things, allow to conclude that COMSOL Multiphysics is a software that provides a broad framework that allows to study real-world engineering problems like the one presented on this work.

# 3.2.2 System to be Modeled: VFInsat

The system modeled in this work is the vertical flow constructed wetland that operates in unsaturated conditions (VFInsat) located in Lesvos, Greece, part of the HYDROUSA project site. Specifically, the numerical model focuses on a one dimensional (1D) representation of the porous medium below one of the 144 holes that compose the distribution system of one of the VFInsat lines. This simplification will allow the investigation of both hydraulic and biochemical processes at the same time in pore microscale on the porous medium, without risking the computational efficiency and accurateness of results.

#### Geometry of the Basin

The full VFInsat unit contains three beds, each composed of four treatment lines (A, B, C, and D), where lines C and D share the same bed. Each of these lines has an approximate surface area of  $153 \text{ m}^2$  ( $18 \times 8.5 \text{ m}$ ), with bottom dimensions of  $16 \times 6.5 \text{ m}$ , and a depth of 1.3 m. In such way, the total net surface area of the VFInsat stage is approximately  $612 \text{ m}^2$  and the volume of  $113.85 \text{ m}^3$ . [26]

The porous medium of the VFInsat basin is made up of multiple layers of washed gravel and sand, and it is isolated from the soil around by a HDPE geomembrane of 1.5mm thickness. Layers are arranged as listed below (from surface downward) [28]:

- 0.20 m of washed gravel, 5–10 mm diameter,
- 0.40 m of sand, 0.2–5 mm diameter,
- 0.20 m of washed gravel, 5–10 mm diameter,
- 0.20 m of washed gravel, 20–40 mm diameter,
- HDPE geomembrane, 0.0015 m.

The bed is planted through a combination of macrophytes, usually utilized in unsaturated CWs, such as: Typha latifolia, Iris pseudacorus, Carex spp., and Scirpus lacustris which enhance oxygen transfer and promote nitrification.

#### Feeding and Drainage System

The VFInsat basin operates with an intermittent pressurized feeding, in which wastewater is distributed all over the surface using perforated PVC distribution pipes (ND 63, internal diameter 34 mm, perforations every meter). Each line uses 8 parallel distribution pipes with a perpendicular connection to a main manifold (ND 125) that is also connected to the pumping system (ND 160). In such way, intermittent pulses allow infiltration and re-oxygenation of the porous medium to happen.

Through 8 parallel HDPE pipes (ND 125) it's possible to have drainage. These are connected to a main collector (ND 160), then on one side the pipes are linked to the outlet chamber and on the other one they emerge vertically above the surface to allow aeration of the layers below. Finally, a level-control valve must be installed in the outlet chamber in order to facilitate three modes of operation: standard, denitrification, and flooding or startup:

- 1. **Standard operation:** fully unsaturated conditions, rapid drainage after each pulse,
- 2. **Denitrification mode:** partial saturation by maintaining the water level at  $\approx 30$  cm above the bottom, supporting anoxic zones,
- 3. Flooding/start-up mode: temporary saturation up to  $\approx 10$  cm above the gravel surface, used for system start-up and vegetation growth.

#### 1D Model Representation

During the modeling processes it is fundamental to find a balance between the desired level of detail and the available resources for computational processes. As previously mentioned, the real distribution system is made up of 144 feeding holes per line (18 m x 8 distribution pipes). In this thesis a 1D vertical domain is made in representation of the infiltration and percolation process occurring under one single hole. In such way, the infiltration dynamics and biochemical reactions are isolated within the porous medium but preserves the key aspects of the geometry of the basin including its composition by layer, depth and hydraulic boundary conditions. Hence this approach provides a balance between physical representativeness and computational effort.

# 3.2.3 Input flowrate characteristics

The input data required for the model is given my data measurements for both the constructed wetland and the UASB. The available data comprehends the period from February 2021 to February 2023 and includes physical and biochemical parameters. The phisical parameters are:

- 1. Flowrate
- 2. Temperature
- 3. Depth of the VFInsat

The biochemical parameters are:

- 1. pH
- 2. TSS (Total suspended soils)
- 3. COD Total (Total chemical oxygen demand)
- 4. COD Sol (Soluble chemical oxygen demand)
- 5. BOD (Biochemical oxygen demand)
- 6. NO3-N
- 7. NH4-N
- 8. TN (Total nitrogen)
- 9. TP (Total phosphorus)
- 10. PO4 (Phosphate)
- 11. Turbidity
- 12. E.coli
- 13. TC (Total carbon)
- 14. EC (Electrical conductivity)

Not all data was evaluated, but specifically flowrate, depth, COD total, NH4-N and NO3-N. It was first processed to be adequate as input for the software used. See Appendix A (Table A.1) for the full dataset.

# 3.2.4 Simulation's parameters

#### Geometrical characteristics

To begin with the construction of the model, it is fundamental to define the computation domain. The software used, COMSOL MultiphysicsTM, allows to simulate systems in one, two or three dimensions. Even if many studies use 2D geometries to represent the vertical cross-sections of saturated and unsaturated beds, as mentioned earlier this thesis approached a 1D vertical model. [28]

Given this simplification it is possible to focus on the combined hydraulic and biochemical behavior along the vertical profile of the bed. Such configuration leads to a representation of the percolating flow in the model, and the reactions that occur in between the inlet point at the top and the outlet at the bottom, neglecting potential horizontal variations. This assumption relies on the homogenous granular composition of the filter media, that allows the vertical section to represent the overall dynamics.

Once the surface of the planted bed was defined, the computational domain was selected to be set at elevation X=0 and the bottom of the filter at X=-1, consistent with the actual design depth, on following simulations this parameter was changed. The assigned inflow was set to enter through the upper boundary, and on the contrary, the outflow was set on the lower boundary. Both of these conditions were set as boundary conditions corresponding to the internal dimensions in the constructed wetland and in order to match the feeding conditions and the drainage conditions. That was done so the inlet simulates the introduction of wastewater from the feeding system, and later the outlet reproduces the collection and drainage of treated outflow.

Lastly, both inlet and outlet boundaries were calculated for the first hydraulic simulation as if a spersion hole was exactly above the drainage hole, and on the second one the inlet represents a single point in the surface and the outlet the exact point underneath of this 1D section of the constructed wetland.

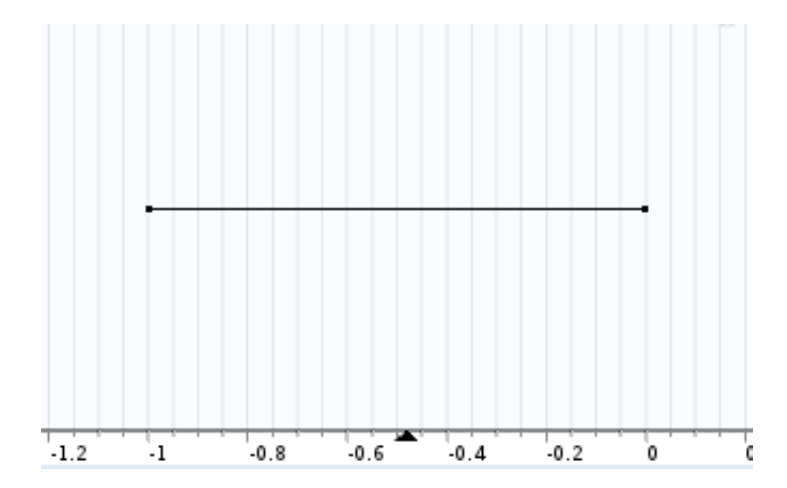


Figure 3.12: Model geometry

For the mentioned second hydraulic simulation a change was done to the geometrical characteristics of the model, in order to comply with the 1D representation of reality, the first 10 cm of depth will be neglected from the simulation as water passes easily through them and is in this where the expansion of the fluid happens mainly, changing what the 1D real result is.

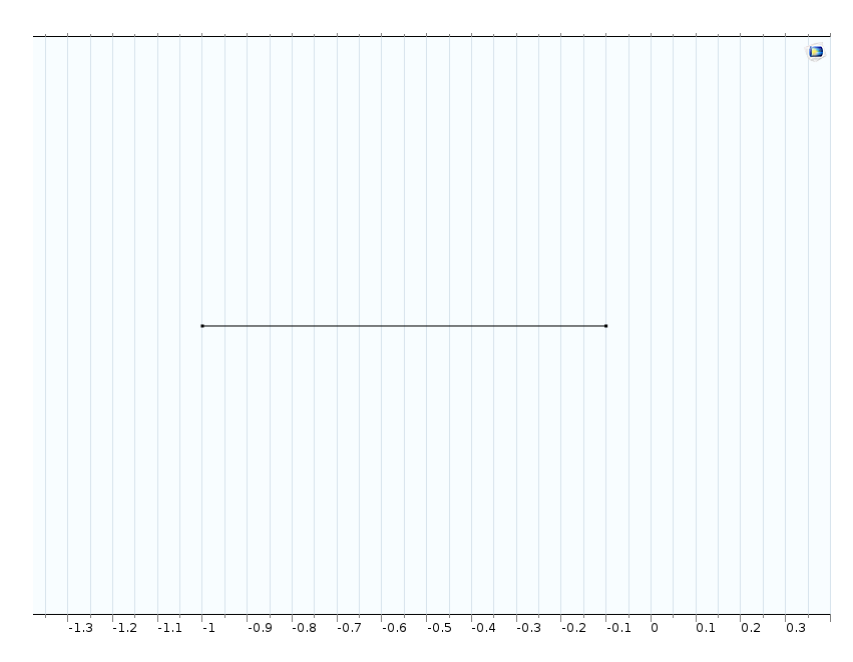


Figure 3.13: Model geometry for the second hydraulic version

#### Materials

COMSOL Multiphysics allows the user to access a wide library of predefined materials, these materials are each characterized by some parameters that can be added, removed or modified by the user. In this work, to represent the constructed wetland bed and obtain a virtual model that accurately represents the reality, three main materials are usually considered within the virtual volume of constructed wetlands: Water, oxygen and mineral medium like granite, sand or gravel [28]. The materials defined for the model will determine the hydraulic and biochemical behavior of the system, given that the properties of this materials will have a direct effect in the transport and the reaction processes.

However, in this model, the case was different, given that the model was developed in 1D along the vertical profile, this type of model does not allow for different type of materials to be used unless the section is subdivided, which would not be an accurate representation of reality. For this reason, one only material was chosen to represent the entire computational domain, this beign a simplification that given the model type, still allows to represent the combined hydraulic and biochemical processes while ensuring model stability while reducing computational complexity.

	Property	Name	Value	Unit	Property group
/	Density	rho	2600	kg/m³	Basic
	Thermal conductivity	k	k(T[1/K])	W/(m-K)	Basic
	Heat capacity at constant pres	Ср	C(T[1/K]	J/(kg·K)	Basic
	TD	TD	TD(T[1/	m²/s	Basic
	Porosity	epsilon	0.35	1	Basic
	Coefficient of thermal expansion	alpha	7e-6	1/K	Basic
	Dynamic viscosity	mu	1e-3	Pa⋅s	Basic

Figure 3.14: Material properties

#### Hydraulic parameters

All the hydraulic data used in this work was taken from Montagna [28] and later on adapted to the 1D vertical configuration of the model, even if the original model he designed was in a 2D representation scenario, the data can be simplified in this case to describe both hydraulic and biochemical behavior while only simulation a single vertical line with only one inlet and one outlet. The characterization of the hydraulic properties in this case of the granular medium, assimilates sandy gravel, according to the parameters reported by Pucher 2019 [29], for sands that

have grain sizes ranging from 0.06 to 4 mm, the parameters that Van Genuchten uses from Pucher are:

$$\alpha = 6.5 \,\mathrm{m}^{-1}, \quad n = 3.64, \quad l = 0.974$$

Nevertheless, throughout the simulations done in COMSOL, the convergence of the model was only achieved with a slight change in the parameter n, the value got a bit reduced and therefore the final parameters used are:

$$\alpha = 6.5 \,\mathrm{m}^{-1}, \quad n = 3.1, \quad l = 0.974$$

On the other hand, for the evaluation of hydraulic conductivity, instead of adopting the value from Pucher's tables which would be  $(K_s = 128 \,\mathrm{cm/h})$ , a more suitable number was applied:

$$K_s = 86.4 \,\mathrm{m/d} \approx 1 \times 10^{-3} \,\mathrm{m/s},$$

With this value it is possible to match the characteristics of a sandy soil that holds the following granulometric characteristics:

- $0.2 \le d \le 5 \,\mathrm{mm}$ ,
- $d_{10} > 0.4 \,\mathrm{mm}$ ,
- $d_{60}/d_{10} < 2$ .

In different literature, there is also the recommendation that Ks should not be lower than  $6 \times 10^{-4} \,\mathrm{m/s}$  ( $K_s \ge 51.84 \,\mathrm{m/d}$ ), which confirms that the chosen value is indeed appropriate for this simulation. This parameter was established in the "definitions" section of the software as  $K_1$ .

After the hydraulic conductivity was fixed, the following step was to consider hydrodynamic dispersion, in this process, it is reflected how water flowing through porous media can follow different paths, which all have different size and direction, this generates spreading of solutes and/or pollutants that go beyond advection. The dispersion coefficient D is expressed as:

$$D = a_{ijkm} \frac{\overline{V_k} \, \overline{V_m}}{\overline{V}} f(Pe, \rho),$$

where:

- $\overline{V}$  is the mean velocity,
- $f(Pe, \rho)$  accounts for molecular diffusion at the pore scale (often assumed equal to 1),
- $\rho$  represents characteristic pore lengths,
- $Pe = \frac{L\overline{V}}{D_d}$  is the Peclet number, with  $D_d$  the molecular diffusion coefficient and L the characteristic pore length,
- $a_{ijkm}$  is the dispersivity tensor of the porous medium.

In the case of isotropic porous media, the tensor reduces to non-zero components: the longitudinal dispersivity  $a_L$  and the transverse dispersivity  $a_T$ , with  $a_T$  typically one order of magnitude smaller. In this study, the adopted values were:

$$a_L = 0.15 \,\mathrm{m}, \qquad a_T = 0.01 \,\mathrm{m}.$$

Lastly, porosity was derived from the design data and was set to:

$$n = 0.35$$

This parameter was taken into account in both the global parameter list and inside the material definition (granite) inside the COMSOL model, like that, it was possible to call it during simulations.

### Physical parameters

Similar to the case of material selection, as it was mentioned before, the software provides a wide range of physical models to choose from. In the Montagna model, two different interfaces were applied to analyze the behavior of the saturated and unsaturated units, for the first one it was Darcy's law, while for the second one, it

was Richard's law. Both of these physical models were explained on Chapter 2 [15]. For the purpose of the present work only the unsaturated unit will be taken into account and therefore the only physical model used was Richard's law.

Some properties were considered for all the simulations, among them, the gravitational effects and a reference temperature were included, by setting first, the gravitational acceleration to  $9.8\,\mathrm{m/s}^2$  and second, the temperature to  $20\,^\circ\mathrm{C}$ .

In the case of the unsaturated unit, due to the variability in the water content (theta), and therefore the variability in the hydraulic conductivity K, which will depend on it  $(K = K(\vartheta))$ , the Richards equation was adopted. After the introduction of this interface in the COMSOL model, the fluid and matrix properties were defined.

With respect to the fluid, for the Montagna model, "water" was chosen from the COMSOL library, which recalls the default density  $\rho$ . For the porous medium "granite" was assigned, with parameters like porosity set to n=0.35 (saturated liquid volume fraction), hydraulic conductivity set to  $K_1=K_s=46\,\mathrm{m/d}$ , and residual liquid volume fraction set to  $\theta_r=0.1$ . This last value guarantees that the domain is never completely dry during simulation.

Regarding the hydraulic conductivity, the value used was derived from some trial simulations that aimed to ensure convergence. These simulations started from the value adopted for the saturation unit ( $K_s = 86.4 \,\mathrm{m/d}$ ) and started comparing to the values found in literature for similar types of constructed wetlands which were around ( $K_s = 37.7 \,\mathrm{m/d}$ , [30]), after a few simulation trials, they found that an intermediate value allowed stable convergence:

$$K_s = 46 \,\mathrm{m/d}.$$

In the "Retention model" section of the Richards equation, the Van Genunchten parameters reported in literature for vertical flow wetlands with clean sand [29] were used:

$$\alpha = 6.5 \,\mathrm{m}^{-1}, \quad n = 3.64, \quad l = 0.974.$$

Nevertheless, just like the saturated case, in order to convert, it is require to reduce the exponent n, which means that the final parameters implemented in the model are:

$$\alpha = 6.5 \,\mathrm{m}^{-1}, \quad n = 3.1, \quad l = 0.974.$$

Also in this case, initial boundary conditions were introduced, the first one was

setting the domain boundaries as no flow zones, which makes them impermeable, the second was the inlet and outlet boundaries, that were assigned to the boundary type of their corresponding function. In the case of the unsaturated unit the inlet boundary was provided with a function time series which reproduces the daily feeding regime, on the work of Montagna, the model was built for the maximum capacity of the basin, meaning 25 m<sup>3</sup> a day divided into 9 flushes per day, each one lasting 5 minutes and separated by two hours and forty-two minutes.

For the construction of this series, the inlet velocity was set to the calculated inflow value while the flush is on, while during the intervals between flushes it was set to a very small nonzero value to avoid the numerical instabilities that could be caused by assigning a zero in the model. Montagna prepared this time series in excel and imported it to COMSOL as an interpolation function to later apply it as the normal inflow velocity. Ensuring that the model follows the real pattern and applying the correct inflow during flushes.

On the other hand, for the outlet boundary the concept used is "Hydraulic head", this condition was set corresponding to the drainage pipes.

Finally, for the initial conditions, the pressure head Hp was calculated from the Van Genuchten equations as a function of the degree of saturation Se. Assuming that the residual water content is 0.1 and that the porosity is 0.35, the initial saturation can be calculated as:

$$S_e = \frac{\theta_r}{n} = \frac{0.1}{0.35} = 0.28.$$

Using the Van Genuchten relationship with the optimized parameters  $\alpha = 6.5 \,\mathrm{m}^{-1}$ , n = 3.1, l = 0.974, m = 0.677, the corresponding pressure head was obtained as:

$$H_p = -0.24 \,\mathrm{m},$$

This is a negative value which matches what is expected under unsaturated conditions.

On the topic of the inflow velocity, it was calculated from the hydraulic configuration of the pilot plant, the calculation done was based on the fact that the three beds are divided into 4 wetland units "lines" located in 2 sectors, the whole plant was design for a peak flow of  $100\,\mathrm{m}^3/\mathrm{d}$ , with each sector getting  $50\,\mathrm{m}_3/\mathrm{d}$  and each line  $50\,\mathrm{m}_3/\mathrm{d}$ . The feeding system consists of 8 pipes with 18 nozzles each which creates 144 total nozzles. For one line, the  $25\,\mathrm{m}_3/\mathrm{d}$  are divided among the 144 nozzles to obtain the daily flow rate through one nozzle, then later divided among the 9

daily flushes to obtain flowrate in a flush, afterwards, divide in 300 s which is the duration of the flush getting a flowrate in m3/s and finally dividing by the area of the nozzle obtaining the velocity:

$$v_{in} = \frac{0.000064}{0.034} = 0.0021 \,\text{m/s}.$$

Finally, for the drainage boundary, the hydraulic head was calculated as:

$$H = Z + \frac{P}{\gamma},$$

In the case of Montagna the geodetic elevation was  $Z = -0.9 \,\mathrm{m}$  meanwhile for the case of this work it was  $Z = -1.0 \,\mathrm{m}$ , and for both cases the pressure head was  $H_p = -0.24 \,\mathrm{m}$ . The initial total head at the drain is in the case of Montagna:

$$H_0 = -0.9 - 0.24 = -1.14 \,\mathrm{m}.$$

And in this work:

$$H_0 = -1.0 - 0.24 = -1.24 \,\mathrm{m}.$$

In the same way as the saturated case, Montagna stablished all other boundaries as no flow to ensure impermeability.

#### **Biochemical** evaluation

To complement the hydraulic description of the system with a biochemical component, the BIO\_PORE model done by Samso and Garcia [19] and later modified by Santelia [18] was selected and integrated to the simulations. This addition made it possible to reproduce at the same time the hydraulic performance and the biochemical reactions that govern the degradation of contaminants, both models done simultaneously provides a more complete representation of the constructed wetland. Sice the study focuses on the unsaturated vertical-flow system, several modifications had to be done to the original model, which was initially formulated for saturated conditions in horizontal flow.

This section will briefly describe the numerical characteristics of the BIO\_PORE model and the original parameters used by Samso and Garcia and the disscuss the issues encountered by Santelia and which changes were made to model to arrive to the preliminary version this work will use.

Using BIO\_PORE within the COMSOL Multiphysics platform was particularly advantageous because of its complexity, like that it was avoided the need to rewrite all the code in another programming environment. The original model was developed as mentioned before by Samso and Garcia but for the purpose of this study it was more manageable to use Santelia's corrected version. Nevertheless, working with a model developed and adapted by others required a detailed understanding of the conceptual basis and the coded structure.

The main simulation difficulties came up in relation to the data handling, and that part was critical for performing the simulations of interest. The problems can be grouped into:

- **pre-processing problems**, concerning the preparation of data before running a simulation,
- **simulation issues**, related to strategies used to improve performance during runs, and
- **post-processing problems**, involving the interpretation and analysis of the simulation results.

#### Original Model by Samsó and Gracía

The BIO\_PORE model provided by Samso and Garcia [19] is based on the domain structure and sub/models described in chapter 2 and was implemented in the COMSOL Multiphysics platform. In the work they did, these two authors made simulations of the behavior of a constructed wetland over a period of three years. The initial conditions and the parameters used for the interpretation of the results they used will be shown below.

**Initial conditions** The fraction that composes the COD that comes in were divided from the values reported by Henze [31]. According to the data, the percentages of each COD fraction were:

- 15% SF
- 20% SA
- 5% SI
- 50% XS.m
- 0% XS,f
- 10% XI,m
- 0% XI,f

Another important point was to minimize the influence of arbitrary initial conditions on the distribution of bacteria, to do so the initial values of all bacterial groups and substrates were set to very small concentrations, much lower than typically expected in a granular medium, this was also a good factor in terms of replicating the start-up phase of the model.

The inflow concentrations of all other considered substances are shown table 3.1 with the exception of dissolved oxygen (So) that was taken from the studies of Garcia on the same pilot wetland. Also the initial concentration of oxygen was set to zero, since wastewater subjected to primary treatment typically contains very low level of dissolved oxygen [32]

Contaminant removal efficiency To study the presence and concentration of each bacterial group within the wetland, it was necessary to estimate the total biomass concentration of each group. The effective biomass that will be expressed in kg of COD was calculated by the interpretation of the concentration along the longitudinal section of the domain and later multiplying by the width of the wetland. The calculated biomass was later normalized by dividing it by the total wet volume, therefore obtaining a value expressed per cubic meter of granular material.

During the simulations, the concentration of the wastewater constituents were monitored both inside the domain and at the outlet point, which made it possible to evaluate pollutant removal efficiency as well as potential inhibitory effects on the bacterial groups.

In order to determine the removal efficiency of COD, nitrogen and sulfur, the initial concentration values of these compounds had to be defined. In the case of COD

and sulfur, the process was done by adding all the values and using the formulas ??. On the contrary, for nitrogen, the calculation required taking into account that some of the total biomass and some of the organic fractions contain a certain quantity of nitrogen, given in percentages, they are denoted by the composition of the parameters, they were all included in the calculation of the initial nitrogen concentration that is expressed in the formula 3.3.

$$COD_0 = \sum COD_i \tag{3.1}$$

$$S_0 = \sum S_i \tag{3.2}$$

$$N_0 = \sum (i_{N,sost} \cdot \text{fraction}_i) \tag{3.3}$$

It is important to highlight that not all organic nitrogen is immediately available for bacterial growth or for nitrification and denitrification processes, because it first has to be released through degradation of organic compounds in which is bound.

**Stability indicators** Three indicators were used to assess bacterial stability:

- 1. the consolidation of the total biomass amount within the wetland domain,
- 2. the stabilization of effluent pollutant concentrations, i.e., when no further variations occur in the outflow, and
- 3. the stabilization of Shannon's diversity index [33], expressed in equation (3.4):

$$H = \sum \left(\frac{X_i}{X_{tot}} \ln \frac{X_i}{X_{tot}}\right) \tag{3.4}$$

where n is the total number of functional bacterial groups,  $X_i$  is the biomass of group i, and  $X_{tot}$  is the total biomass of all groups.

#### Santelia's BIO\_PORE adaptation

This subsection synthetizes how Santelia [] obtained the BIO\_PORE results that serve as reference for the present thesis. The implementation is based on the Samso and Garcia formulation explained above and it is also run in COMSOL Multiphysics, the work Santelia did includes:

- 1. establishment of a long-term baseline to dynamic equilibrium
- 2. rigorous data handling to hand over consistent initial states to subsequent studies
- 3. a correction to one reaction-rate sign in the carbon matrix
- 4. a set of one-year step-load experiments to probe resilience and performance under abrupt influent changes

Baseline to dynamic equilibrium Santelia's first step was to execute the three-year simulation performed by Samso and Garcia using the BIO\_PORE reactive transport framework. The model is in charge of the COD partitioning into soluble and particulate fractions, therefore, the activity of the key microbial guilds, like heterotrophs, fermenters, acetotrophic sulfate reducer, acetotrophic methanogens and nitrifying autotrophs, and the stoichiometrically coupled production and consumption of intermediates, most important ones are acetate and sulfide. The three year run is used both purge transients that might come from the arbitrary start up conditions and also helps characterize a steady behavior using three type of stabilization criteria, the first one is consolidation of total biomass, second stabilization of inflow concentration and finally the stabilization of Shannon's diversity index H [33]. The terminal fields of all state variables at the third year represent the reference state.

Initial-state transfer and data handling In order to reuse the final fields of the first three year simulation as initial conditions for the additional studies, then Santelia made a comparison between several export and reimport strategies. Some of the exported fields introduced special artifacts in reinterpolation; in consequence, two steps were adopted:

1. A short transition study initialized exactly the same as the three year terminal state

2. Subsequently, the studies were started from the transition study's terminal fields, making sure it avoids discontinuities between plotted initial fields and the values at time zero ensure the numerical consistency from the first step and on.[18]

Model correction (carbon matrix) Later, the verification of the reaction network was done, and during this verification Santelia identified a sign error that slowly affected the slowly biodegradable particulate in solid phase, Xs,f. In the original model, the heterotrophic lysis term was contributing with the wrong sign, which implies that there is net consumption rather than production of Xs,f. The correct stoichiometric entry restores the Xs,f production from the heterotrophs lysis, and this aligns with the implementation of the conceptual model of Samso and Garcia [16]. Simulations of the three year, both uncorrected and corrected showed some small changes in the bulk particulate COD, the mean Xs,f differs on domain by a few percent but there is anyway a sizeble3 redistribution across guilds, for example on heterotrophs there was a variation of about 70% in some zones. Two independent checks confirmed the veracity of the correction:

- 1. The steady segment variability of Shannon's index remained low and reproductable
- 2. Integrated carbon balances (inflow export added to domain storage) increased by a consistent amount and restoring the particulate production pathways [18]

Step-load experiment design From the corrected reference state, Santelia design a continuous one year study with a reference case of So and 3 different load scenarios with different increments of incoming COD, +10%, +30% and +50%. This step was applied on day 10 with a short ramp of about 10 minutes, that is because nitrogen species are coupled to organic loading in the BIO\_PORE, the total inflow nitrogen was increased accordingly. The nominal inflow values reported by Santelia [18] on her thesis were: COD = 260 mg/L (S0) and 286/338/390 mg/L for +10/+30/+50%, with total N rising from 64.3 mg/L to 65.0/66.5/67.9 mg/L.

These scenarios probe the resilience window while keeping COD/S ratios within the coexistence range discussed by Samsó and García [17].

**Solver control and numerical choices** The transients are stiff in the flushes, moreover in the rapid acetate and sulfide excursions. Santelia limited the maximum

timestep with the COMSOL's time integrator, and with it, it is possible to avoid solver stalls and at the same time mitigate spurius overshoots that might happen during the sharp transients. This cap was tuned iteratively because one that was too loose was causing intermittent failure to converge and on the contrary, one that was too strict was computationally expensive. The adopted bounds balance robustness and wall time [18].

**Performance metrics and stability criteria** Santelia evaluated system behavior using:

- 1. Biomass consolidation: total (and guild-resolved) biomass trajectories approaching steady envelopes;
- 2. Effluent stabilization: flattening of outlet concentrations for regulatory surrogates (e.g., COD, total N);
- 3. Shannon diversity  $H = \sum_{i} \left( \frac{X_i}{X_{\text{tot}}} \ln \frac{X_i}{X_{\text{tot}}} \right)$  [33] to track ecological structure.

At the same time, mass balances of C were done by integrating domain storage and cumulative inflow export to verify global consistency.

Key responses under load steps Immediately after the COD step, the fermenters bacteria grow due to the higher availability of fermentable substrate which raises acetate Sa, and this gives power to the growth of acetotrophic sulfate reducers bacteria and methanogens bacteria, the first one produces sulfide which inhibits the nitrifying autotrophs and partially the methanogens, this explains the observed decline in nitrification capacity.

Across all the scenarios that Santelia examined [18], the COD/S ratios always remained in the coexisting window that was reported by Samso and Garcia [19], so the acetotrophic sulfide reducers and the methanogens bacteria persist without competitive exclusion. On the other hand, total biomass increases with step magnitude and takes longer to stabilize, the results show that it takes about 7 months for the +10% and about 8 months for the +30% and +50%.

The inert particulate Xi accumulates close to the inlet, which reduces local porosity and moves the centroid of the active biomass downstream. Within the analyzed reach, this change does not cause hydraulic failure but it does narrow the safety margin because it moves the majority of the reaction zona to a place closer to the outlet.

The performance of the inflow shows slight changes that tend to decline modestly relative to So, for example, the COD removal decreases from about 91 to 88% for over +50% and the total N removal on the order of 17 to 19%, this data is consistent with the acetate plumes extending further downstream and with the sulfide mediated inhibition of Xa [18].

Methodological takeaways from the reference model Santelia's study establishes a consistent reference state for BIO\_PORE with:

- 1. corrected carbon stoichiometry
- 2. reproducible initial-state transfer via a transition study
- 3. solver settings that stabilize stiff transients

The step-load experiments prove that the wetland can absorb shocks of COD with a limited time-average efficiency penalties over one year, at the same time, highlighting mechanisms that govern the resilience, like acetate-centered carbon pathways, sulfide inhibition of nitrification, and progressive downstream displacement of activity due to particulate accumulation. The results and datasets create the basis upon which the following adaptations and scenarios analyses can be constructed [18, 19].

### Model adjustments implemented

The numerical model used in this study was not applied exactly as the ones received, instead some adaptations have to be made in order to combine both models and to make them suitable to represent the specific conditions of the case study. The adjustments made followed a structure sequence which first ensured the hydraulic behavior of the system, followed by the incorporation of the biochemical transformation applied in a way that mirrors the conditions of an unsaturated vertical flow constructed wetland (VFCW). This methodological choice allowed both hydraulic and biochemical processes to be consistent, which made it possible to later analyze the combined performance of the system.

#### Hydraulic model

The first part on the adjustments done was to create a dedicated hydraulic description of the inflow that in reality enters the domain. Following the approach

described in Montgna's work [28], the Richards equation was selected to represent the flow conditions in the variably saturated bed, this is expressed in COMSOL in terms of Darcy's velocity. The Richard's formulation is essential for this type of system as it combines the continuity equation for the cases of water with pressure saturation and also for the cases in which water content changes with the matric pressure head. This allows the system to assimilate the real infiltration dynamics of a porous medium that alternates from saturated to unsaturated states along the day during the feeding cycles.

In Montagna's earlier work, the inflow was idealized with distribution pulses that matched the maximum daily flowrate, this simplified representation works in that case as it still represents the hydraulic load and at the same time reproduces the maximum hydraulic stress that the bed can experience. As it was mentioned before the flushes done by Montagna were for 25 m3/day devided into 9 equally distributed flushes, each lasting 300s.

In the present work, this representation was redefine to introduce more realistic conditions, using real measure daily volumes, to do so, two main corrections had to be applied, the first one is that the interpolated function no longer works because contrary to the two days simulation performed by Montagna, this one aims to simulate 6 months, which would imply a heavy computational load. The second one was, rather than assuming that every day has the same inflow, the real inflow of each day was divided by the standard volume of a single flush and the result was rounded to the nearest integer to obtain the daily number of pulses for each day, ensuring that the maximum load is not exceeded but reproducing real daily load variations.

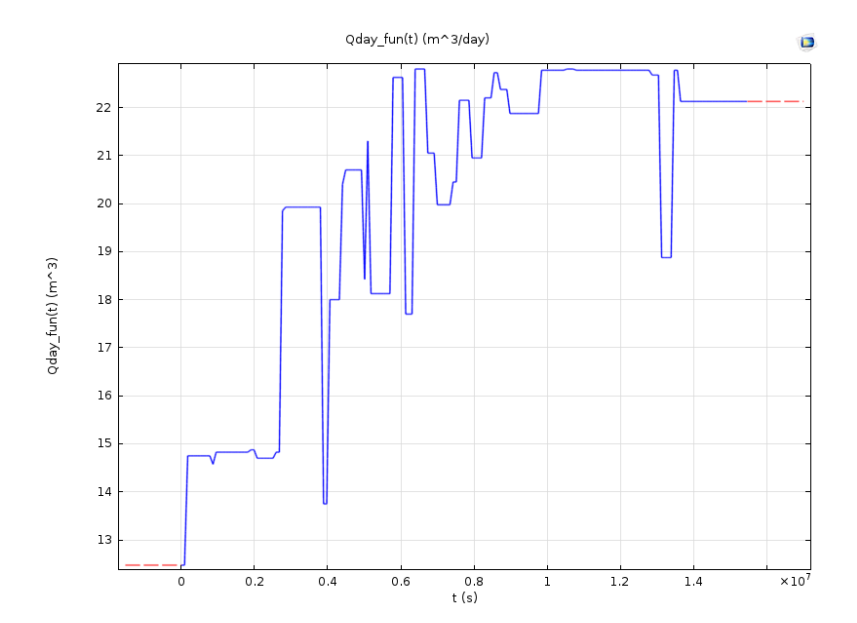


Figure 3.15: Daily flowrate function

To do so, it was necessary to introduce an interpolated function of the daily inflow conditions as shown in 3.15, also some auxiliary variables that distributed the pulses within a day of simulation cycle 86400 seconds. Each cycle begins with 300 seconds of inflow with constant velocity imposed, this is followed by a zero inflow period lasting until the beginning of the next pulse, the duration of each cycle is the variable depending on the daily required number of pulses, the quantity of pulses is distributed as seen in the picture 3.17 and then the density of daily flushes is seen in the picture 3.16 to more detail. The only discrepancy with this method is that since pulses must be integer numbers, some minor differences were introduced but always keeping a very small margin error.

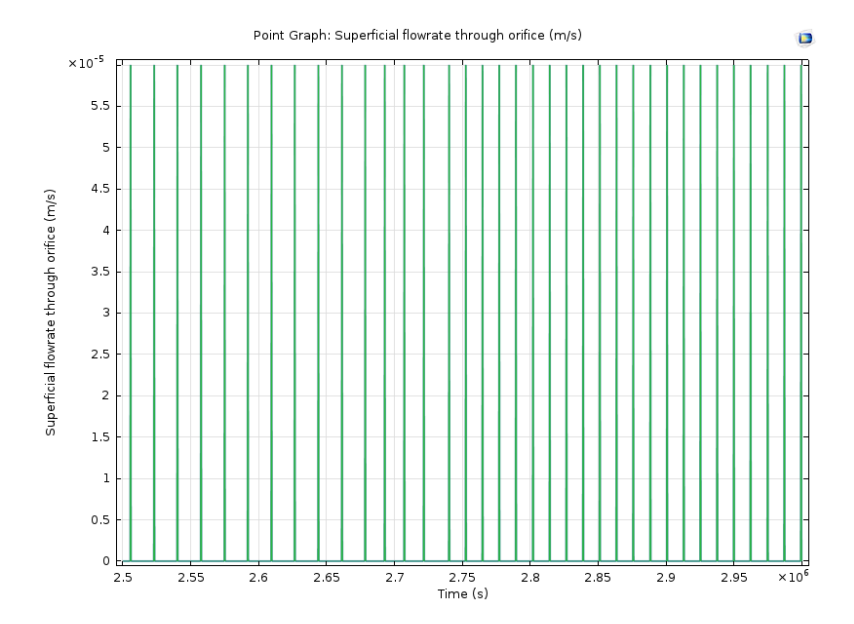


Figure 3.16: Q inlet for 6 days zoom

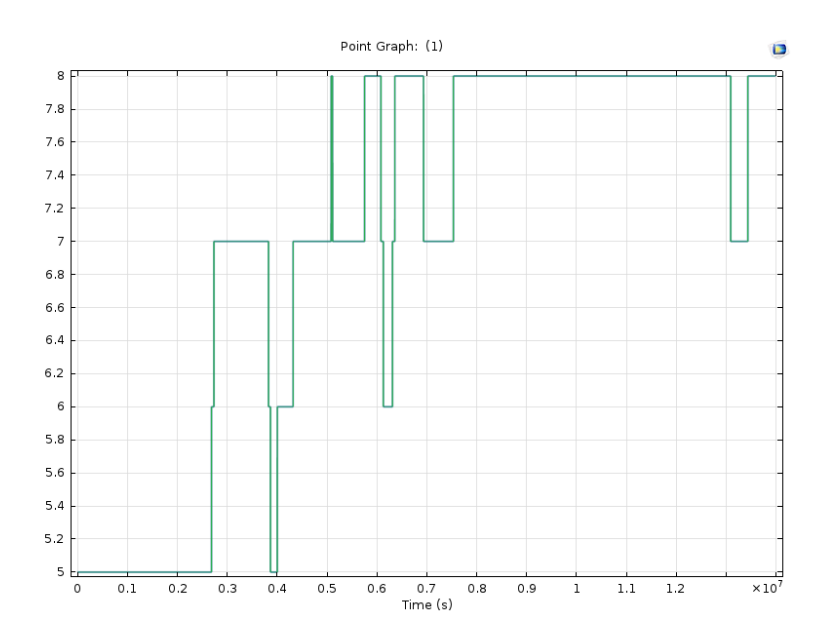


Figure 3.17: Total daily number of pulses

The correct implementation of the inflow scheme was verified through a daily mass balance, this is a very important verification because the timing and frequency of pulses strongly affect all the system behavior including both hydraulic and biochemical. In vertical flow constructed wetlands, when flushes are shorter and more frequent, oxygen transfer and limited clogging are both promoted, on the contrary, long rest periods favor anaerobic transformations. Comparing the daily water balance obtained from COMSOL with measured filed data so it was confirmed that the adjusted inflow model reproduced the expected behavior, which gave confidence to follow with the biochemical simulations. Later on, once the biochemical model was stablished, and calibrated some discrepancies were found in the functioning of the system which led to a further modification from Montagna, as inlet and outlet are not aligned the 1D reproduction using the inflow velocity calculated by Montagna failed to represent any point inside the wetland as it neglected the effect of full bed filling, therefore a new velocity was calculated as

$$\frac{25 \text{ m}^3/\text{day}}{9 \text{ flush/day}} = 2.77 \text{ m}^3/\text{flush}$$

$$\frac{2.77 \text{ m}^3/\text{flush}}{300 \text{ s/flush}} = 0.0092 \text{ m}^3/\text{s}$$

$$\frac{0.0092 \text{ m}^3/\text{s}}{153 \text{ m}^2} = 0.0000603 \text{ m/s}$$
(3.5)

This implied also removing the first 10 cm of depth which as Montagna's work displays that are the part that receives faster and directly the flushes so the regular inflow starts the 10 cm down with the new calculated velocity.

### Biochemical model

Once the biochemical model was calibrated, the next part was adapting the biochemical model, as known before, the BIO\_PORE model was originally developed for a horizontal flow under saturated construction wetlands, due to that fact a few adjustments had to be done in order to adapt it to simulate the present one-dimensional vertical unsaturated case.

The first adjustment concerned the molar weight units, in COMSOL, for the chemical formulation, specifically in this case the Transport of Diluted Species interface must be expressed in mol/m3, while in the original model they were in kg/m3. This required converting all inflows and state variables to the correct units, referring to the point in which they were supposed to be use either molar or weight. The conversions used depended on the compound that was being referred to, the ones used are displayed on table 3.1.

Table 3.1: Molar masses used for unit conversion in the biochemical model

Compound	Molar mass (g/mol)
$O_2$	32.00
$\mathrm{NH_4}$	17.00
$NO_3$	62.00
COD	113.12
$SO_4$	96.00
$H_2S$	34.00

This conversion was not only a numerical requirement but also it was a fundamental step to ensure that there is consistency with the biochemical reaction network as all the stoichiometric coefficients are defined on molar units.

A second adjustment was the partitioning of the COD fractions. In the original model, the COD was distributed according to typical assumptions of saturated systems. Nevertheless, real measurements of total and soluble COD in this work showed that there is a bigger fraction of COD that was soluble and therefore the partition was changed to the percentages shown in table 3.2.

**Table 3.2:** COD fractionation adopted in the biochemical model

COD fraction	Percentage (%)
Sa (soluble acetate)	45
Sf (soluble fermentable COD)	15
Si (soluble inert COD)	5
Xi (particulate inert COD)	10
Xs (slowly biodegradable COD)	25

This change had an important impact on the dynamics of microbial guilds, since soluble fractions are more readily available for uptake, while particulate fractions occur during slower hydrolysis. Increasing the share of Sa made the model more sensitive to oxygen availability and to the activity of fast-growing heterotrophs, which is consistent with observed field behavior.

The final but most important change was the introduction of oxygen dynamics, in unsaturated conditions, oxygen enters through two mechanisms:

- 1. entrainment during the injection of water pulses
- 2. diffusion from the atmosphere through the partially filled pore space

Both of this processes are difficult to represent in a one dimensional model but to fix this problem, oxygen availability was added with a saturation-dependent aeration function:

Aeration = 
$$k \cdot f_{\text{oxy}}(\theta) \cdot (S_{O,\text{sat}} - S_O)$$

where k is a calibrated constant,  $f_{\text{oxy}}(\theta)$  is a function that scales from 0 to 1 depending on the water content  $\theta$ ,  $S_{O,\text{sat}}$  is the oxygen solubility in water at 20 °C ( $\approx 9 \text{ mg/L}$ ), and  $S_O$  is the actual dissolved oxygen concentration. The function  $f_{\text{oxy}}(\theta)$  ensures that oxygen transfer is promoted under unsaturated conditions and reduced when the bed is near saturation. The shape of this function is shown in the following figure 3.18.

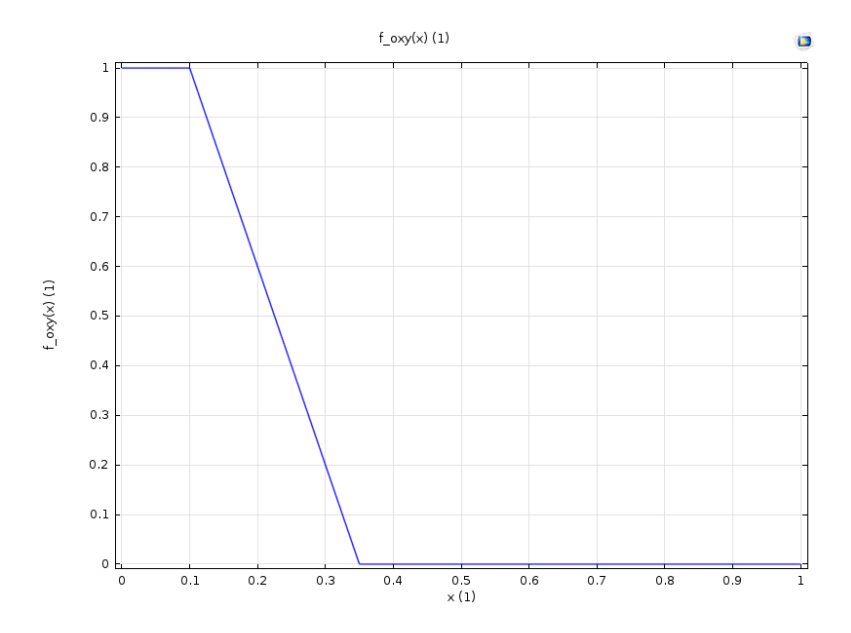


Figure 3.18:  $f_o xy$ 

Adding to the changes, the initial concentrations of the microbial groups were set to small values, in order to simulate start-up conditions and allow microbial communities to evolve dynamically, but the are slightly higher that the ones implemented by the original BIO\_PORE model. This approach avoids biasing

the system with artificially high initial biomass levels, while ensuring that each functional group is represented from the beginning:

Table 3.3: Initial concentrations of microbial groups

Bacterial type	Initial concentration (mg/L)
$X_{Ai}$	1
$X_{Hi}$	1
$X_{FBi}$	1
$X_{AMBi}$	1
$X_{ASRBi}$	1
$X_{SOBi}$	1

Finally, instead of assuming constant influent concentrations, the measured influent data were implemented directly in the model. This ensured that the simulated system responded to realistic boundary conditions, making it possible to later compare results with field measurements and evaluate the predictive capability of the model.

#### Simulations performed

The simulation performed in this work followed the same general procedure as in [28], but with adjustments required by the one–dimensional vertical configuration adopted. The verification and calibration process was structured to first ensure that the hydraulic regime driven by the intermittent flushes was correctly reproduced, and subsequently to confirm that the coupled biochemical transformations produced realistic contaminant removal behavior. Unlike the structure in which hydraulics and biochemistry are simulated in fully independent stages, here the two components were activated together, since the biochemical reactions cannot be validated without an accurate hydraulic description of the inflow and water content. Nevertheless, for clarity the methodology and results are presented in two steps: first the hydraulic verification (with pulse distribution and daily mass balance), and then the hydraulic–biochemical combined simulation with COD and nitrogen transformations.

Hydraulic verification: pulse feeding and daily mass balance The first step consisted in verifying that the inflow pulses were correctly implemented

and that the daily water balance closed within acceptable error. The Richards equation, expressed in terms of Darcy's velocity, was used to describe variably saturated flow. The basin was driven by a pulse schedule consistent with operational conditions: each day receives a maximum of  $25~\mathrm{m}^3$  (corresponding to one of the four unsaturated units of the full–scale system), distributed in several flushes of approximately  $2.77~\mathrm{m}^3$  each, lasting  $300~\mathrm{s}$ . Between pulses, the inflow boundary condition was set to zero so that the bed could drain and return to unsaturated conditions before the next pulse.

In general, the COMSOL model was constrained to resolve these sharp inflow events. The solver time step was limited to a maximum of 60 s to guarantee that each 5-minute pulse was sampled by several internal points, and with this constraint, avoiding numerical smoothing of the rectangular inflow profile. Without this precaution, the software would every once in a while take steps longer than the pulse itself, which would miss an entire inflow events and producing and that would produce unrealistic mass balances.

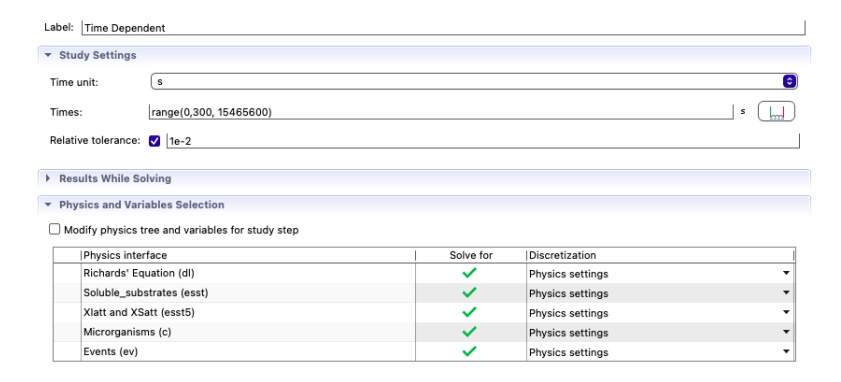


Figure 3.19: Solver configuration

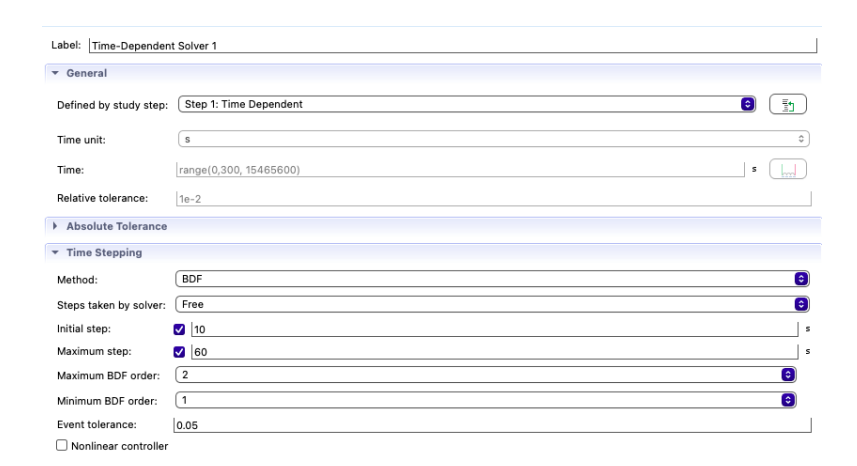


Figure 3.20: Time stepping configuration

Verification of the hydraulic implementation was performed through a daily water balance. The inlet flux was integrated over the pulse windows to obtain the daily volume entering the basin, and the outlet flux was integrated over the same period to obtain the daily discharge. The difference between inflow and outflow represents the transient storage in the porous medium, which should remain well below the pore volume to guarantee that the bed is never saturated throughout the cycle. This procedure follows exactly the reasoning outlined by [28].

In the 1D vertical model, the results showed that the given daily inflows were accurately reproduced and that the outlet flux matched the expected values within a very small margin of error. The transient storage fluctuated during the day but always returned to its initial value by the end of the 24 hour cycle, demonstrating that the system remained in a periodic regime consistent with the physical operation of the wetland. This verification confirmed that the hydraulic driver was reliable and that the model could be used as a basis for simulating the biochemical transformations.

Coupled hydraulic—biochemical simulations Once the hydraulic representation was verified, the biochemical reactions were activated, and the system was simulated in its coupled configuration. In this phase, the focus was on reproducing the observed behavior of COD and nitrogen species under the validated hydraulic regime. This approach reflects the fact that the biochemical module cannot be meaningfully tested without the correct hydraulic context: substrate availability, residence times, and oxygen transfer all depend directly on the pulse—driven infiltration pattern.

The biochemical model included the COD fractions (Sa, Sf, Si, Xi, Xs) defined previously, that together with the microbial guilds responsible for their transformation. The nitrification—denitrification sequence was represented explicitly, with ammonium oxidized to nitrate by nitrifiers in the presence of oxygen, and nitrate subsequently reduced under more anoxic conditions. Oxygen availability was controlled by the saturation—dependent aeration function, which increased gas transfer during unsaturated phases and reduced it when the pores approached full saturation. The calibration of microbial growth and death coefficients ensured that the activity levels reflected those of biofilm—dominated vertical—flow systems, rather than the much higher values typical of completely mixed suspended biomass.

The simulation of both hydraulic and biochemical at the same time was run for the entire monitoring period, with measured daily inflow values used as inputs. For each day, the number of pulses was calculated from the real flowrate and applied in the model. At the same time, the influent concentrations of COD,  $NH_4^+$ , and  $NO_3^-$  were introduced as time–dependent boundary conditions in interpolated functions, following the measured dataset. In this way, the model reproduced not only the correct hydraulic load but also the variability in pollutant concentrations actually observed during operation.

The outputs analyzed included:

- daily COD,  $\mathrm{NH_4^+}$ , and  $\mathrm{NO_3^-}$  at the outlet compared to measured concentrations,
- depth-profiles of substrate and biomass to visualize how reactions were distributed along the vertical profile,
- daily mass balances of COD and nitrogen species, computed as the difference between integrated inflows and outflows, and
- time series of oxygen concentration, showing the alternating cycles of consumption during pulses and partial re—oxygenation during resting phases.

The results demonstrated that the model was able to reproduce the main trends observed in the field. COD removal efficiencies were consistent with measured values, showing the expected dominance of soluble COD removal in the upper layers of the bed. Ammonium decreased significantly due to nitrification during pulse phases, while nitrate appeared as a product, with subsequent partial removal linked to denitrification in deeper layers. Oxygen dynamics followed the cyclic pattern imposed by the flushes, with peaks of concentration immediately after each pulse and depletion during the resting intervals.

# Chapter 4

# Results

This chapter presents the results that were obtained from the numerical simulations that were done with the adjusted combination of the models done by Montagna and Santelia [28, 18] in COMSOL Multiphysics. The discussion of the results is organized in two main parts: The first one, contains the hydraulic verification of the one dimensional variation of the vertical unsaturated model model of Montagna, and the second part, includes the results of joining to the previous hydraulic metioned model with the adjusted biochemical model of BIO\_PORE that was previously adjusted by Santelia including the simulation of the COD, nitrogen and oxygen dynamics. This part displays the results of the staged methodology that was adopted, in which a hydraulic functioning had to be confirmed before analyzing the full biochemical response of the system.

## 4.1 Hydraulic verification

The first step was to verify that the hydraulic system of the model was working and its results were consistent with the expected conditions of the unsaturated vertical/glow unit. Specifically, it was tremendously important to confirm that the numerical series of pulses imposed at the inlet reproduced the real measured inflows and represented the design logic of daily feeding through flushes performed by the pump.

In order to implement this scheme, as described in the methodology, the system produces daily inflows that are devided in fixed flushes of about 3 m3 of wastewater that are spread in the basin for exactly 5 minutes, and then between flushes the

system remains with no inflow, which allows the system to drain and re-aerate the pore spaces. To verify the implementation of pulses for different daily total volume inflows, a daily water balance was implemented, this process was done by integrating the inlet flushes over each 24 hour cycles and ensuring is closeness to real data inlet information. Also a mass balance check was be performed, to do this the verification says that the difference between the inlet and outlet has to be the storage volume and this ensures that the bed never approaches saturation between pulses.

The time dependent Darcy's velocity confirms the expected pattern, which is a sharp increment of inflow that lasts 300 seconds, which are the inflow windows, that are next followed by a rapid decline once the pump in real life is turned off and then a space with zero inflow in-between pulses. The velocity is then propagated in the porous medium and gets dissipated after only a few minutes after each pulse, consistent with the design assumption, which said that the unsaturated flow regime is dominated by percolation.

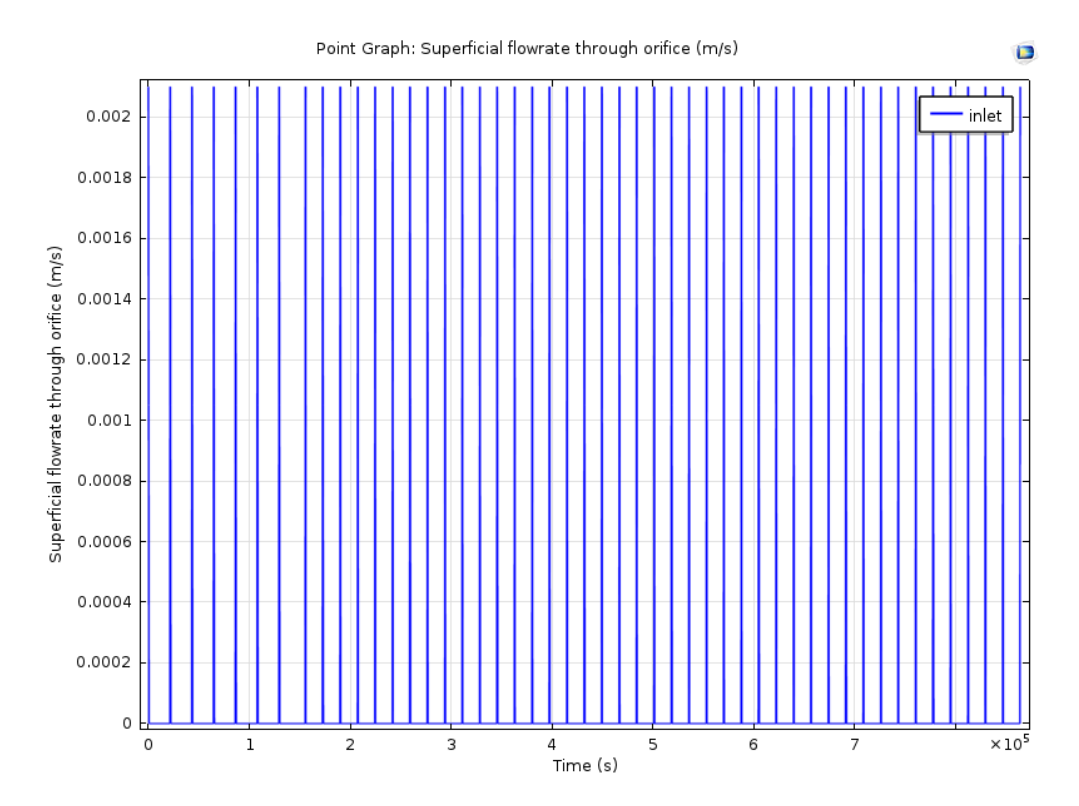


Figure 4.1: Series of inlet pulses for 30 days

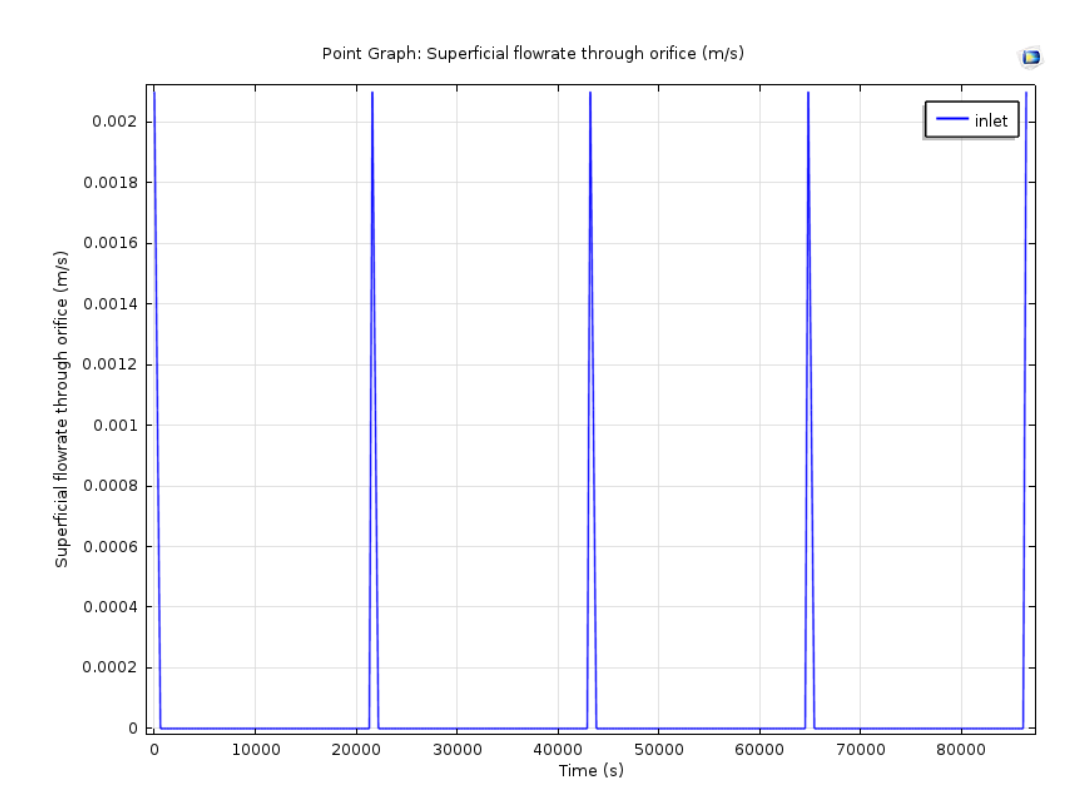


Figure 4.2: Series of inlet pulses for 1 days

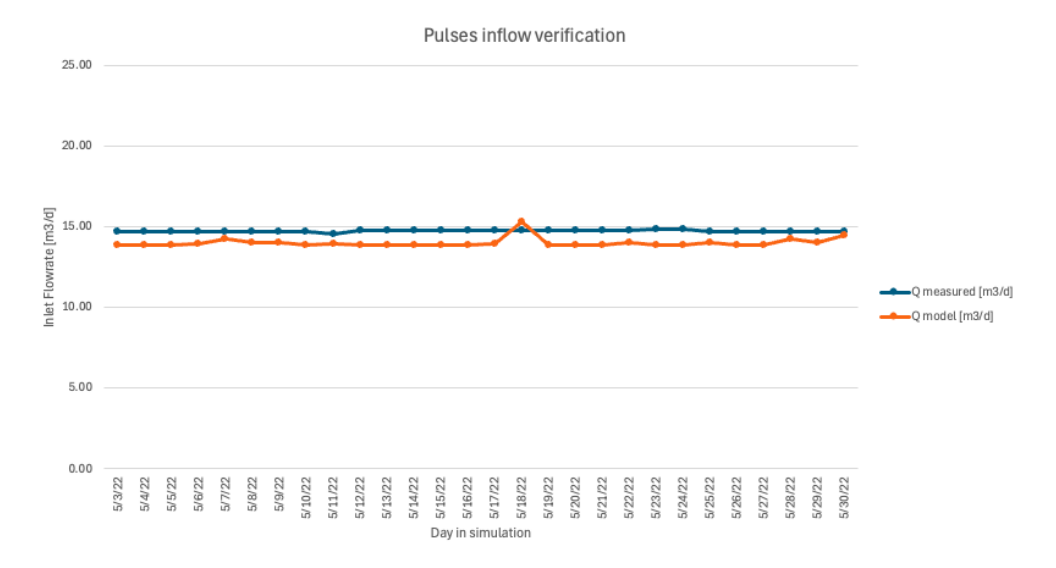


Figure 4.3: Flushes inflow verification

The pictures below 4.4 shows that the water content and effective saturation indeed follow the expected behavior, after each pulse, the pore spaces is filled partially and then progressively drains until the arrival of the next inflow event, and this behavior was consistent during the following days, which proves that the wetland indeed operates under unsaturated conditions.

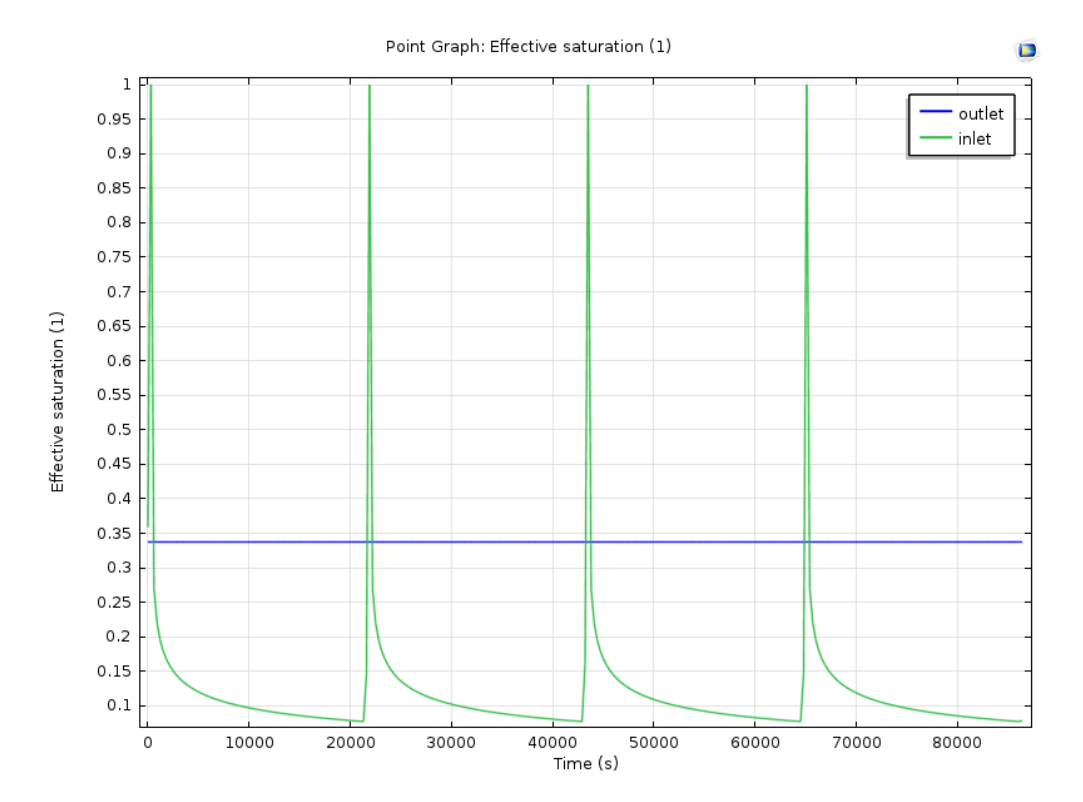


Figure 4.4: Effective saturation over one day

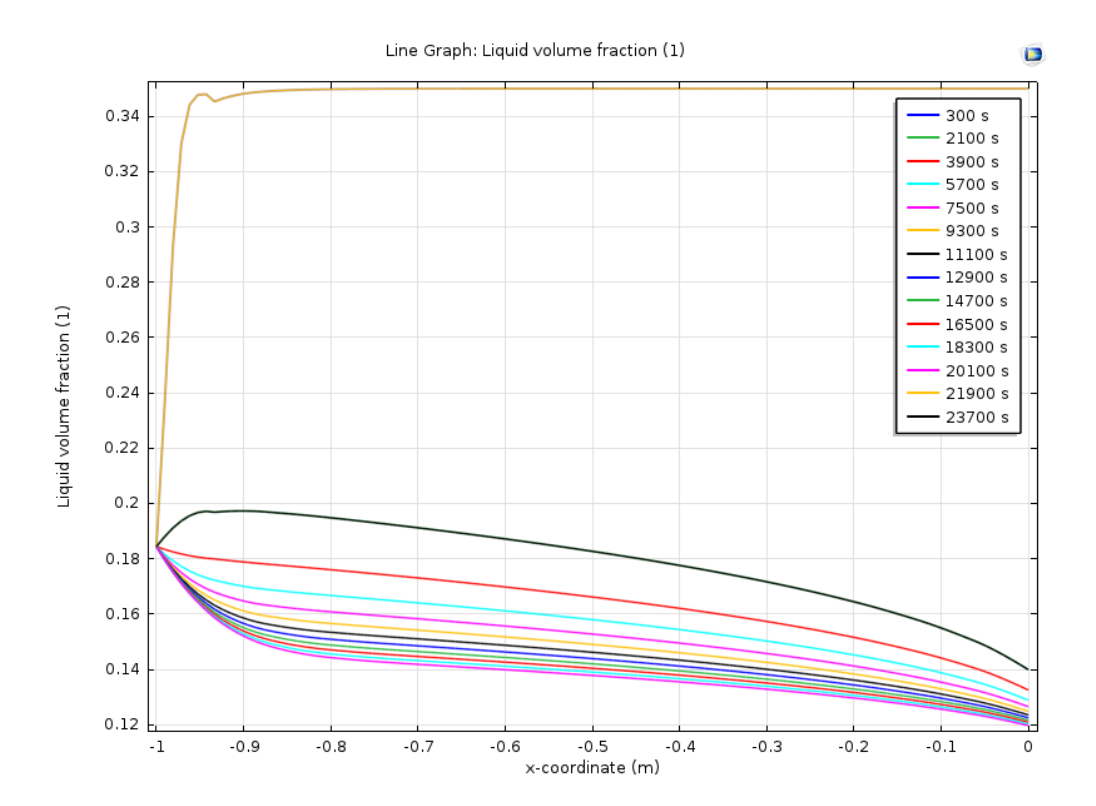


Figure 4.5: Liquid volume fraction over one flush for the first hydraulic simulation

The inlet pulse series ?? demonstrates that the dosing strategy imposed in the model successfully reproduces the experimental pulsed loading of the VFInsat system. The flush frequency and amplitude are consistent with the measured operation of the Lesvos pilot plant, validating the imposed boundary conditions. Effective saturation dynamics (4.4) reveal rapid increases following each flush, followed by drainage toward unsaturated conditions, which are characteristic of vertical flow wetlands. The liquid volume fraction (4.5) shows that drainage occurs efficiently, confirming that the selected Van Genuchten parameters allow for a realistic representation of infiltration and emptying processes. This hydraulic reliability is critical for coupling with the biochemical model, as oxygen replenishment depends directly on the alternation between saturated and unsaturated conditions.

In general, the hydraulic verification consisted on applying the methodology for accurate pulses during a day and checking that indeed the 1D vertical model correctly implemented this intermittency in the feeding strategy and that the Richards equation captures the infiltration and drainage cycle to correctly assimilate the real-life measured data.

## 4.2 Coupled hydraulic-biochemical results

Once the hydraulic verification was performed, the biochemical reactions were applied to analyze the behavior of both systems coupled. In order to analyze this part, some parameters were chosen for verification, among them the model includes COD divided into Sa, Sf, Si, Xs and Xi, oxygen transfer through aeration, once given the aeration term, and nitrogen transformation due to nitrification a denitrification measured in NH4 and NO3.

The daily inflows are the same ones used for the hydraulic simulation alone and they perfectly match the operational values measured in the used data, at this point is important to specify that the data was all taken from the date mentioned in the methodology, nevertheless, in this case the biggest simulation performed includes data from the 1st of May 2022 until the 31st of October 2022. For each day, both flowrates and pollutant concentrations loads were imposed at the inlet boundary as time dependent boundary conditions, making the simulation as real as possible. This allows

The most important part of the simulation was to calibrate the oxygen aeration, this part was done with the first simulation and the aim was to arrive to a oxygen fluctuation that helped the constructed wetland receive oxygen to saturation point in the moments where the wetland itself was not saturated and that this saturated condition helped create enough oxygen to reach the oxygen consumption rates that in reality help the reactions occur. The k obtained for the function was started first with 1 second and then the reaction time began to grow to the real response time, this was done through an iterative process that required running simulations with a time increase of about 20 seconds each until arriving to the real result, which in this case is 200 seconds and made the aeration function look like 4.6.

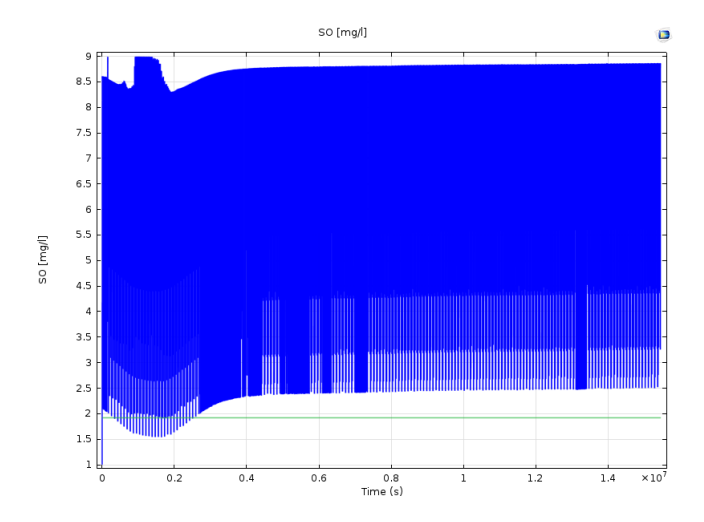


**Figure 4.6:** Simulated oxygen concentrations in time for the first hydraulic simulation

Once this part was calculated, the nitrification reaction was checked, ammonium  $(NH_4^+)$  concentrations decreased significantly after each pulse, due to the activity of nitrifying bacteria supported by the oxygen introduced during infiltration. Nitrate  $(NO_3^-)$  appeared as the main product of nitrification and was partially reduced under anoxic conditions in deeper layers. The temporal evolution of  $NH_4^+$  and  $NO_3^-$  matched the general behavior observed in the experimental data.

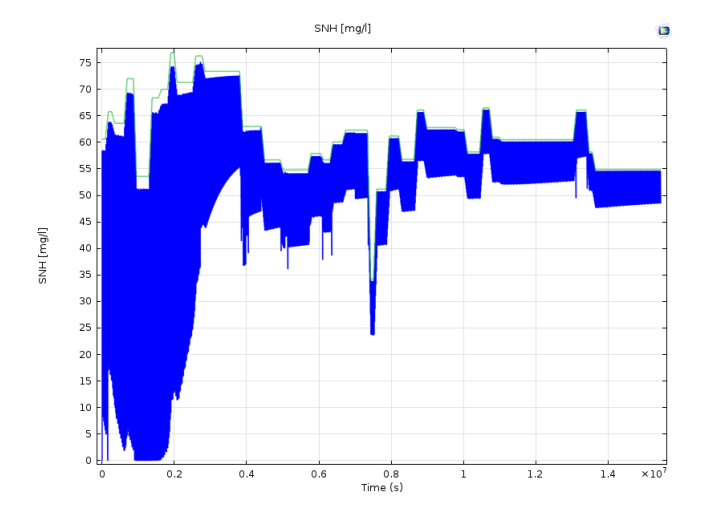


Figure 4.7: Simulated NH4 concentrations in time for the first hydraulic simulation

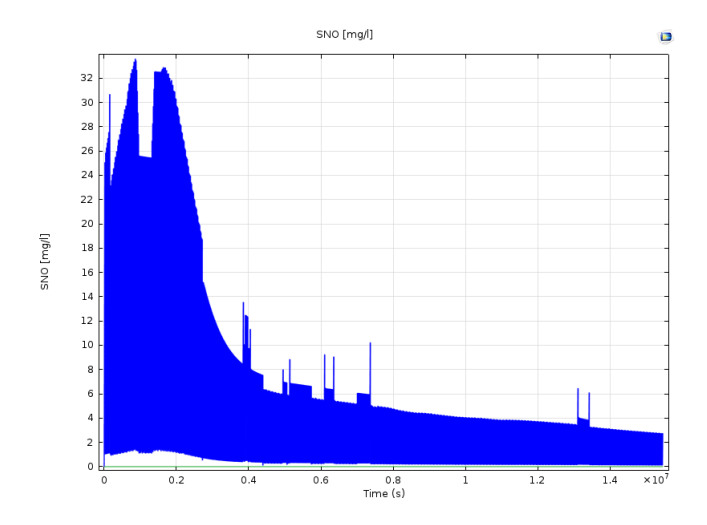
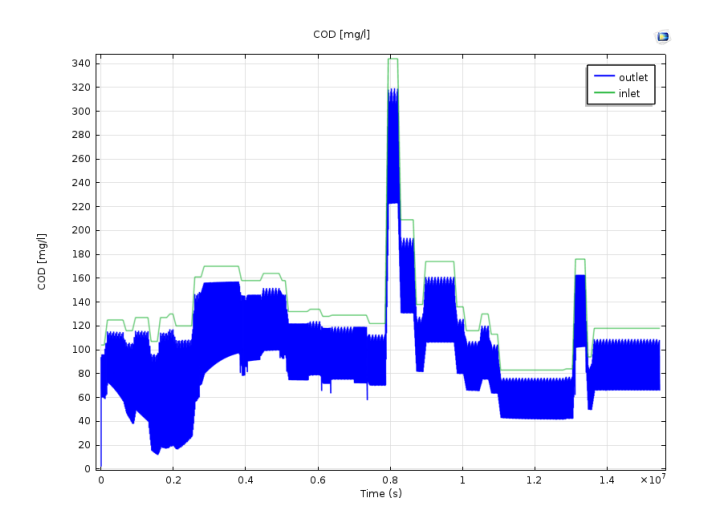


Figure 4.8: Simulated NO3 concentrations in time for the first hydraulic simulation

The results of the nitrification show, first a weird behavior give the fluctuation in the outlets which are all represented in blue, this would mean that during the moment of the flush, the exiting water would be going out with almost the exact same concentration as the one they had when they entered, this does not only divert from reality but also would not comply with government regulation. The second relevant result is that once the bacteria stabilizes, the nitrification process decreases efficiency also diverging from the real results. Given this two alerts the COD results were also checked as seen in figure 4.9



**Figure 4.9:** Simulated COD concentrations in time for the first hydraulic simulation

The initial simulation shows the interdependence between oxygen, nitrogen species, and COD dynamics. Dissolved oxygen concentrations (4.6) change strongly with flushing, with peaks after inflow events due to atmospheric refueling. Ammonium removal (4.7) is partially achieved but limited, with residual NH4 remaining after each cycle, suggesting not enough nitrification capacity. The nitrate profile (4.8) shows incomplete accumulation, which shows a combination of oxygen limitation and restricted autotrophic growth. COD removal (4.9) is significant, but residual concentrations point that hydrolysis and microbial growth processes were not fully balanced under the first parameterization. These results underline the need for model correction, particularly in the representation of oxygen transfer and microbial kinetics.

Once all the parameters were checked, a following change had to be done to arrive to the real results, after a deep analysis it was discovered that there was a problem in the hydraulic part, as a 1D model is not supposed to represent one inlet node but a vertical section in any point of the constructed wetland so the new inflow velocity was calculated as it was explained in the Methodology chapter.

#### 4.2.1 Corrected simulation

Then the simulation showed that not only the results were consistent with reality and the removal patterns are accurate as shown in the following graphs.

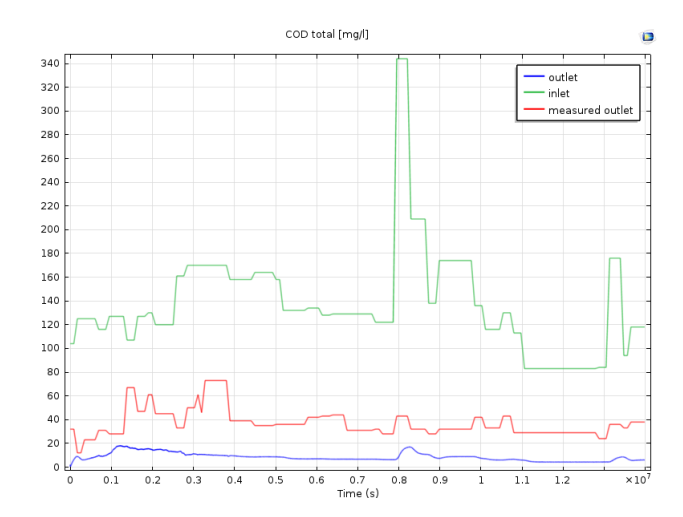


**Figure 4.10:** Simulated COD concentrations in time for the second hydraulic simulation

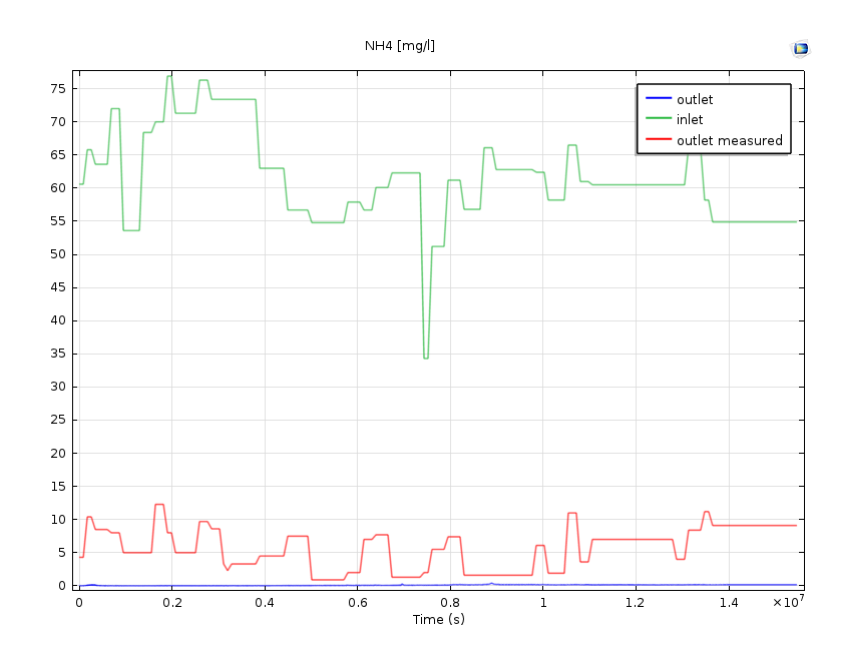


Figure 4.11: Simulated NH4 concentrations in time for the second hydraulic simulation

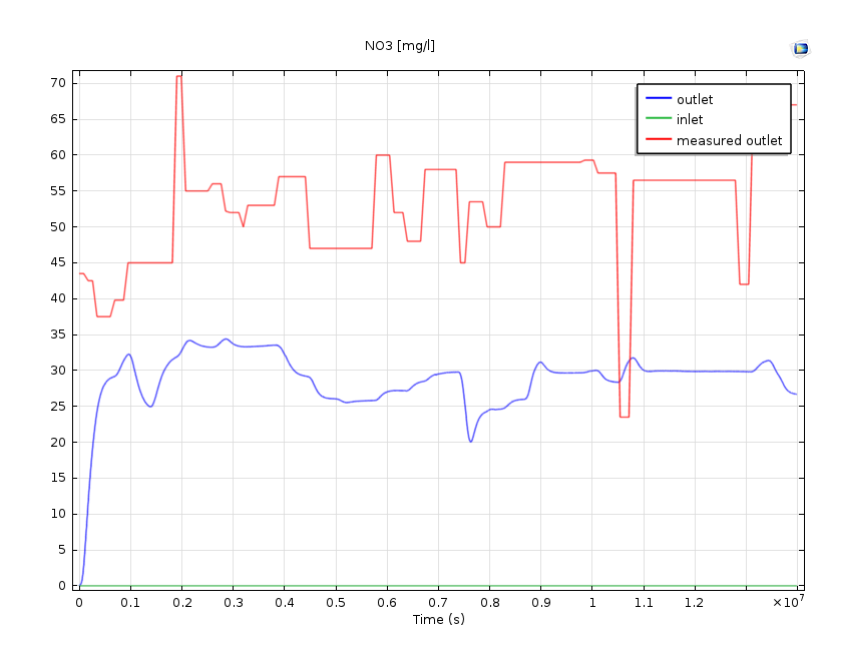


Figure 4.12: Simulated NO3 concentrations in time for the second hydraulic simulation

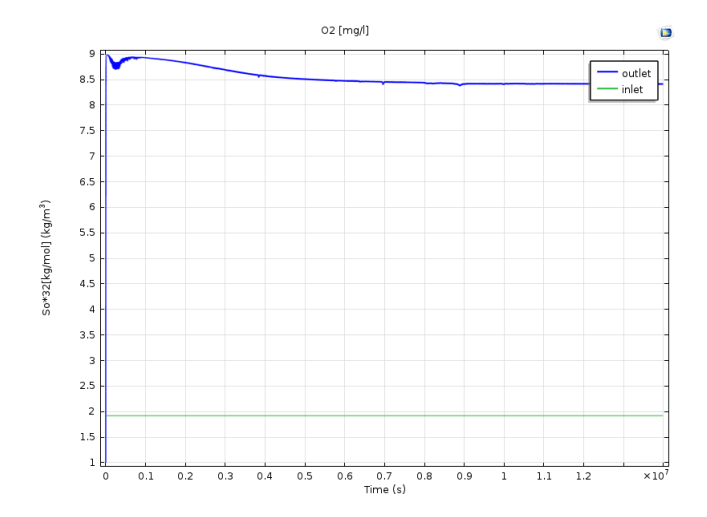


Figure 4.13: Simulated O2 concentrations in time for the second hydraulic simulation

This results show a realistic behavior of the components that were evaluated in the study so a further analysis was done, which included checking the correct behavior of the main bacterial groups shown in the following graphics

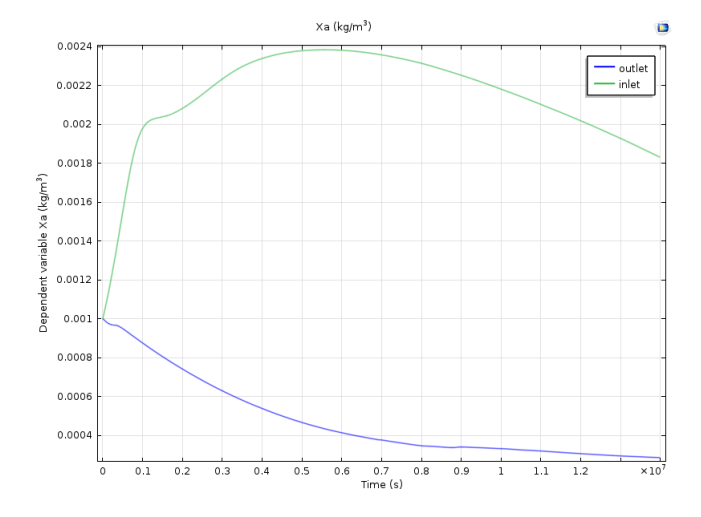
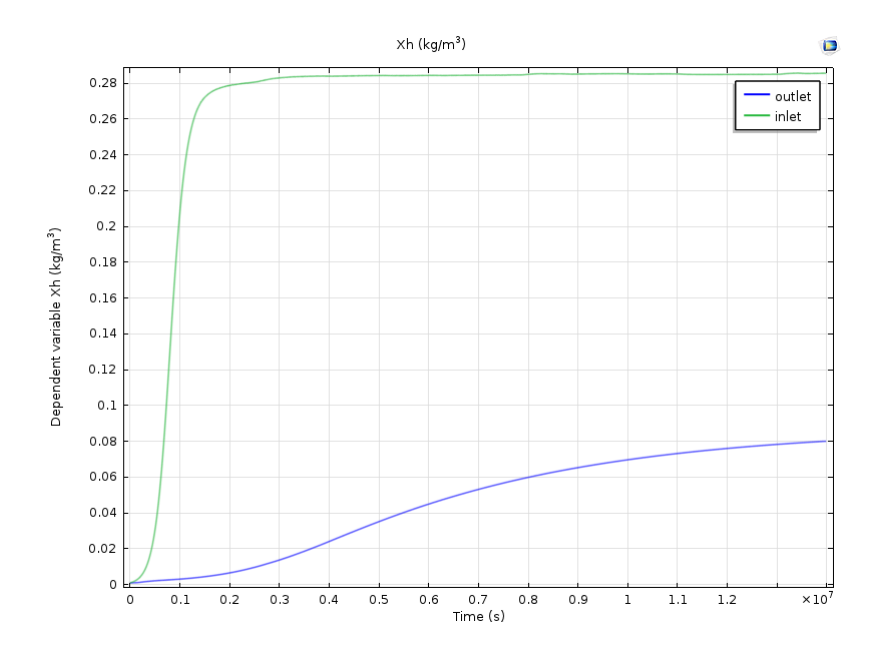


Figure 4.14: Simulated Xa concentrations in time for the second hydraulic simulation



**Figure 4.15:** Simulated Xh concentrations in time for the second hydraulic simulation

After refining the hydraulic boundary conditions and adjusting oxygen transfer coefficients, the corrected simulations show improved pollutant removal. COD concentrations (4.10) decrease more consistently, which aligns with field data trends. Ammonium levels (4.11) are significantly reduced compared to the first simulation, and nitrates (4.12) increase accordingly, indicating that nitrification was better captured. Oxygen dynamics (4.13) remain pulsed but maintain higher baseline concentrations, which is crucial keeping nitrifiers. The microbial populations (??) show stabilization: autotrophs (XA) grow steadily, while heterotrophs (XH) oscillate in relation to COD availability. These microbial patterns confirm that the biopore scheme can reproduce realistic ecological interactions within the wetland bed.

The behavior seen is similar to the expected results, the bacteria grow with the income of contaminants and later on the heterotrophs stabilize in a higher concentration while nitrifying autotrophs take longer to stabilize because they grow faster at the beginning and then lower, this also matches the fact that even though NH4 is basically going to zero, NO3 does not completly appear as expected.

Two last checks were performed, the first one was the behavior of the contaminants on a profile view during a flush. In this case the displayed profiles are for the first flush in the case of O2, NH4 and NO3, and for the last flush in the case of COD.

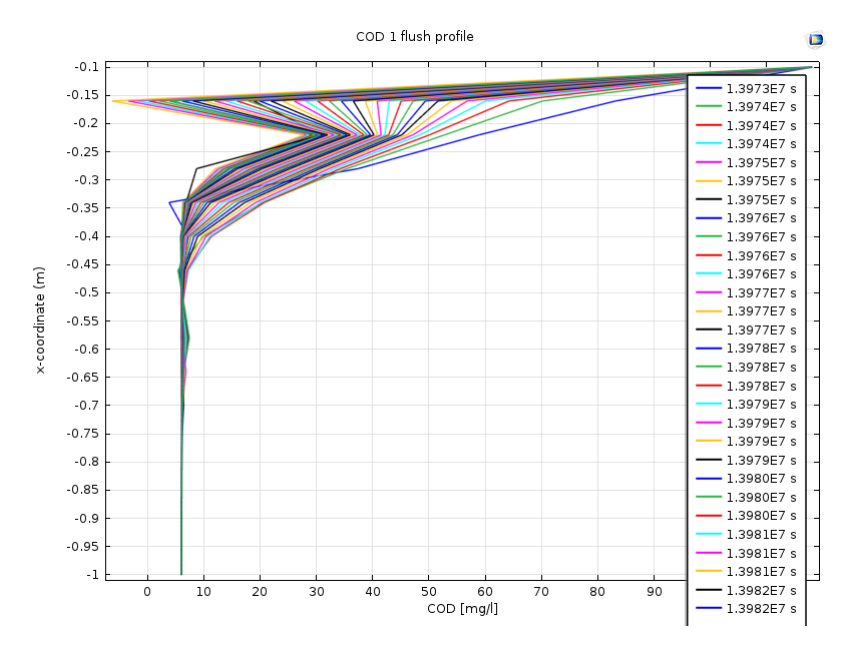


Figure 4.16: Simulated COD concentrations in profile for the second hydraulic simulation during the last flush

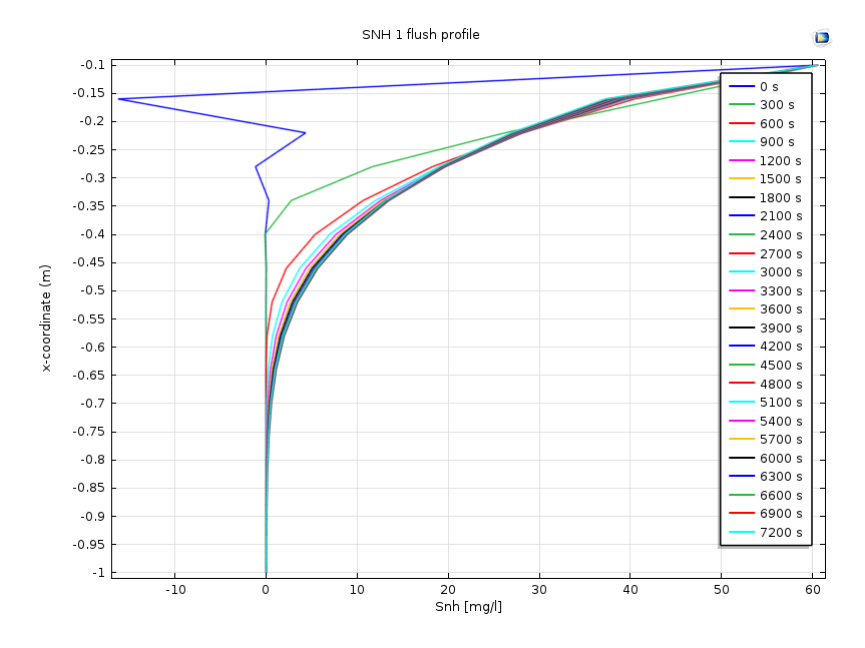


Figure 4.17: Simulated SNH concentrations in profile for the second hydraulic simulation during the first flush

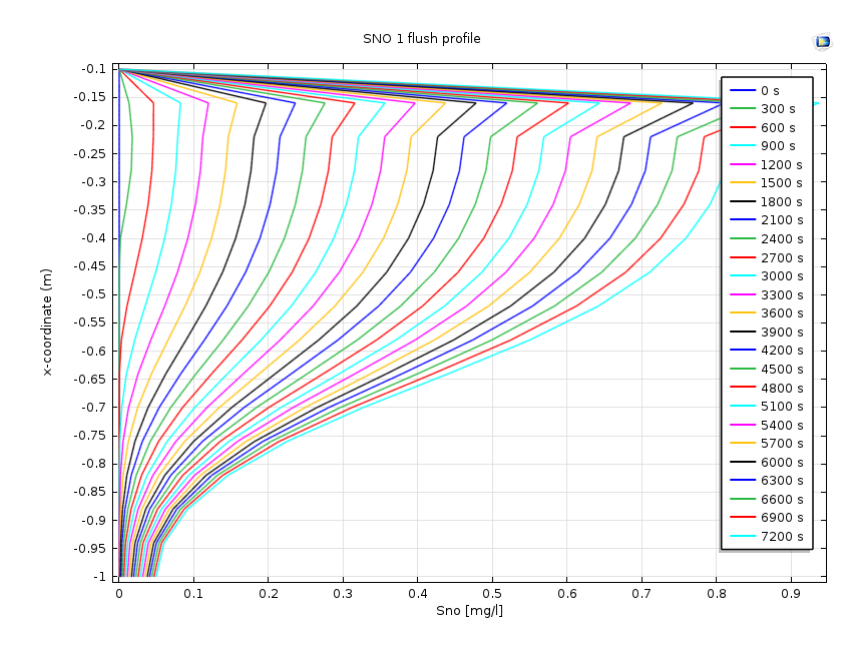


Figure 4.18: Simulated SNO concentrations in profile for the second hydraulic simulation during the first flush

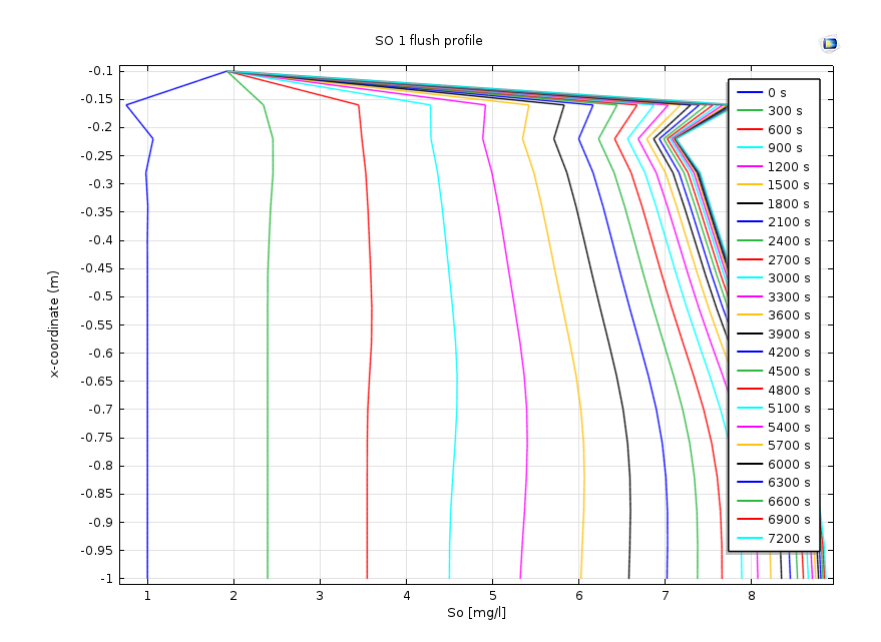


Figure 4.19: Simulated SO concentrations in profile for the second hydraulic simulation during the first flush

Concentration profiles along the wetland depth provide further insight into process localization. COD (4.16) is rapidly consumed in the upper layers, highlighting the dominance of aerobic degradation near the surface where oxygen is most available. Ammonium and nitrate profiles (4.18)(4.17) confirm the stratification of nitrification and denitrification processes: ammonium is oxidized in the upper layers, while nitrate consumption occurs deeper in anoxic zones. Oxygen profiles (4.19) demonstrate strong gradients, with high concentrations near the surface decreasing rapidly with depth, consistent with diffusion-limited aeration. These vertical patterns match well with conceptual expectations of VF wetlands, strengthening the model's credibility.

Finally, the oxygen consumption rate was calculated as:

OCR = 
$$\frac{[1.0(\Delta M_{\text{COD}}) + 4.5(\Delta M_{\text{TKN}})]}{A}$$
(4.1)

As proposed by Nivala [34], this equation allows estimating the areal oxygen consumption rate (OCR) in constructed wetlands based on the mass removal of COD and TKN, normalized by the wetland surface area. Therefore, the OCR obtained from the simulation compared from the ones measured look like this:

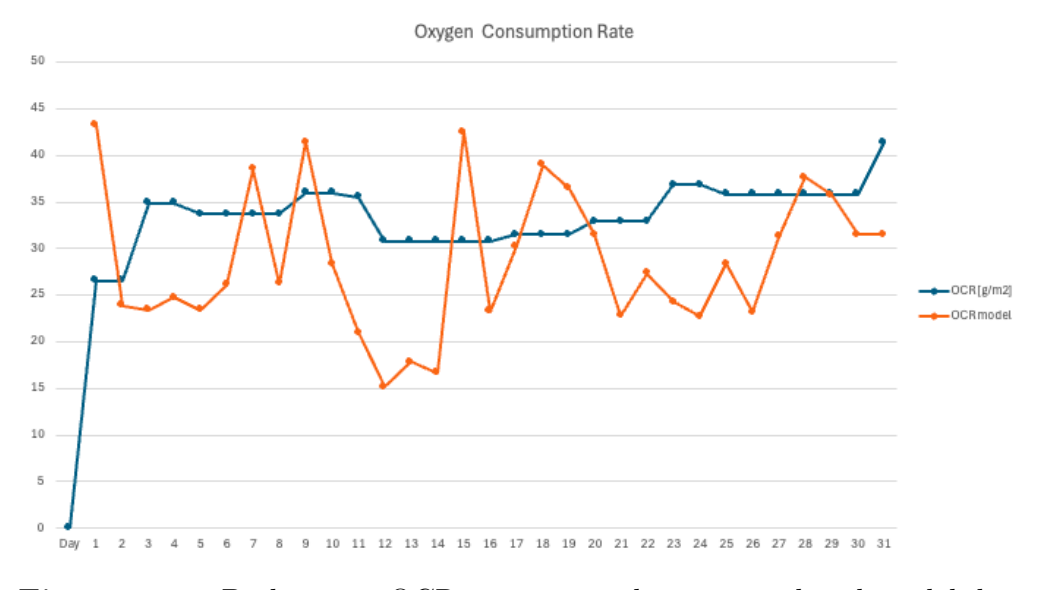


Figure 4.20: Daily mean OCR comparison between real and model data

The comparison between simulated and measured daily mean Oxygen Consumption Rate (OCR) shows good agreement, with the model capturing both magnitude and temporal variability. This agreement validates the oxygen balance formulation introduced in the adapted BIO\_PORE model, confirming that atmospheric replenishment as a function of water content is a critical improvement for unsaturated vertical systems. Minor deviations can be attributed to simplifications in root oxygen release and uncertainties in microbial activity parameters. Nonetheless, the OCR validation demonstrates that the model can reliably reproduce the overall aerobic capacity of the system, which is essential for COD and nitrogen removal.

In summary, the coupled hydraulic–biochemical simulations demonstrated that the model is capable of reproducing the main features of the observed system behavior. The hydraulic pulses structured the oxygen regime and substrate availability, while the adjusted COD partition and microbial kinetics ensured that the degradation pathways were consistent with measured removal efficiencies. The results highlight the robustness of the 1D vertical BIO\_PORE based model as a tool for analyzing constructed wetland performance under variable loading.

#### Chapter 5

#### Conclusions

In this work it was developed and applied a one dimensional numerical model of an unsaturated vertical flow constructed wetland (VFInsat), to do so, the HYDROUSA pilot system in Lesvos, Greece was used as case study. the work done combined Richards' equation for the hydraulic part and the BIO\_PORE framework for the biochemical part, both of them were modified to match the unsaturated vertical conditions. This model was calibrated and validated against the historical operational data of inflow, COD, NH4 and NO3.

The hydraulic verification proved that the imposed flush feeding regime in the model correctly matched real life functioning, which ensures a realistic behavior and shows the variation between saturated and unsaturated conditions. This dynamic proved fundamental for oxygen replenishment, which directly supports aerobic biodegradation. The chosen Van Genuchten parameters effectively captured infiltration and drainage behavior, confirming the reliability of the hydraulic submodel.

Coupled simulations highlighted the central role of oxygen transfer in determining treatment performance. In the first hydraulic-biochemical simulation, COD removal was partially achieved but with residual concentrations, and ammonium oxidation was incomplete due to oxygen limitation. After correcting the oxygen exchange formulation and refining key parameters, the second simulation produced more consistent pollutant removal. COD was effectively reduced, ammonium was oxidized with corresponding nitrate formation, and microbial populations reached stable dynamics. These results confirmed that the adapted BIO\_PORE scheme can reproduce the complex interactions among carbon, nitrogen, and oxygen cycles under unsaturated vertical flow conditions.

The spatial profiles of COD, ammonium, nitrate, and oxygen further validated the model by showing realistic stratification along the wetland depth. COD degradation and nitrification were concentrated near the upper layers where oxygen was more available, while denitrification processes were enhanced in deeper, oxygen-limited zones. This stratified behavior is consistent with empirical knowledge of vertical flow constructed wetlands, supporting the conceptual soundness of the numerical framework.

The comparison of simulated and measured Oxygen Consumption Rate (OCR) demonstrated that the model successfully captured the aerobic capacity of the wetland. This validation is a significant achievement, as oxygen availability has traditionally been one of the most difficult aspects to reproduce in process-based wetland models. The inclusion of water-content-dependent gas exchange proved essential for reproducing dissolved oxygen dynamics under variably saturated conditions.

The main contribution of this thesis lies in extending the applicability of process-based wetland models to unsaturated vertical systems. By coupling Richards' equation with the adapted BIO\_PORE biochemical framework, the work bridges the gap between conceptual understanding and numerical simulation of pollutant removal in VF wetlands. The framework can be applied for the optimization of design and operation strategies, including dosing regimes and recirculation, to enhance treatment performance under real-world conditions. Despite these achievements, the model presents limitations. The one-dimensional representation simplifies lateral heterogeneity and root-zone interactions. Some biochemical processes, such as methanogenesis and phosphorus dynamics, were excluded or simplified. Parameter uncertainty, particularly in microbial kinetics, remains a challenge for long-term predictions. Moreover, seasonal variability and long-term clogging phenomena were not explicitly addressed within the current framework.

Future research should focus on extending the model to two- or three-dimensional configurations, enabling representation of spatial heterogeneity and preferential flow paths. Incorporating seasonal datasets would allow testing model robustness under variable climatic conditions. Additional work is also required to refine plant—microbe interactions, particularly the role of root oxygen release. The potential of recirculation strategies, which motivated this study, can be fully explored using the validated model as a decision-support tool for design and management of constructed wetlands.

In conclusion, this thesis demonstrates that process-based modeling of unsaturated vertical flow constructed wetlands is feasible and effective for reproducing both hydraulic and biochemical dynamics. The validated framework provides a valuable tool for optimizing treatment efficiency, supporting the wider implementation of constructed wetlands as nature-based solutions for decentralized wastewater management. This contribution strengthens the scientific basis for advancing sustainable water treatment technologies that align with circular economy principles and environmental protection goals.

## Appendix A

# Input data for the model

**Table A.1:** VF CW monitoring data: flow, saturation depth and effluent concentrations (sat/unsat) for COD,  $NO_3$ -N and  $NH_4$ -N.

Date	$\frac{Q}{[\mathrm{m}^3/\mathrm{d}]}$	$\begin{array}{c} \mathrm{sat} \\ \mathrm{depth} \\ [\mathrm{cm}] \end{array}$	$COD_{tot}$ [mg/L]		NO <sub>3</sub> -N	NO <sub>3</sub> -N [mg/L]		$\mathrm{NH_{4}\text{-}N}~\mathrm{[mg/L]}$		
			OUT VF SAT	OUT VF UNSAT	OUT VF SAT	OUT VF UNSAT	OUT VF SAT	OUT VF UNSAT		
Limits										
07/02/21										
16/02/21		30								
10/03/21		30								
11/03/21		30								
12/03/21		30								
15/03/21		30								
16/03/21		30								
18/03/21		30								
19/03/21		30								
22/03/21		30								
23/03/21		30								
25/03/21		30								
26/03/21		30								
27/03/21		30								
29/03/21		30								
30/03/21		30								
01/04/21		30								
02/04/21		30								
05/04/21		30								
07/04/21		30								
08/04/21		30								
12/04/21		30								
14/04/21	16.4	30								
						Continu	ued on ne	ext page		

Continued fr Date	Q [m <sup>3</sup> /d]	sat depth [cm]	$\mathrm{COD}_{\mathrm{tot}}$	[mg/L]	NO <sub>3</sub> -N	[mg/L]	$\mathrm{NH_{4} ext{-}N}~\mathrm{[mg/L]}$	
		. ,	OUT VF SAT	OUT VF UNSAT	OUT VF SAT	OUT VF UNSAT	OUT VF SAT	OUT VF UNSAT
16/04/21	16.2	30						
19/04/21	15.9	30					39.9	1.4
20/04/21	16.1	30						
21/04/21	16.1	30		25				
22/04/21	16.2	30						
23/04/21	14.6	30						
26/04/21	12.0	30						
27/04/21	16.0	30						
28/04/21	16.5	30						
29/04/21	16.4	30						
05/05/21	7.3	30						3
07/05/21	12.0	30						
10/05/21	16.3	30				27.2		0.69
11/05/21		30						
13/05/21	16.1	30						
17/05/21	16.2	30		30				
20/05/21		30						
21/05/21	5.7	30						
24/05/21	16.5	30		19				
25/05/21		30				25.5		0
27/05/21	16.3	30						
08/06/21	16.2	30		49		29.7		0.2
11/06/21	33.6	30		46		30		0.4
14/06/21	28.0	30						
17/06/21	33.6	30		53		30.9		0.2
22/06/21	33.5	30		33		33		0.4
24/06/21	26.6	30						
25/06/21	17.8	30		16		33		0.1
28/06/21	33.6	30						
29/06/21		30						
30/06/21	33.6	30						
01/07/21	33.6	30						
06/07/21	32.8	30		25		42		0.1
07/07/21	52.8	30						0.1
08/07/21	67.2	30		35		35.4		0
12/07/21	67.2	30	97	35		32.7	39.6	1.1
14/07/21	67.2	30	01	90		02.1	00.0	1.1
16/07/21	63.4	30						
19/07/21	00.1	30				31.5	39.9	1.4
21/07/21	53.1	30	85	42		01.0	30.0	
23/07/21	46.3	30	100	36				
27/07/21	57.5	30	103	36		40.5	47.2	2.1
30/07/21	34.9	30	91	35		46.5	48.3	4.2
03/08/21	49.7	30	87	35		50	44.8	1.6
06/08/21	67.2	30	104	49	1.5	32	49.8	12.7
10/08/21	62.2	30	89	38	1.0	40	54.5	6.1
12/08/21	67.1	30	94	40	0.6	40	57.9	6.8
14/08/21	07.1	30	34	40	0.0	40	91.9	0.0
14/08/21 $17/08/21$	67.3	30	106	40	0.8	42	61.5	5.3
							ued on ne	

Date	from previous $Q$ [m <sup>3</sup> /d]	sat depth [cm]	$COD_{tot}$ [mg/L]		NO <sub>3</sub> -N [mg/L]		$\mathrm{NH_{4}\text{-}N}~\mathrm{[mg/L]}$	
			OUT VF SAT	OUT VF UNSAT	OUT VF SAT	OUT VF UNSAT	OUT VF SAT	OUT VF UNSAT
20/08/21	67.2	30	107	40	1	52	60	5.3
24/08/21	61.2	30	106	40	1.2	48	59.8	5.4
27/08/21	66.1	30	97	27		49	56	5.8
30/08/21	60.9	30	107	37	0	44	58.6	8.3
02/09/21	67.2	30	111	43		40	59.2	8.5
07/09/21		30						
13/09/21	67.2	30	78	20		49.5	58.9	5.4
15/09/21	67.3	30	75	31		39.5	59.1	4.5
20/09/21	66.0	30	107	41		49	58.5	7.4
21/09/21		30						
24/09/21	67.3	30	98	37		48.5	60	8.1
29/09/21	67.2	30	115	41		51	65.8	6.3
01/10/21	67.2	30	112	38		57	76.4	7
04/10/21	67.2	30	86	36		49	66.9	9.9
07/10/21	67.2	30	93	36		51		4.9
12/10/21	53.7	30	97	29		50		10
14/10/21	67.2	30	97	33		65		5.1
18/10/21	67.3	30						
19/10/21	65.1	30						
20/10/21	67.2	30						
21/10/21	67.3	30		21		39		6.6
22/10/21		30		21		39		7.4
23/10/21		30		20		35.5		12
25/10/21	66.9	30	98	22		50		5.6
26/10/21	0010	30						
27/10/21	66.4	30						
28/10/21	00.1	30						
29/10/21	67.2	30	119	44		37.5		11.2
30/10/21		30						
01/11/21	67.2	30	125	39		39.4		13.1
02/11/21	02	30	120	30		30.1		10.1
04/11/21	67.3	30	167	36		41.8	60.8	12.7
06/11/21		30						
09/11/21		30						
10/11/21	67.2	30	70	13		38.4		4.5
12/11/21	67.2	30	100	21		41.4	61.8	4.8
13/11/21	01.2	30	100			11.1	01.0	1.0
15/11/21		30						
16/11/21	66.9	30	98	30		38		9.1
17/11/21	00.0	30	00	30		90		0.1
19/11/21	64.9	30	111	27		52.5		4.7
22/11/21	67.1	30	97	6		57.5	68.4	4.6
23/11/21	01.1	30	91	U		51.5	30.4	4.0
25/11/21	67.3	30	83	14		43		7.1
30/11/21	57.0	30	66	5		38		1.8
$\frac{30/11/21}{02/12/21}$	33.6	30	86	29		36 46		1.6
02/12/21 $06/12/21$	33.6	30	57	29 24		47.5	47.8	0.7
00/12/21 $09/12/21$	33.6	30	63	24		34	41.0	
$\frac{09/12/21}{10/12/21}$	55.0	30	03	21		54		0.4
10/14/41		90						

Continued fr Date	Q [m <sup>3</sup> /d]	sat depth [cm]		[mg/L]	$ m NO_3$ -N	[mg/L]	NH <sub>4</sub> -N [mg/L]	
			OUT VF SAT	OUT VF UNSAT	OUT VF SAT	OUT VF UNSAT	OUT VF SAT	OUT VF UNSAT
13/12/21	30.8	30	51	5		31		0.7
17/12/21	33.6	30	63	23		30	31.7	0.2
21/12/21	33.7	30		7		27		0.7
23/12/21	33.5	30	83	23		28		1
27/12/21	33.6	30	104	21		26		3
28/12/21		30						
30/12/21	33.6	30	93	21		24	41.7	2.1
03/01/22	37.8	30	72	30		26	27.4	1
14/01/22		30						
17/01/22	24.8	30	45	9		26.5	21.5	0.5
20/01/22	27.5	30	69	27		18.5	26	0.6
25/01/22	26.7	30	71	31		24	38	1.3
27/01/22	26.3	30	48	20		24.5	33	1.3
31/01/22	22.1	30	34	7		32	38.5	0.2
04/02/22	24.7	30	42	18		26	32.5	0.8
07/02/22	24.1	30	45	21		27	28	0.7
10/02/22	25.2	30	36	27		25	28.2	5.8
14/02/22	24.0	30						
16/02/22	24.0	30						
18/02/22		30						
21/02/22		30	41				32.1	
23/02/22		30						
24/02/22		30		17		27		1.4
25/02/22	24.6	30	56	15		26.5	38.9	1.6
28/02/22		0						
01/03/22	24.3	0	58	27		34.5	41.6	0.5
03/03/22	24.2	0						
04/03/22	24.2	0	54	8		35.5	40.2	0.8
08/03/22	24.2	0	40	10		19.5	34	0.7
09/03/22	25.0	0						
11/03/22	26.2	0	43	24		26.5	29.8	0.6
15/03/22	24.0	0	44	25		10	25.9	0.1
17/03/22	30.7	0	40	16		25.4	28.4	0.7
21/03/22	39.8	0	70	10		10.5	15.7	1.1
23/03/22	39.8	0	78	35		22	33.1	1.2
30/03/22	39.6	0	156	10		30.5	40.3	1.5
31/03/22	39.8	0						
01/04/22	39.8	0	148	25		29.5	44.4	4.1
04/04/22	39.8	0						
05/04/22	39.8	0	53	13		37.5	50	4.5
06/04/22	39.8	0		61		52		3.3
07/04/22	39.4	0		46		50		2.3
08/04/22	39.8	0		73		53		3.3
09/04/22	39.8	0						
15/06/22	55.0	0	158	39		57	63	4.5
17/06/22	72.0	0						
21/06/22	81.6	0				57		
22/06/22	82.8	0	164	35		47	56.7	7.5
28/06/22	73.7	0	158	36		=•	54.8	0.9
- / /			100				0 1.0	0.0

Date	Q [m <sup>3</sup> /d]	sat depth [cm]	$COD_{tot}$ [mg/L]		$ m NO_3$ -N $ m [mg/L]$		$\mathrm{NH_{4}\text{-}N}~[\mathrm{mg/L}]$	
			OUT VF SAT	OUT VF UNSAT	OUT VF SAT	OUT VF UNSAT	OUT VF SAT	OUT VF UNSAT
29/06/22	85.2	0						
30/06/22	72.5	0	132	36				
07/07/22	90.5	0	134	42		60	57.9	2
11/07/22	70.8	0	128	43		52	56.7	7
14/07/22	91.2	0	129	44		48	60.1	7.7
18/07/22	84.2	0	129	31		58	62.3	1.3
21/07/22	79.9	0						
26/07/22	81.8	0	122	32		45	34.3	2
28/07/22	88.6	0	122	28		53.5	51.2	5.5
01/08/22	83.8	0	344	43		50	61.2	7.4
05/08/22	88.8	15	209	32		59	56.8	1.6
08/08/22	90.9	15						
10/08/22	89.5	15	138	28			66.1	
13/08/22	87.5	15	174	32			62.8	
23/08/22	91.1	30	136	42		59.3	62.4	6.1
26/08/22	91.1	30	116	33		57.5	58.2	1.9
31/08/22	91.2	30	130	43		23.5	66.5	11
03/09/22	91.1	30	113	29		56.5	61	3.6
06/09/22	91.1	30	83	29			60.5	7
27/09/22	90.7	30	84	24		42	60.5	4
30/09/22	75.5	30	176	36		67	66.1	8.4
04/10/22	91.1	30	94	33		67	58.2	11.2
06/10/22	88.5	30	118	38			54.9	9.1
03/11/22	48.5	30	106	84			77.2	22
07/11/22	43.4	30	103	62		47	65.5	16
10/11/22	24.2	30	96	56		50	66.9	12.3
14/11/22	59.5	30	106	50		46	68.6	13.5
17/11/22	56.0	30	112	46		66	69.6	6.4
22/11/22	65.9	30	127	44		65	76.4	12.5
25/11/22	81.2	30				63	54.5	5.3
30/11/22	67.3	30	102	42		53	63.8	8.9
02/12/22	81.5	30	112	60		26	42.7	2.2
05/12/22	81.6	30	84	36		37	45.6	2.8
08/12/22	71.0	30	102	36		47	59.7	2.8
13/12/22	80.8	30	119	40		21	64.4	7
14/12/22	80.0	30	157	37		54.2	64.7	8.2
15/12/22	67.8	30	138	35		57.5	67.6	10.2
20/12/22	66.2	30	122	46		49	61.6	11.5
23/12/22	79.5	30	207	34		53.5	61	5.6
10/01/23	47.6	30	112	43		59.5	77.2	10.5
12/01/23	46.1	30	110	52		61	59.6	5
16/01/23	43.0	30	105	40		43	54.1	7.1
19/01/23	38.2	30	87	38		50	59.6	5.8
26/01/23	44.2	30	107	33		38.5	49.4	1.3
30/01/23	38.2	30	132	33		36	39.5	2.6
03/02/23	38.0	30	66	27		34	41.9	2
08/02/23		30	71	29		40.5	49.1	0.5
14/02/23		30	68	32		45.5	55.5	0.8
14/02/20								

Continued for Date	$ m rom\ previo\ \it Q\ [m^3/d]$	us page sat depth [cm]	$COD_{\mathrm{tot}} \ [\mathrm{mg/L}]$		NO <sub>3</sub> -N	[mg/L]	$ m NH_4$ -N $ m [mg/L]$	
			OUT VF SAT	OUT VF UNSAT	OUT VF SAT		OUT VF SAT	OUT VF UNSAT
21/02/23		30				50		1.9

## **Bibliography**

- [1] Robert H. Kadlec and Scott D. Wallace. *Treatment Wetlands*. 2nd. Boca Raton: CRC Press, 2009. ISBN: 9781566705264 (cit. on pp. 1, 5–11).
- [2] UNEP. Constructed Wetlands Manual. Online. Accessed: 2025-07-09. 2015. URL: https://www.unep.org/resources/report/constructed-wetlands-manual (cit. on p. 1).
- [3] Guillermo Dotro, Günter Langergraber, Pascal Molle, Jaime Nivala, Jaume Puigagut, Otto Stein, and Marcos von Sperling. *Treatment Wetlands*. Biological Wastewater Treatment Series. IWA Publishing, 2017. ISBN: 9781780408774 (cit. on pp. 1, 5–10).
- [4] Jan Vymazal. «Constructed Wetlands for Wastewater Treatment: Five Decades of Experience». In: *Environmental Science & Technology* 45.1 (2011), pp. 61–69. DOI: 10.1021/es101403q (cit. on pp. 5, 6).
- [5] S. Salvati, A. Bianco, G. Bardasi, M. Cecilia, M. C. De Mattia, L. Giovannelli, R. Canapel, and M. C. Natalia. *Guida tecnica per la progettazione e gestione dei sistemi di fitodepurazione per il trattamento delle acque reflue urbane*. Tech. rep. ISPRA Istituto Superiore per la Protezione e la Ricerca Ambientale, 2012 (cit. on pp. 5, 7, 8).
- [6] Jan Vymazal. «Horizontal Sub-surface Flow Constructed Wetlands: The Most Successful Artificial Wetland Type for Wastewater Treatment». In: *Ecological Engineering* 37.3 (2011), pp. 487–490. DOI: 10.1016/j.ecoleng.2010.11.007 (cit. on p. 7).
- [7] Jan Vymazal. «Constructed Wetlands for Wastewater Treatment: Vertical Flow Systems». In: *Ecological Engineering* 37.3 (2011), pp. 390–406. DOI: 10.1016/j.ecoleng.2010.12.010 (cit. on pp. 8, 9).
- [8] Günter Langergraber and Rudolf Haberl. «Constructed Wetlands for Water Treatment: Minimizing Clogging and Sustainability Issues». In: Water Science and Technology 48.5 (2003), pp. 1–8 (cit. on p. 9).

- [9] Lewis A. Rossman, Beverly Pucher, and Mark G. Healy. «Clogging Processes in Constructed Wetlands: Role of Suspended Solids and Microbial Growth». In: *Ecological Engineering* 23.2 (2004), pp. 77–90. DOI: 10.1016/j.ecoleng. 2004.07.011 (cit. on p. 9).
- [10] Jan Vymazal. «Clogging and Sustainability of Constructed Wetlands Used for Wastewater Treatment». In: *Ecological Engineering* 120 (2018), pp. 1–8. DOI: 10.1016/j.ecoleng.2018.05.032 (cit. on p. 9).
- [11] Joan García. «Constructed Wetlands for Wastewater Treatment». In: *Hand-book of Environmental Engineering*. Springer, 2010, pp. 121–154. DOI: 10.1007/978-1-60327-031-1\_5 (cit. on p. 10).
- [12] J. D. Baptista, R. J. Davenport, T. P. Curtis, and E. Reid. «Aerobic and Anaerobic Pathways of Organic Matter Degradation in Constructed Wetlands». In: Water Science and Technology 48.5 (2003), pp. 125–131 (cit. on p. 11).
- [13] P. Aguirre. «Performance of Constructed Wetlands Treating Municipal Wastewater». PhD thesis. Universitat de Barcelona, 2005 (cit. on p. 11).
- [14] Otto R. Stein and Paul B. Hook. «Temperature, Oxygen, and Plant Effects on Wastewater Treatment in Constructed Wetlands». In: *Ecological Engineering* 30.2 (2007), pp. 142–152. DOI: 10.1016/j.ecoleng.2007.01.001 (cit. on p. 12).
- [15] Veronica Montagna. «Modellazione di un Sistema di Fitodepurazione a Flusso Verticale Insaturo». MA thesis. Politecnico di Torino, 2020 (cit. on pp. 13, 55).
- [16] Roger Samsó and Joan García. «BIO\_PORE, a New Mechanistic Mathematical Model for Substrate and Bacterial Dynamics in Horizontal Subsurface Flow Constructed Wetlands». In: *Ecological Engineering* 53 (2013), pp. 156–168. DOI: 10.1016/j.ecoleng.2012.12.014 (cit. on pp. 19, 22, 24, 62).
- [17] Roger Samsó and Joan García. «BIO\_PORE: A Model for the Simulation of Biofilm Processes in Horizontal Subsurface Flow Constructed Wetlands». In: Water Research 47.13 (2013), pp. 4790–4802. DOI: 10.1016/j.watres.2013.05.040 (cit. on pp. 19, 62).
- [18] Valeria Santelia. «Risposta di una constructed wetland ad incrementi di carico inquinante: analisi numerica con il software BIO\_PORE». Tesi di Laurea Magistrale in Ingegneria Civile, Indirizzo Idraulica. MA thesis. Torino, Italia: Politecnico di Torino, 2014 (cit. on pp. 19, 20, 22, 24, 57, 62–64, 75).
- [19] Roger Samsó. «Development and Application of the BIO\_PORE Model». PhD thesis. Universitat Politècnica de Catalunya, 2014 (cit. on pp. 24–27, 30, 33, 57, 58, 63, 64).

- [20] Günter Langergraber. «CWM1: A General Model to Describe Biokinetic Processes in Subsurface Flow Constructed Wetlands». In: Water Science and Technology 59.9 (2009), pp. 1687–1697. DOI: 10.2166/wst.2009.131 (cit. on pp. 26, 27, 29, 30, 33).
- [21] L. A. Richards. «Capillary Conduction of Liquids Through Porous Mediums». In: *Physics* 1.5 (1931), pp. 318–333. DOI: 10.1063/1.1745010 (cit. on p. 32).
- [22] R. Rosenzweig, A. Furman, Z. Ronen, and B. Berkowitz. «Biofilm Clogging in Sand Columns: Conceptual Models». In: *Water Resources Research* 45.10 (2009), W10414. DOI: 10.1029/2009WR007769 (cit. on p. 34).
- [23] UNESCO. Lesvos Island UNESCO Global Geopark. Accessed: 2025-07-09. 2023. URL: https://www.unesco.org/en/iggp/lesvos-island-unesco-global-geopark (cit. on p. 35).
- [24] Greeka.com. Lesvos Geography. Accessed: 2025-07-09. 2023. URL: https://www.greeka.com/eastern-aegean/lesvos/geography/(cit. on p. 36).
- [25] Encyclopædia Britannica. Lésbos / Greece, Map, Sappho, & Facts. Accessed: 2025-07-09. 2023. URL: https://www.britannica.com/place/Lesbos-island-Greece (cit. on p. 36).
- [26] F. Masi, R. Bresciani, A. Rizzo, and G. Cipolletta. Constructed Wetland Installed and Operating (Deliverable D3.4). Tech. rep. Revised February 2022. Grant Agreement No. 776643. HYDROUSA Project, Horizon 2020, 2020 (cit. on pp. 36, 47).
- [27] HYDROUSA Consortium. Design of the Constructed Wetland (Deliverable D3.2). Tech. rep. Grant Agreement No. 776643. HYDROUSA Project, Horizon 2020, 2022 (cit. on p. 36).
- [28] Giuseppe Montagna. «Modellazione numerica di una Constructed Wetland sita in Lesbo (Grecia)». Tesi di Laurea Magistrale in Ingegneria Civile, Relatore: Prof. Fulvio Boano, Correlatore: Ing. Anacleto Rizzo. MA thesis. Torino, Italia: Politecnico di Torino, 2021 (cit. on pp. 47, 50, 52, 65, 71, 73, 75).
- [29] B. Pucher. «Hydraulic and treatment performance of vertical flow constructed wetlands». English. PhD Thesis. Universität für Bodenkultur Wien (BOKU), 2019 (cit. on pp. 52, 55).
- [30] F. Masi, R. Bresciani, A. Rizzo, A. Edathoot, N. Patwardhan, D. Panse, and G. Langergraber. «Green walls for greywater treatment and recycling in dense urban areas: a case-study in Pune, India». In: *Water Science and Technology* 76.1 (2017), pp. 15–29. DOI: 10.2166/wst.2017.201 (cit. on p. 55).

- [31] Mogens Henze, Mark C. M. van Loosdrecht, George A. Ekama, and Damir Brdjanovic. *Biological Wastewater Treatment: Principles, Modelling and Design*. London: IWA Publishing, 2010. ISBN: 9781843391883. DOI: 10.2166/9781780401867 (cit. on p. 58).
- [32] Lucía Tyroller, Diederik P. L. Rousseau, Silvia Santa, and Joan García. «Dynamics of oxygen transfer through the air—water interface in constructed wetlands». In: *Water Science and Technology* 61.3 (2010), pp. 631–638. DOI: 10.2166/wst.2010.861 (cit. on p. 59).
- [33] Claude E. Shannon. «A mathematical theory of communication». In: *Bell System Technical Journal* 27.3 (1948), pp. 379–423. DOI: 10.1002/j.1538-7305.1948.tb01338.x (cit. on pp. 60, 61, 63).
- [34] Jaime Nivala, Scott Wallace, Tom Headley, Kinfe Kassa, Hans Brix, Manfred van Afferden, and Roland Müller. «Oxygen transfer and consumption in subsurface flow treatment wetlands». In: *Ecological Engineering* 61 (2013), pp. 544–554. DOI: 10.1016/j.ecoleng.2012.08.028 (cit. on p. 89).